The modelling of transition metal centres using molecular mechanics and density functional theory

Paget, Veronica J.

Award date:
1996

Awarding institution:
University of Bath

The Modelling of Transition Metal Centres using Molecular Mechanics and Density Functional Theory

submitted by Veronica J. Paget

for the degree of PhD

of the University of Bath

1996

ProQuest LLC
789 East Eisenhower Parkway
P.O. Box 1346
Ann Arbor, MI 48106-1346

For my parents,

with love.

Acknowledgements.

The end of my thesis is nearly in sight and all that remains (apart from the viva) is to say a big thank you to the many people who have helped me get this far. First I must thank Dr. Rob Deeth, for all his supervision and guidance over the last three years, for all the many references that he wrote for me and all the several hours he must have spent reading and correcting this final 'masterpiece'??!! Also to Mr. Mark Bray for his help in many areas of my work, from listening to my rantings and ravings, to setting up the computers in Warwick so I could actually get some work done. Thank you also Mark for keeping me company at lunch, and in the bar, and generally being an excellent 'tea boy'! Past members of the group, Dr. Paul Sheen and Miss Sarah Langford have also helped me a great deal in the first two years of my PhD. Thanks for a great time in Prague, and also Newcastle. An extra big thank you must also go to Sarah for not only being my 'chem pal' in my PhD years but my undergraduate ones as well. I would also like to thank Jack (Andrew) Smith for showing me the ropes at Warwick University, and helping me to settle in there. There are many other people to mention at Bath University. I am very grateful to Mrs. Sylvia Hodges, who put in all my travel claim back forms and generally kept me solvent financially over the last year, and I would also like to thank Dr. Dennis Edwards and Dr. Brian Brisdon for writing numerous references for me. Last, but certainly not least, I would like to thank Tim Paget, for all his support and encouragement, especially in my year at Warwick. Thanks Tim, I couldn't have done it without you.

Summary

This thesis illustrates two important areas of computational chemistry. The first is Molecular Mechanics, (MM). Here, the development and improvement of this method in application to transition metal complexes is discussed. A ligand field stabilisation energy term is included in the MM calculations, and a transferable force field for the following has been developed:

i) high and low spin Ni(II) complexes

ii) a variety of different stereochemistries of Cu(II) amine complexes. For the six-coordinate species the Jahn Teller distortions were automatically generated.

iii) low spin Co(III) amines

iv) Mixed ligand systems of the type $[ML_4X_2]$ (where M = Co(III), Ni(II) and L=amine, X=Cl), and $[MA_xB_y]^{2+}$ (where M = Ni(II), Cu(II) and A=amine, B=imine, and $0 \leq x \leq 6$, $0 \leq y \leq 6$).

The inclusion of an electrostatic term to the force field has been discussed and a transferable force field which takes into account charges has also been developed. Initial studies of modelling Pt(II) complexes have also been carried out, and a novel method for the simulation of the trans influence has been developed.

The second part considers a completely different computational method, Density Functional Theory. Here, this ab initio method is applied to the investigation of the factors which effect the acidity of metal hexaaquo ions, and the importance of this to biological systems. Molecular geometries of $[M(H_2O)_6]^{n+}$ and $[M(H_2O)_5(OH)]^{(n-1)+}$ (where M = Fe(III), Cr(III), Al(III), Zn(II), Fe(II), Ni(II) and Mn(II)) are calculated and the correlation between the energy of H^+ dissociation and pK_a is discussed.

Contents

Part 1

A Novel Molecular Mechanics Force Field with a Cellular Ligand Field Stabilisation Energy Term for the Accurate Modelling of Coordination Complexes.

Introduction

The success of a computational technique may depend on how well the approach is developed in the first place. Part 1 discusses Molecular Mechanics, and how, in this study, it has been developed to give an accurate and general computational approach for determining the structures of transition metal complexes.

The first section deals with a detailed discussion of the basic principles of Molecular Mechanics, along with the recent and exciting developments in this area. Subsequent chapters deal with the role of the Cellular Ligand Field Stabilisation Energy term, and how a transferable force field has been developed to bring about DOMMINO (D-Orbitals in Molecular Mechanics for INOrganics). This has then been successfully applied to the determination of geometries of several Ni(II), Cu(II) and Co(III) complexes.

The importance of including π interactions is discussed and the inclusion of an electrostatic term into the force field is also considered. A new Morse function is also introduced between ligands which are trans to each other, so that the modelling of the trans influence exhibited by Pt(II) square planar complexes can be simulated.

All of this leads to many significant advances which have been made with this method, and have not previously been achieved using conventional Molecular Mechanics. These include:

i) the determination of high and low spin complexes using the same force field.

ii) the automatic generation of Jahn Teller distorted Cu(II) complexes.

iii) the modelling of the trans influence of Pt(II) complexes (though this is still in the earlier stages of development).

Chapter 1

Molecular Mechanics

1.1 Theory

Molecular Mechanics is an empirical method which is commonly used to predict geometries and determine conformational energies[1]. Its advantages are:

i) limited computer resources are required

ii) little experience is necessary to use the method

iii) the results obtained can reproduce experimental data accurately.

Within the Molecular Mechanics method the molecule is viewed as a collection of atoms held together by elastic forces. These forces can be described by potential energy functions of structural features like bond lengths, bond angles, non bonded interactions and torsional terms. The combination of these potential energy functions is the force field. The total strain energy, E_{tot}, of the molecule in the force field arises from deviations from ideal structural features, and can be approximated by the sum of the energy contributions (equation 1.1).

$$E_{tot} = \Sigma E_{str} + \Sigma E_{bend} + \Sigma E_{tors} + \Sigma E_{vdw} + \ldots\ldots \qquad (1.1)$$

where

E_{str} = the energy of a bond stretched or compressed from its natural bond length
(this corresponds to nearest neighbour interactions)

E_{bend} = the energy of bending bond angles from their natural values
(this corresponds to next nearest neighbour interactions)

E_{tors} = the torsional energy due to twisting about bonds
(this corresponds to interactions due to rotation about bonds)

E_{vdw} = the energy due to van der Waals non bonded interactions
(this corresponds to non bonded interactions)

If there are other intramolecular mechanisms affecting the energy such as Coulombic interactions, or out of plane deformations, for example, then these too may be added to the force field. In general, there are no strict rules concerning what types of potential energy functions should be used. This has led to the development of many different Molecular Mechanics force fields[2-5].

Once the force field has been constructed, a trial geometry is specified in terms of atomic coordinates, and an initial strain energy is calculated. Thereafter, the geometry is optimised by a minimisation procedure.

These procedures are iterative methods in which the atomic coordinates are modified from one iteration to the next, in order to obtain the smallest possible strain energy.

1.2. Potential Functions of Force Fields

1.2.1. E_{str}

Most force fields employ a harmonic potential with Hooke's law functions for bond stretching (equation 1.2).

$$E_{str} = 1/2k_r(r_{ij}-r_0)^2 \qquad (1.2)$$

where k_r is the force constant

r_{ij} is the actual bond length

r_0 represents the ideal bond length

However, at very large deformations from the ideal bond length, deviations from the harmonic potential are observed, thus a Morse function[6] can be employed.

The Morse potential is given by

$$E_{str} = D_0[1-e^{-\alpha(r_{ij}-r_0)}]^2 - D_0 \qquad (1.3)$$

where D_0 is the bond dissociation energy

α is the force constant

r_{ij} is the actual bond length

r_0 represents the ideal bond length

Figure 1.1. A schematic representation of the Morse function.

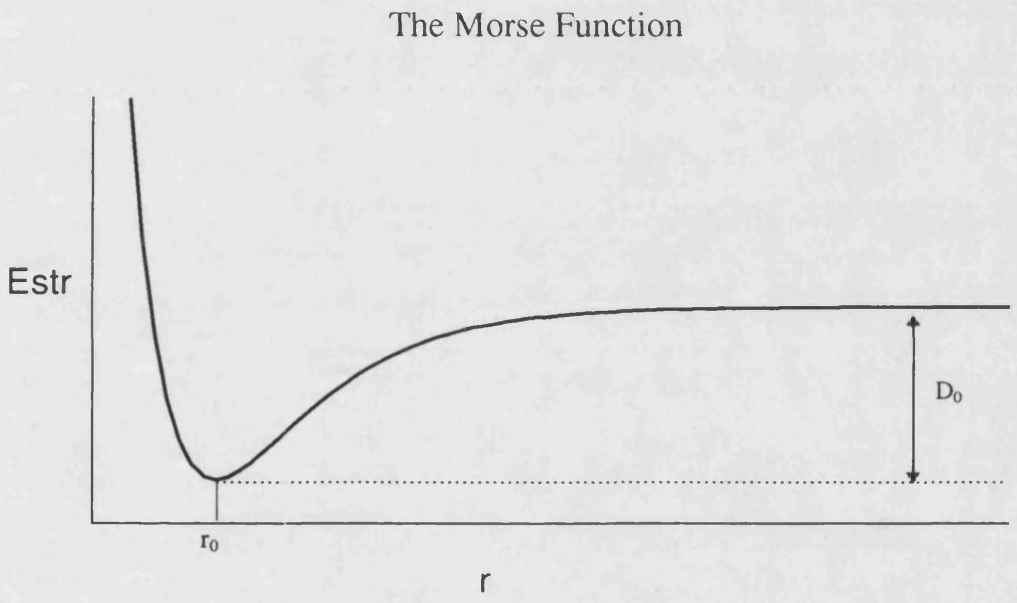

Other approximations have also been designed which give equivalent results to the Morse function, provided the deviation from the equilibrium bond length is not too large. One such approximation is to include a cubic term into equation 1.2 as shown in equation 1.4.

$$E_{str} = 1/2k(r-r_0)^2 + k'(r-r_0)^3 \qquad (1.4)$$

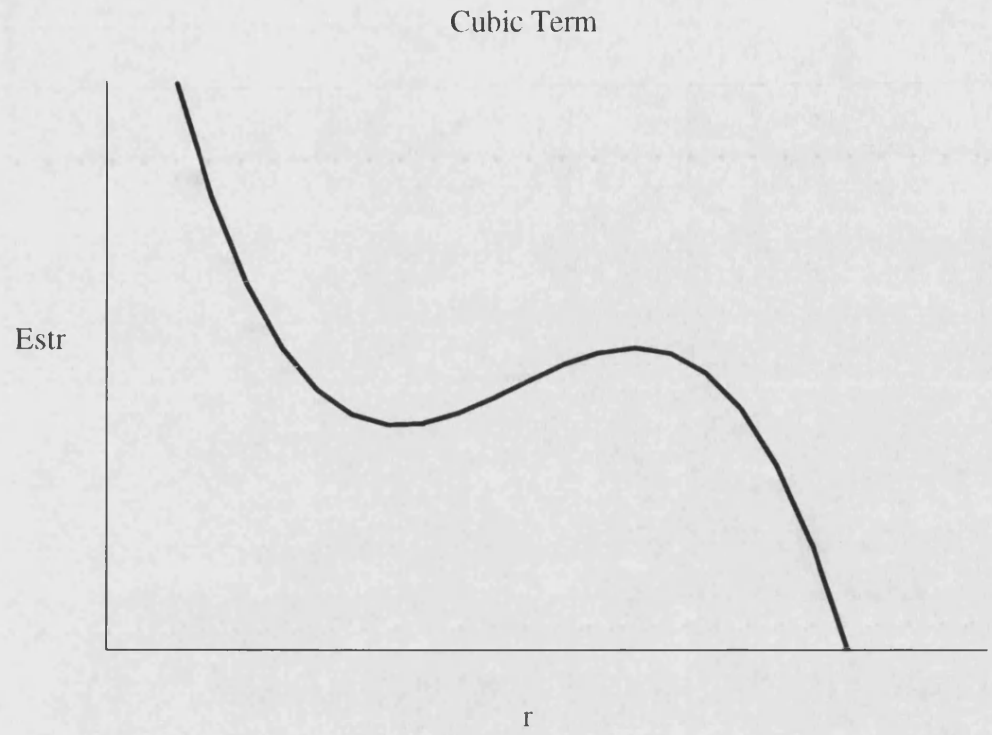

Figure 1.2. An illustration of a cubic term.

The disadvantage of cubic terms is that at very large distortions the function inverts. Thus, the Morse function is a more accurate description of bond stretching since it includes anharmonic terms and leads to a finite energy, D_0, for breaking bonds.

1.2.2. E_{bend}

Angle bending terms can also be expressed by harmonic potentials.

$$E_{bend} = (1/2)\, k_\theta\, (\theta - \theta_0)^2 \qquad (1.5)$$

where θ is the bond angle, θ_0 is the equilibrium bond angle and k_θ is the force constant.

A problem involving the use of a harmonic angular potential concerns the behaviour of the function at the angular limit (e.g. $\theta_{L\text{-}M\text{-}L} = 180°$). At this limit, harmonic functions peak, whereas the slope should be zero. This shows the anharmonicity of the angular potential particularly in the region of large distortions.

1.2.3. E_{tors}

Internal rotation about bonds are most commonly described in terms of a torsional angle, ω, defined according to Figure 1.3.

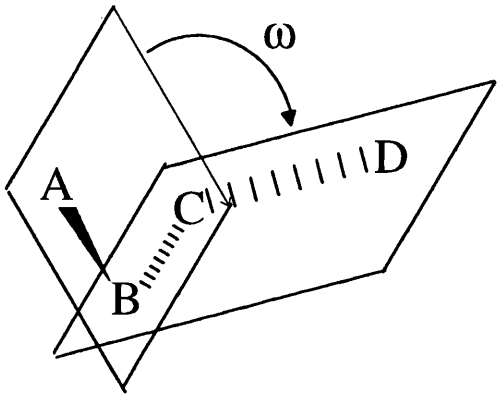

Figure 1.3. Definition of torsional angle ABCD

The torsional energy term has usually been thought of as resulting from a repulsion between bonds not covered by van der Waals interactions. Modern Molecular Mechanics force fields describe the change in energy of the molecule as the torsion angle, ω, changes in terms of the Fourier series shown in equation 1.6.

$$E_{tors} = (1/2)\, V\, (1\text{-}\cos(j\omega)) \qquad (1.6)$$

In this equation V is the force constant, j is the periodicity and ω is the torsion angle.

1.2.4. E_{vdw}

Also included in the Molecular Mechanics scheme is the energy term relating non-bonded interactions of atoms. As two atoms approach one another there are the usual attractive forces, for example dipole-dipole interactions, dipole-induced dipole interactions, and dispersion forces (interactions between fluctuating dipoles in molecules or atoms, i.e. induced dipole-induced dipole interactions). These are then opposed by repulsion when the two atoms become too close. All these interactions are assembled in the van der Waals term.

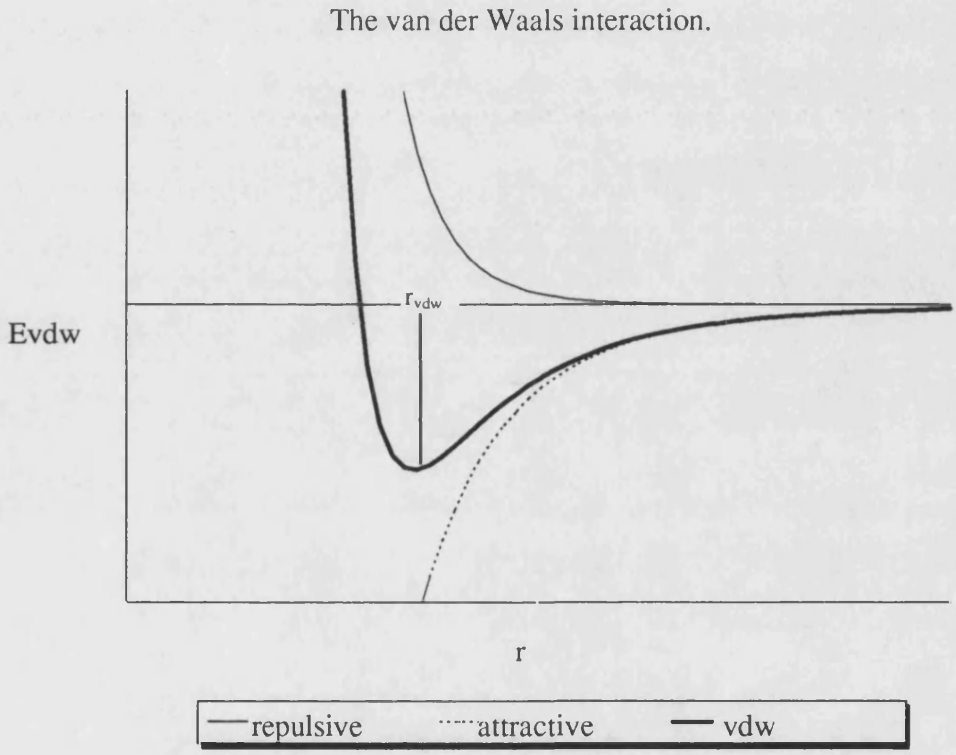

Figure 1.4. An illustration of the van der Waals potential.

r_{vdw} is defined as the van der Waals radius which corresponds to maximum stabilisation.

At distances below r_{vdw} the atoms repel each other, and above r_{vdw} they attract each other. The attractive force is usually modelled by a $1/r^6$ dependence while various possibilities exist for the repulsion. Two examples of the functions used in modern programs to calculate the van der Waals term are the Lennard-Jones[7] potential,

$$E_{vdw} = A/r^{12} - B/r^6 \qquad (1.7)$$

where A and B are constants

r = distance between atoms

or the Buckingham potential[8],

$$E_{vdw} = A\exp(B/r) - C/r^6 \qquad (1.8)$$

where A, B, and C are constants

r = distance between atoms

Non bonded interactions could be defined as anything from 1,3 and 1,4 and 1,5 and upwards. However in MM, the E_{vdw} term usually only considers terms from 1,5 interactions and above as the 1,3 and 1,4 interactions are subsumed within other force field terms.

1.2.5. E_{tot}

All these potential functions combine together to give the total steric or strain energy, E_{tot}. It is important to recognise that the energy E_{tot} by itself has no physical meaning, it is only a measure of intramolecular strain relative to a hypothetical situation. It is the differences in E_{tot} for a given set of calculations that are appropriate for comparison with experimentally observed properties such as rotational barriers or conformational energies of a given molecule.

1.3. Modelling of Coordination Compounds.

Molecular Mechanics is a popular method for modelling geometry and energetics, and it has been used for many years to study the structures and properties of organic molecules[9]. This is because of fairly complete force fields for this class of compounds. The same cannot be said about transition metal compounds because of the large number of elements and the diversity of both geometries and oxidation states. Despite this, many applications of Molecular Mechanics to transition metal complexes have been reported and many reviews have been published[10,11].

The prediction of isomer distribution of Co(III) and Ni(II) complexes has been investigated[12,13], and other conformational analysis of coordination complexes includes work by Hambley et al.[14]. Drew et al.[15-19] have studied macrocyclic ligands bound to various transition metal species, and an extensive study on Ni(II) macrocycles has been carried out by Adam et al.[20]. Force fields for Cr(III), Fe(III), Ni(II), Zn(II) complexes have been reported by Bernhardt et al.[21]. Metal ion size-based selectivity studies for Cu(II), Ni(II), and Zn(II) complexes have been carried out by Hancock et al.[22] and Evers et al.[23], and Bernhardt et al.[24] have extended this work. Molecular Mechanics calculations have also been applied to the prediction of spectroscopic properties. Bernhardt et al.[25] have combined Molecular Mechanics with the Angular Overlap Model to predict the d-d electronic structure of a variety of hexammine complexes of Co(III), Cr(III) and Ni(II). Work has also been carried out on the chelate effect by studying the strain energy of Ni(II) complexes containing chelate rings of different sizes[26-27]. Force fields for metal carbonyl clusters[28-30] and metallocenes[31,32] have also been reported.

Recently Molecular Mechanics methods have been combined with Quantum Mechanical, (QM), methods[33-36]. The reason for this is that Quantum Mechanical methods are able to model bond making/breaking processes (which Molecular Mechanics can not), but they are unable to model large systems, e.g. proteins. As Molecular Mechanics can handle these relatively easily, then by combining the two techniques, it is envisaged that the

reaction profiles of biological systems could be investigated. A full discussion of the combined QM/MM method is beyond the scope of this thesis.

Also Molecular Mechanics has been combined with semi empirical methods by Hancock[37]. Here it is used in the calculation of steric activation energy between the ground state and intermediates of some Co(III) complexes.

Despite the growing number of applications of Molecular Mechanics to transition metal complexes, there are significant difficulties in the parameterisation of those parts of the structure involving the metal. These will now be discussed in detail.

1.4. Angular Potential Function

As mentioned earlier, the angular potential, particularly in the region of large distortions, exhibits anharmonicity. This anharmonicity needs to be included in the modelling of transition metal complexes, as these often show a wide variety of geometries.

Allured et al.[4] have addressed this problem in reporting a force field, SHAPES, that differs from conventional force fields in that the angular potential used to describe the ligand-metal-ligand (L-M-L) bond angles take the form of a Fourier term, i.e. a periodic function, shown in equation 1.9.

$$E_{bend} = k^F[1+\cos(n\phi+\psi)] \qquad (1.9)$$

where ϕ represents the bond angle

n is the periodicity of the cosine function

ψ is the phase shift which determines the position of the minima

k^F is the 'force constant' which determines the steepness of the function about the minima.

It is suggested that this Fourier term is a superior representation of the distortion potentials at large bond angles, and does not show the inappropriate behaviour of harmonic potentials.

Another problem is encountered in the definition of unique angles and corresponding equilibrium values. This is referred to as the unique labelling problem. For example cis-diamminedichloroplatinum(II), $[Pt(NH_3)_2(Cl)_2]$, requires two N-Pt-Cl equilibrium values, 90° and 180°. The unique labelling problem arises for any molecular shape with the possibility of cis and trans ligand orientations. This includes T-shaped, square planar, trigonal bipyramidal and octahedral idealised geometries (i.e. geometries which are often observed for high coordination complexes). Since cis and trans orientations are not possible for tetrahedral, trigonal planar, and linear geometries, the problem of defining unique angles and equilibrium values is not usually an issue for organic molecules.

Weisemann et al.[38] suggest that the unique labelling problem can be resolved by assigning every L-M-L type with several bond angle reference values and their corresponding force constants. Then prior to a single energy calculation, the program chooses the reference value closest to the actual bond angle in the current geometry. This reference value and the force constant is then retained throughout the energy calculations.

Another strategy to evade the unique labelling problem and the problems encountered due to the use of harmonic angular functions, is to set the angle bend force constant for the L-M-L angles to zero, and to allow ligand-ligand 1,3 non bonded interactions, usually in the form of Lennard-Jones or Buckingham potentials. This approach has been used by Bernhardt et al.[39].

A recent method for modelling the angular geometry about the metal centre has been developed by Comba et al.[40]. This strategy is based on the combination of 1,3 nonbonded interactions around the metal centre and a harmonic sine function with a ligand field dependent force constant for the L-M-L terms. For octahedral geometries, the ligands are

located along the cartesian x, y, and z axes. So the L-M-L angles will be 90° and 180°. The simplest function with minima at these respective angles is a harmonic sine function of 2θ.

$$E_\theta = 1/8k_\theta \sin^2(2\theta) \qquad (1.10)$$

k_θ is then given by

$$k_\theta = cn1/2(k_{ML} + k_{ML'}) \qquad (1.11)$$

where k_{ML} and $k_{ML'}$ are the bond stretching force constant of M-L and M-L', which are related to the ligand field strength of the ligand, c is defined as a normalisation constant, n accounts for the d orbital occupancy, and is given by the linear dependence of the ligand field stabilisation energy nDq, i.e. for d^0, high spin d^5, and d^{10} configurations, n=0; d^3, n=12; low spin d^6, n=24.

In this way computed angular geometries of metal complexes have been more accurately determined. This is of importance in the calculation of spectroscopic properties in the MM-AOM technique mentioned earlier.

1.5. Universal Force Field (UFF)

A problem of Molecular Mechanics is that many of the force fields are limited to a particular class of species, for example, those of proteins, organics and nucleic acids[41,42]. Rappé et al.[43] have tried to overcome this by developing a force field which could, in principle, be extended to the entire periodic table. The approach that they have used, involves the utilisation of a generic force field. Generic force fields employ simple algorithms that generate the parameters needed, from atom-based parameters and the molecule's connectivity. The advantage of this approach is that once an atom type has been parameterised, it can be modelled in any environment. This force field they

developed is referred to as the Universal Force Field. The estimation of these force field parameters is based only on the element, its hybridisation and connectivity. The potential energy of a complex is described by various two-body(bond-stretch), three-body(angle bend) and four-body interactions(torsional and non-bonded interactions).

The bond stretch term is described by harmonic or Morse potentials (see equation 1.2 and 1.3). For the harmonic term, the bond length, r_{ij}, is assumed to be the sum of atom type specific single bond radii, e.g. $r_i + r_j$, plus a bond order correction, r_{bo}, plus an electronegativity correction, r_{en}.

$$r_{ij} = r_i + r_j + r_{bo} + r_{en} \qquad (1.12)$$

r_{bo} is then given by:

$$r_{bo} = -\lambda(r_i + r_j) \ln (n) \qquad (1.13)$$

where λ is a proportionality constant

n is the bond order between centres i and j

The electronegativity term was suggested by O'Keefe and Brese[44] and is shown in equation 1.14.

$$r_{en} = r_i r_j(\sqrt{\chi_i} - \sqrt{\chi_j})^2/(\chi_i r_i + \chi_j r_j) \qquad (1.14)$$

Here χ is a dimensionless parameter which is proportional to the electronegativity[45] of, for example, atom i.

The force constant, k_{ij}, is determined such that

$$k_{ij} = 644.12\, Z_i\, Z_j/r_{ij}^3 \qquad (1.15)$$

where Z is the effective atomic charge.

For the Morse function, the dissociation constant D_{ij} is given by:

$$D_{ij} = 70(n) \qquad (1.16)$$

where n = bond order between i and j

and α is given by

$$\alpha = [k_{ij}/2D_{ij}] \qquad (1.17)$$

where k_{ij} is described as above.

Thus the parameterisation of the bond stretch term relies only on atomic radii, bond order and effective atomic charge.

The angle bend term is described by a cosine Fourier expansion

$$E_\theta = k_{ijk} \Sigma C_n \cos n\theta \qquad (1.18)$$

where k_{ijk} is the force constant

C_n is a coefficient

θ is the natural bond angle

Again k_{ijk} is derived from an analytical function which depends on the natural angle, atomic radii and effective nuclear charge.

The torsional term is a Fourier expansion, which is a function of a torsional barrier parameter which is defined for each atom type, an equilibrium torsion angle and its periodicity.

The nonbonded terms are van der Waals and electrostatic. The van der Waals term is described by a Lennard-Jones type expression, and the electrostatic term (where it is included) depends on the charges q_i and q_j of atoms i and j respectively and also on r_{ij} and the dielectric constant.

The force field described is thus constructed from simple rules and atomic parameters and is capable of reproducing many structural features across the periodic table[46,47].

The UFF has been used successfully with organics, main group elements and some transition metal complexes. However, with the transition metal species[48], the errors are somewhat larger than those for organic compounds (the M-L bond distance error ranging from less than 0.05 Å to as much as 0.15 Å). It is also unable to predict the trans influence exhibited in Pt complexes, and reproducibility of d orbital stereochemical activity, such as Jahn Teller effects, have not been reported.

The modelling of such Jahn Teller effects of Cu(II) systems has posed many problems for conventional Molecular Mechanics, and this is now discussed in detail.

1.6. Simulating the Plasticity of the Cu(II) Coordination Sphere: The Challenge for Molecular Mechanics!

The distribution of electrons within a transition metal species can exert a large influence over the geometry of the complex. One such 'electronic effect' due to partly filled d orbitals is the Jahn Teller distortions which are often observed. Molecular Mechanics force fields can not easily reproduce the geometry of a Jahn Teller distorted structure. For example, in order to reproduce the elongated octahedral geometry of a CuL_6 species, it is necessary to define different parameter sets for the axial and equatorial ligands in order to give different axial and equatorial metal-ligand bond lengths, even though L is identical in both cases[49]. Complexes where equatorial and axial ligands are different are treated more easily without any apparent anomalies, as different force field parameters can be defined

for each[50]. However, if in one complex the ligand, L, was in an axial position, and in another molecule, L occupied an equatorial site, then different sets of parameters would be required for each situation.

Square planar 4-coordinate complexes, being at the extreme of the Jahn Teller distortion are less plastic and thus have been handled quite well with Molecular Mechanics[51].

For some Cu(II) 4-coordinate complexes, e.g, when coordinated to amino acids, the geometry can exhibit an intermediate structure between 'regular' planar and tetrahedral structures. A Molecular Mechanics approach developed by Sabolovic et al[52] has been designed to simulate these complexes. In this procedure, dummy atoms, X and X', are defined above and below the plane of the chelate ligands and the coordination sphere around the central metal atom is determined by considering only the bonding interactions with the central atom and Coulombic interactions between all nonbonded atoms except X and X'. This was then modified later[53] to include the Coulombic interactions between apically placed charges. The disadvantage of these strategies is that tetrahedral configurations would only be possible if the X atoms were so far away that their influence is very weak. Thus, prior knowledge of the geometry of the system to be modelled is necessary. Clearly, this method would then have no great predictive utility.

A variation on the 'dummy atom' model[54], with angle bending interactions between 'real' ligands and two 'dummy' apically placed ligands, has also been used. This method has proved successful in conformer analysis[55,56].

For 6-coordinate Cu(II) species, Jahn-Teller distortions are frequently observed. Systems where different force field parameters are used for axial and equatorial ligands have proved to give reasonable accuracy[49]. However, for a CuL_6 system where all the ligands are the same, then a prior knowledge of the geometry is required. This method is then lacking, if a prediction of structure is required.

A recent methodology reported by Comba et al.[57] has an additional term which mimics the Jahn-Teller stabilisation energy, EJT. For this to be determined a prior knowledge of the ligand field spectrum is required.

Consider a Cu(II) hexacoordinate complex. The distortions that can occur by splitting the e_g orbitals are shown in Figure 1.5 below.

Figure 1.5. Illustration of the distortions that can occur by splitting the e_g orbitals.

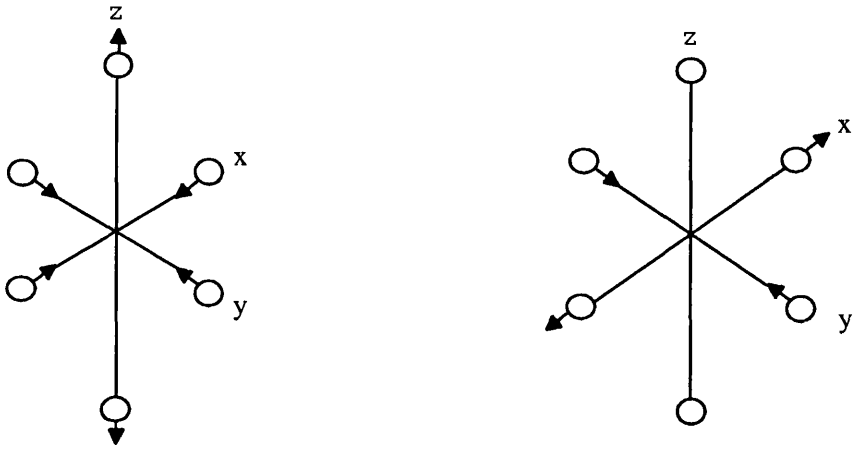

Mode 1 Mode 2

Based on the harmonic first order model and equations[58] for mode 1, then EJT as a function of the in plane displacement ($\delta x=\delta y$) is described by

$$EJT = \{(-0.01198)(\delta x)(\Delta')\}/r_0 \qquad (1.19)$$

where Δ' is the energy of d orbital splitting between the e_g and t_{2g} orbitals in cm^{-1}.

In the calculations, the complex is first minimised without involving a Jahn Teller distortion. Then the total strain energy and the Jahn Teller stabilisation energy, can be calculated by systematically changing the constrained bond lengths of the in-plane and

axial ligands. For each in-plane contraction, an axial elongation of twice the distance is applied.

This method has worked well for some Cu(II) complexes[59]. The advantages of the method are that the Cu-L distances of dynamically Jahn Teller distorted complexes, or of complexes which have not been crystallographically characterised can be obtained. Also steric and electronic contributions can be analysed. However, this strategy can be quite cumbersome, in as much as minimisation in each direction of possible distortion, needs to be carried out, in order to assess which geometry is the most energetically stable. This method has also been problematic in that at large axial distortions, the in-plane equatorial compression is overestimated. For example, $[Cu(imid)_6]^{2+}$, (imid=imidazole), where Cu-N(ax) = 2.59 Å, this method predicts the Cu-N(eq) distance to be 1.91 Å, compared with an experimentally observed bond length of 2.03 Å. Thus, this approach may be accurate at small Jahn Teller deformations, but falls short for complexes with large distortions.

1.7. Conclusion.

Molecular Mechanics is a simple technique for locating a local minimum on a potential energy surface of a complex. This potential energy surface is computed by using functions whose parameters are derived empirically by reproducing experimental data.

For coordination chemistry, the design of force fields which accurately represent experimental data has been problematic. This is due to the large range of possible coordination numbers, oxidation states, spin states, and electronic effects which are so often observed for these complexes, and which can have significant consequences for the structure.

Many characteristics of coordination complexes can be explained in terms of the ligand field stabilisation energy[60]. The ligand field stabilisation energy is a general concept which, for example, explains the tendency for four-coordinate d^8 metals to be associated with

square planar coordination[61], rationalises the 'double hump' behaviour of the heats of hydration of metal(II) hexaaquo complexes, and can also be used in understanding the Jahn Teller effects exhibited by some open-shell systems.

Thus, it appears that for any general modelling of transition metal systems, the inclusion of a ligand field stabilisation energy expression is necessary. In this study, a Cellular Ligand Field Stabilisation Energy (CLFSE) term has been included in a Molecular Mechanics force field for the determination of structures of coordination complexes.

In the next chapter, the basis of the Cellular Ligand Field Stabilisation Energy Term (CLFSE) is discussed.

1.8. References

1. J. Comp. Chem, 1996, 17, 385, and Refs therein, Edt. N. Allinger, P von R Schleyer; J. Comp. Chem, 1996, 17, 489, and Refs therein, Edt. N. Allinger, P von R Schleger
2. MM2, Quantum Chemical Program Exchange (QCPE), Creative Arts Bldg. 181, Indiana University, 840 Stat Hwy. 46 Bypass, Bloomington, IN 47405, U.S.A.
3. MM3 Technical Utilization Cooperation, Inc., 235 Glen Village Court, Powell, OH 43065, U.S.A.
4. SHAPES, V. S. Allured, C. M. Kelly, C. R. Landis, *J. Am. Chem. Soc.*, 1991, **113**, 1.
5. Sybyl, Tripos Associates, 1699 Hanley Road, Suite 303, St. Louis, MO 63144-2193, U.S.A
6. P. M. Morse, *Phys Rev,* 1929, **34**, 57.
7. J. E. Lennard-Jones, *Proc. R. Soc. London Ser. A*, 1924, **106**, 463.
8. A. D. Buckingham, *Ann. Rev. Phys. Chem.*, 1970, **21**, 287.
9. N. L. Allinger, *J. Am. Chem. Soc.*, 1977, **99**, 8127.
10. P. Comba, *Coord. Chem. Rev.*, 1993, **123**, 1.
11. B. P. Hay, *Coord. Chem. Rev.*, 1993, **126**, 177.
12. P. Comba, T. W. Hambley and L. Zipper, *Helv. Chim. Acta*, 1988, **71**, 1875.
13. P. V. Bernhardt, P. Comba, T. Gyr and K. Varnagy, *Inorg. Chem.*, 1992, **31**, 1220.
14. T. W. Hambley, C. J. Hawkins, A. J. Palmer and M. R. Snow, *Aust. J. Chem.*, 1981, **34**, 45.
15. M. G. B. Drew, S. Hollis and P. C. Yates, *J. Chem. Soc., Dalton Trans.*, 1985, 1829.
16. M. G. B. Drew, D. A. Rice, S. bin Silong and P. C. Yates, *J. Chem. Soc., Dalton Trans.*, 1986, 1081.
17. M. G. B. Drew and P. C. Yates, *J. Chem. Soc., Dalton Trans.*, 1987, 2563.
18. C. Harding, D. NcDowell, J. Nelson, S. Raghunathlan, C. Stevenson, M. G. B. Drew and P. C. Yates, *J. Chem. Soc., Dalton Trans.*,1990, 2521.
19. J. Beech, P. Y. Croggs and M. G. B. Drew, *J. Chem. Soc., Dalton Trans.*, 1994, 719.
20. K. R. Adam, M. Antolovich, L.G. Brigden and L.F. Lindoy, *J. Am. Chem. Soc.*, 1991, **34**, 45.
21. P. V. Bernhardt, P. Comba and T.W. Hambley, *Inorg. Chem.*, 1993, **32**, 2804.
22. R. D. Hancock, *Prog. Inorg. Chem.*, 1989, **37**, 189.
23. A. Evers, P.W. Wade, M.P. Ngwenya, J.C.A. Boeyens and K.P. Wainwright, *J. Am.Chem. Soc.*, 1988, **110**, 2788.
24. P. V.Bernhardt and P. Comba, *Helvetica Chimica Acta*, 1991, **74**, 1834.
25. P. V. Bernhardt and P. Comba, *Inorg. Chem.*, 1993, **32**, 2798.
26. G. J. Mc Dougall, R.D. Hancock and J.C.A. Boeyens, *J. Chem. Soc Dalton Trans.*, 1987, 1438.
27. R. D.Hancock, G.J. McDougall and F. Marsicano, *Inorg., Chem.*, 1979, **18**, 2847.
28. A. Sironi, *Inorg. Chem.*, 1992, **31**, 2467.
29. J. W. Lauher, *J. Am. Chem. Soc.*, 1986, **108**, 1521.
30. A. Sironi, *Inorg. Chem.*, 1996, **35**, 1725.
31. T. N. Doman, T. K. Hollis and B. Bosnich, *J. Am. Chem. Soc.*, 1995, **117**, 1352.
32. T. V. Timofeevan. J. H. Lii and N. L. Allinger, *J. Am. Chem. Soc.*, 1994, **116**, 591.
33. J. Gao and L. Shao, *J. Phys. Chem.*, 1994, **98**, 13772.
34. J. Gao, *J. Phys. Chem.*, 1992, **96**, 537.
35. I. H. Hillier, B. Waszkowycz, N. Gensmantel and D. W. Payling, *J. Chem. Soc., Perkin Trans. 2*, 1991, 225.
36. R. V. Stanton, D. S., Hartsough and K. M. Marz Jr., *J. Comp. Chem.*, 1995, **16**, 113.
37. R. D. Hancock, *J. Chem. Soc., Chem. Comm.*, 1996, 1301.
38. F. Weisemann, S. Teipel, B. Krebs and U. Howler, *Inorg. Chem.*, 1994, **33**, 1891
39. P. V. Bernhardt and P. Comba, *Inorg. Chem.*, 1992, **31**, 2638.
40. P. Comba, T. W. Hambley and M. Stöhle, *Helv. Chim. Acta.*, 1995, **78**, 2042.
41. L. Nilsson and M. Karplus, *J. Comp. Chem.*, 1983, **4**, 187.

42. S. J. Weiner, P. A. Kollman, D. A. Case, U. C. Singh, C. Ghio, G. Alagona, S. Profeta Jr, and P. Weiner, *J. Am. Chem. Soc.*, 1984, **106**, 765.
43. A. K. Rappé, C. J. Casewit, K. S. Colwell, W. A. Goddard III, and W. M. Skiff, *J. Am. Chem. Soc.*, 1992, **114**, 10024.
44. M. O'Keefe and N. E. Brese, *J. Am. Chem. Soc.*, 1991, **113**, 3226.
45. A. L. Allred and E. G. Rochow, *J. Inorg. Nucl. Chem.*, 1958, **5**, 264.
46. C. J. Casewit, K. S. Cowell and A. K. Rappé, *J. Am. Chem. Soc.*, 1992, **114**, 10035.
47. C. J. Casewit, K. S. Cowell and A. K. Rappé, *J. Am. Chem. Soc.*, 1992, **114**, 10046.
48. A. K. Rappé and K. S. Cowell, *Inorg. Chem.*, 1993, **32**, 3438.
49. P. V. Bernhardt and P. Comba, *Inorg. Chem.*, 1992, **31**, 2638
50. P. W. Wade and R. D. Hancock, *J. Chem Soc. Dalton Trans.*, 1990, 1323.
51. M. G. B. Drew, P. C. Yates, B. P. Murphy, J. Nelson and S. M. Nelson, *Inorg. Chim. Acta.*, 1986, **118**, 37.
52. J. Sabolovic and N. Raos, *Polyhedron*, 1990, **9**, 2419.
53. J. Sabolovic, *Polyhedron*, 1993, **12**, 1107.
54. B. Kaitner, N. Paulic and N. Raos, *J. Coord. Chem.*, 1991, **24**, 291.
55. B. Kaitner, G. Ferguson, N. Paulic and N. Raos, *J. Coord. Chem.*, 1992, **26**, 95.
56. B. Kaitner, G. Ferguson, N. Paulic and N. Raos, *J. Coord. Chem.*, 1992, **26**, 105.
57. P. Comba and M. Zimmer, *Inorg. Chem.*, 1994, **33**, 5368.
58. R. J. Deeth and M. A. Hitchman, *Inorg. Chem.*, 1986, **25**, 1225.
59. P. Comba, T. W. Hambley, M. A. Hitchman and H. Stratemeir, *Inorg. Chem.*, 1995, **34**, 3903.
60. D. Nicholls, *Complexes and First Row Transition Elements*, Macmillan Press, New York, 1983.
61. F. A. Cotton and G.Wilkinson, *Advanced Inorganic Chemistry*, 5th edition, Wiley Interscience, New York, 1988.

Chapter 2

Cellular Ligand Field Stabilisation Energy (CLFSE).

2.1. Introduction

The inclusion of the CLFSE term within a Molecular Mechanics routine and the nature of this term under a variety of coordination numbers and d configurations has been discussed by C. M. Kemp[1]. An introduction to the basic concepts and principles will be given here.

In order to generate a CLFSE, it is necessary to calculate a set of one-electron d orbital energies. Then, multiplication of the occupation of the d orbital, by its energy, determines the CLFSE.

Thus, the CLFSE for a d^n system can be defined as:

$$CLFSE = \sum^{n} \rho(d_i)E(d_i) \qquad (2.1)$$

where $\rho(d_i)$ = the occupation number

$E(d_i)$ = the energy of the orbital d_i

The energy of the d orbitals is calculated using

$$E\Phi = H\Phi \qquad (2.2)$$

where Φ is a basis set of d orbitals

H is a Hamiltonian operator

The Hamiltonian makes use of a ligand field Hamiltonian, H_{LF} where

$$H_{LF} = I.E.R + S.O.C. + V_{LF} \qquad (2.3)$$

Here the inter electron repulsion, I.E.R , is assumed to be zero, as only one electron d orbital energies are being considered; the spin orbit coupling, S.O.C, is of little importance and is thus approximated to zero; and thus the Hamiltonian is dependent solely on the ligand field potential, V_{LF} . This V_{LF} is calculated on the basis of Cellular Ligand Field (CLF) theory.

2.2. Cellular Ligand Field (CLF) theory.

In the CLF model, described by Gerloch et al.[2-4], the space around the metal is divided into spatially discrete 'cells'. The ligand field potential in a 'cell' i.e. the local ligand field potential, is assumed to arise exclusively from the electron density in that cell. Each cell is usually associated with a single metal-ligand bond. Local CLF parameters are defined, $e_\lambda = e_\sigma$, e_π and these are now illustrated (Figures 2.1, and 2.2).

Figure 2.1. Definition of e_σ

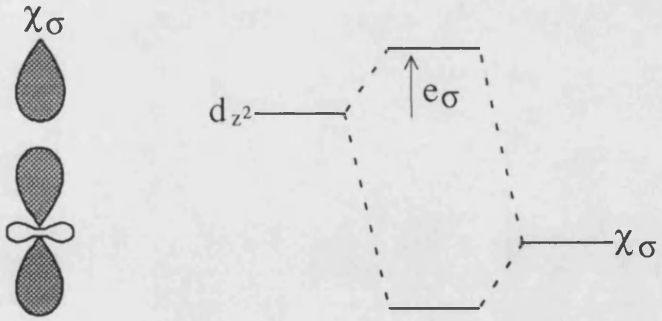

A molecular orbital of σ symmetry, χ_σ, interacts with the d orbital of σ symmetry, resulting in the d orbital being destabilised by the amount e_σ.

Figure 2.2. A definition of e_π for a π donor ligand.

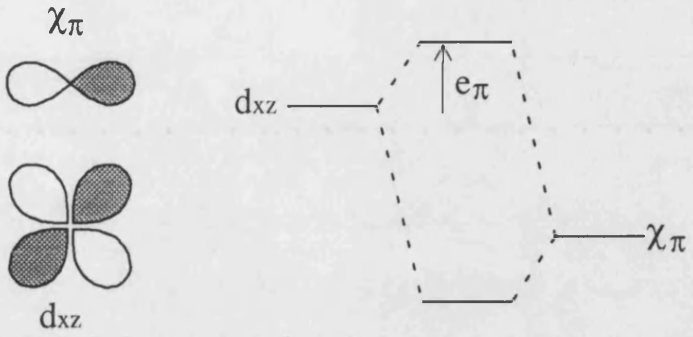

A molecular orbital of π symmetry, χ_π, interacts with the d orbital of π symmetry, resulting in the d orbital being destabilised by the amount e_π.

Figure 2.2 illustrates the situation where e_π is positive. This results when the ligand is a π donor. If the ligand was a π acceptor, then e_π would be negative, as shown in Figure 2.3.

Figure 2.3. The d orbital is stabilised by an amount e_π for π acceptor ligands.

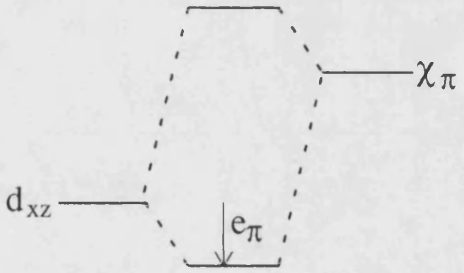

Having chosen the local parameter values and their local directions, it is then assumed that the total perturbation of the d orbital basis is given by transforming the local perturbation into some global frame and then summing over all the contributions to obtain the total global ligand field potential.

The global ligand field potential V_{LF} is now expressed in terms of matrix elements which depend on the molecular geometry and the values of the local e_λ parameters only, as seen in equation 2.4.

$$V_{LF} = \Sigma_i \Sigma_\lambda F_{i\lambda}^2 e_\lambda \qquad (2.4)$$

where $F_{i\lambda}$ is the factor defining the relationship between the local and global axis frame.

Thus, once V_{LF} is calculated the d orbital energies can be determined, and thus the CLFSE may be generated.

2.3. The CLFSE.

In the calculation of the CLFSE, d orbital energies are calculated with reference to a crystal field-like barycentre. This is illustrated in the following example.

Consider a d^1 octahedral complex. The energy levels of the d orbitals are shown in Figure 2.4.

Figure 2.4. Energy levels of d orbitals in a d^1 octahedral complex.

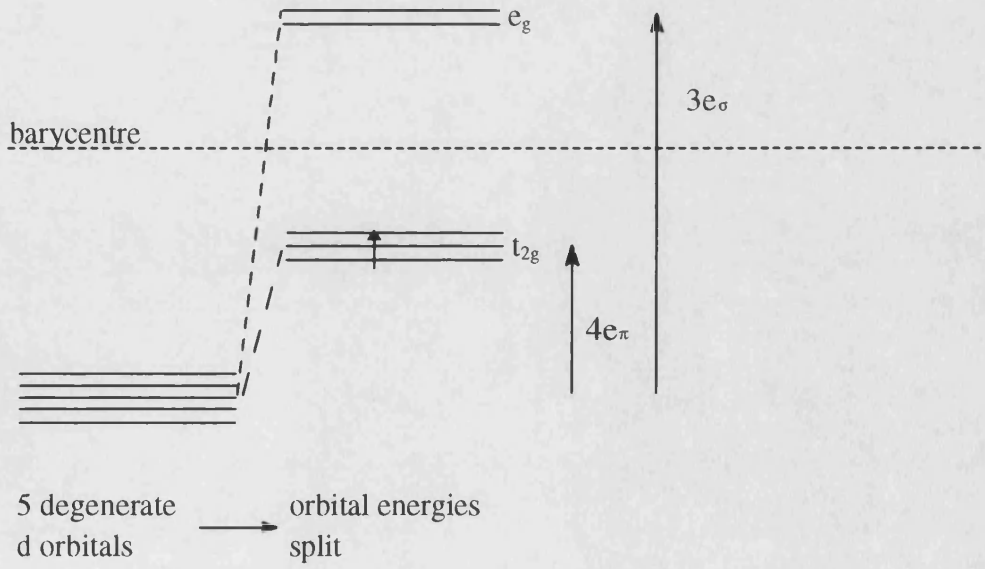

The barycentre (BC) is defined as

$$BC = 1/5\ \Sigma\ (\text{d orbital energies}) \qquad (2.5)$$

The orbital energies can be assigned simply, using CLF theory as,

$$\begin{aligned} E(d_z^2) &= 3e_\sigma \\ E(d_{x^2-y^2}) &= 3e_\sigma \\ E(d_{xz}) &= 4e_\pi \\ E(d_{yz}) &= 4e_\pi \\ E(d_{xy}) &= 4e_\pi \end{aligned}$$

Thus, the BC in this example is given by

$$BC = 1/5(6e_\sigma + 12e_\pi) \qquad (2.6)$$

The CLFSE can then be calculated as

$$\begin{aligned} \text{CLFSE } d^1 &= 1(4e_\pi - BC) + 0(4e_\pi - BC) + 0(4e_\pi - BC) + 0(3e_\sigma - BC) + 0(3e_\sigma - BC) \\ &= 4e_\pi - 1/5(6e_\sigma + 12e_\pi) \\ &= -6/5\ e_\sigma + 8/5\ e_\pi \end{aligned}$$

The CLFSE must be expressed relative to the BC, to ensure that the CLFSE for high spin d^5 and d^{10} configurations is zero.

Therefore, to calculate a CLFSE, a set of d orbital energies must be determined. For this to be achieved, the coordinates of the metal and ligands need to be defined, along with a definition of local axis frame. The CLF parameters, e_λ, need to be assigned. The ligand

field matrix is generated and from the diagonalisation of this matrix, the orbital energies and thus CLFSE can be calculated.

Within the computational scheme, the relevant coordinates are supplied by the energy minimisation routine, the d orbital configuration is predefined, and the CLF parameters, e_λ, (used in the calculation of d orbital energies), are assigned on a parametric basis.

2.4. Parameterisation of e_λ.

The e_λ parameter can be thought of as a measure of charge donation from ligand to metal. Thus, it would seem reasonable to assume that a large charge donation, i.e. large e_λ, would correspond to a shorter bond length. Within the CLF formalism, there is no theoretical justification for a dependence of e_λ upon metal-ligand bond length. However, it would seem feasible that such an empirical relationship would provide a 'first guess' at the value of e_λ for a given metal-ligand interaction at a given bond length. The possibility of a relationship between e_σ and bond length, r, was thoroughly investigated and established by C.M. Kemp[1].

2.5. Conclusion.

In order for the CLFSE to be incorporated in a Molecular Mechanics scheme, it must fit certain criteria:

i) it must be reasonably simple so as not to excessively increase the computational time required for the calculation
ii) it must be independent of assumptions concerning the coordination number and geometry

The CLF model fits these criteria and provides an excellent basis for the calculation of CLFSEs in a Molecular Mechanics routine.

C. M. Kemp[1] first used the CLFSE/MM strategy to model transition metal complexes. However, a transferable force field was not obtained. Subsequent chapters will now describe the implementation of a transferable force field for a variety of Ni(II), Cu(II), Co(III) and Pt(II) systems using the CLFSE/MM method,

2.6. References.

1. C. M. Kemp, *'The Cellular Ligand Field Stabilisation Energy, A New Term for Modelling Open Shell Transition Metals'*, PhD Thesis, University of Bath, 1993.
2. M. Gerloch, J. H. Harding and R. G. Woolley, *Struct. Bonding (Berlin)*, 1981, **46**, 1.
3. M. Gerloch and R. G. Woolley, *Prog, Inorg. Chem.*, 1983, **31**, 371.
4. M. Gerloch, *'Magnetism and Ligand Field Analysis'*, Cambridge University Press, New York, 1983.

Chapter 3

Molecular Modelling of Ni(II) Amine complexes.

3.1. Introduction.

Ni(II) complexes have been widely studied using Molecular Mechanics[1-5], particularly in metal ion size-based selectivity studies[6], elucidation of stability between five- and six-membered chelate rings[7], chelate effects[8] and conformational analysis[9,10]. In all of these studies both four- and six-coordinate complexes have been studied. For the Ni(II) amines, the four-coordinate species are planar and diamagnetic while the six-coordinate structures are octahedral and paramagnetic. However, in modelling these structures, different force fields have been required for both the high and low spin systems, since the Ni-L distances are much shorter in the planar complexes than in the octahedral species. For example, for amine systems, the equilibrium Ni-N distance for a low spin complex is ≈ 1.92 Å, while for high spin species, the Ni-N equilibrium distance is ≈ 2.12 Å. The aim of this investigation is to show that by using a CLFSE/MM treatment, both high and low spin geometries can be accurately modelled using a single force field.

3.2. Theory.

The general form of the CLFSE/MM method is,

$$E_{tot} = E_{str} + E_{bend} + E_{tors} + E_{vdw} + CLFSE \qquad (3.1).$$

These terms refer to the bond stretch, angle bend, torsional, non bonding and CLFSE interactions respectively. These terms, which make up the force field, are constructed from mathematical expressions which, combined, can be used to determine the molecular structures.

These functions used in this study are described in equations 3.2 - 3.6.

$$E_{str} = D_0[1-e^{-\alpha(r-r_0)}]^2-D_0 \qquad (3.2)$$

$$E_{bend} = (1/2)k_\theta (\theta - \theta_0)^2 \qquad (3.3)$$

$$E_{tors} = K[1+S(\cos n\omega)] \qquad (3.4)$$

$$E_{vdw} = \varepsilon[2(r^*/r)^9-3(r^*/r)^6] \qquad (3.5)$$

$$CLFSE = \Sigma p(d_i)E(d_i) \qquad (3.6)$$

Here, equations 3.2, 3.3 and 3.6 have been defined in previous chapters, K is the force constant for ω, the torsion angle, S is the sign to be applied to the cosine function, n is the periodicity, r* is the van der Waals radius and ε is the depth of the potential well.

3.3. Parameterisation of the CLFSE.

As described in chapter 2, the CLFSE is computed from the d orbital energies, which, in turn, are related to the Cellular Ligand Field (CLF) parameters, e_λ. In the complexes studied here, Ni(II) amines, the ligands are simple σ-bonding only ligands, so the d orbital energies will depend solely on e_σ.

In the parameterisation of the CLFSE term, an expression relating the M-L bond length, r, to the CLF parameter value is required. C. M. Kemp[11] looked at the correlation of e_σ with r for a variety of transition metal species including Co(II), Ni(II) and Cu(II) complexes. Here it was implied that the CLF parameter, e_σ, should display a $1/r^5$ dependence. However, work by Bertini et al.[12], Bencini et al.[13] and Lever et al.[14], investigating e_σ values of Ni(II) complexes, suggested that, over the range of about 2.0 to 2.3 Å, e_σ varies linearly with bond length. Accordingly, the expression for e_σ as a function of Ni-N bond length, r, is given in equation 3.7.

$$e_\sigma = 21629 - 8235r \qquad (3.7)$$

The fit between empirical e_σ values and this straight line is shown in Figure 3.1.

Figure 3.1. Graph of e_σ vs M-L bond length.

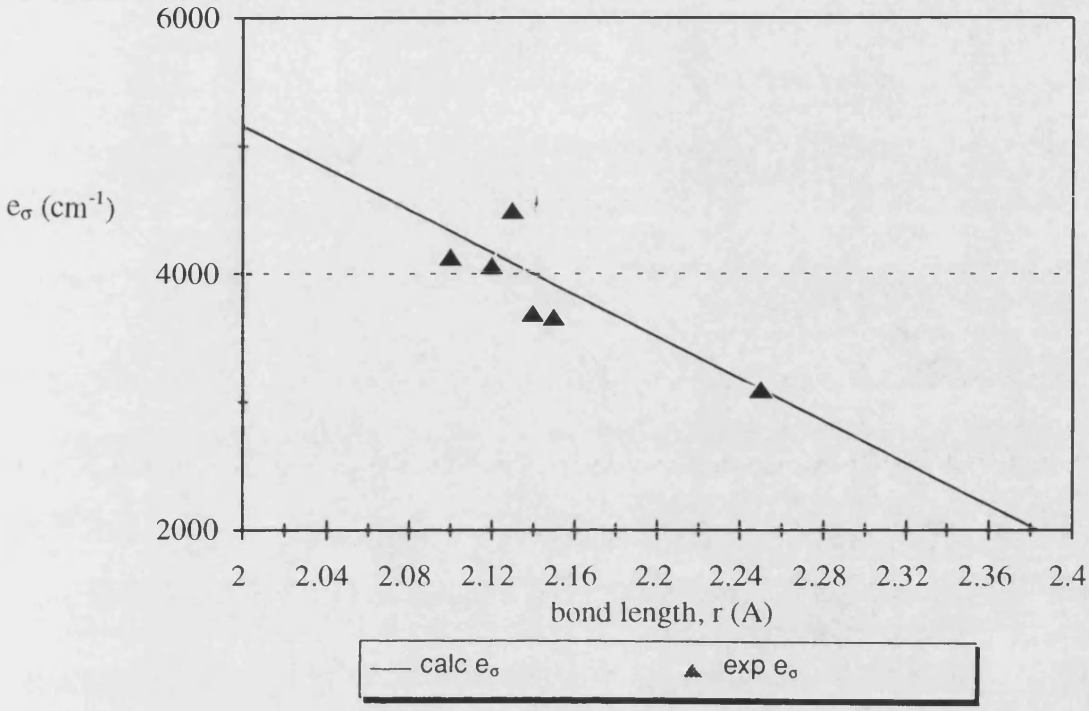

Thus, calculation of e_σ from the chosen functional form, along with the metal configuration and the atomic coordinates, allows the CLFSE to be calculated for a given species.

3.4. Parameterisation of E_{str}.

The metal-ligand bond length is dependent on both the E_{str} and the CLFSE term. This can be illustrated by the following.

Consider a hypothetical Ni(II) high spin complex NiN_6. If only the sigma bonding is taken into account then the d orbital splitting for the octahedral complex is shown in Figure 3.2 overleaf.

Figure 3.2. Schematic diagram of d orbitals in NiN_6.

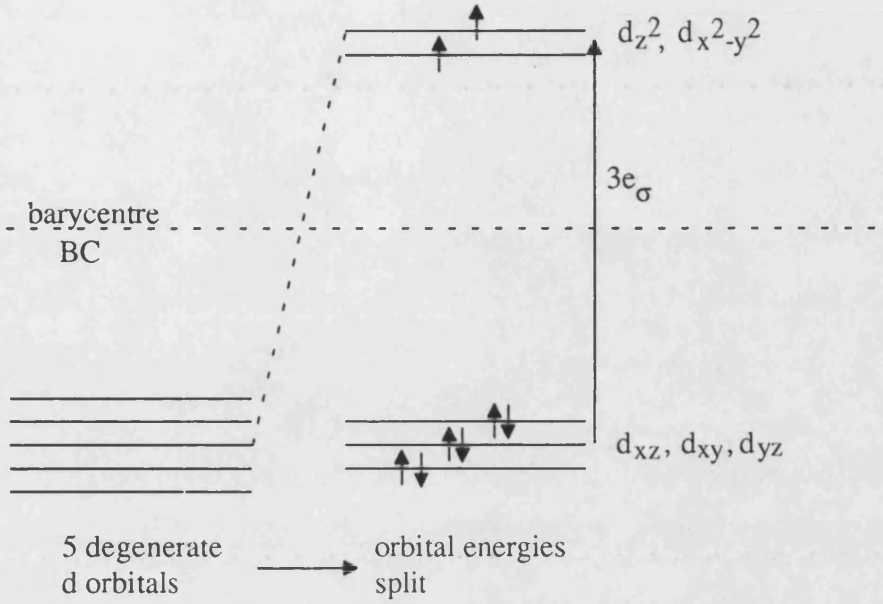

The barycentre, (BC) as defined in chapter 2 is given in equation 3.8.

$$BC = 1/5 \Sigma E(d_i) \qquad (3.8)$$

Thus, for NiN_6,

$$BC = 1/5 (6e_\sigma) \qquad (3.9)$$

The CLFSE must be expressed relative to this barycentre, thus, for a d^8 high spin system the CLFSE is given by,

$$\begin{aligned} CLFSE &= 2[E(d_{xy}) - BC] + 2[E(d_{xz}) - BC] + 2[E(d_{yz}) - BC] + 1[E(d_z^2) - BC] \\ &\quad + 1[E(d_{x^2-y^2}) - BC] \\ &= 2(0-6/5e_\sigma) + 2(0-6/5e_\sigma) + 2(0-6/5e_\sigma) + 1(3e_\sigma-6/5e_\sigma) + 1(3e_\sigma-6/5e_\sigma) \\ &= -3.6e_\sigma \end{aligned}$$

Therefore, for a single Ni-N interaction in an octahedral high spin environment the CLFSE is $-0.6e_\sigma$. As the CLFSE depends on e_σ, which depends on bond length, and the E_{str} term (which is a Morse Function in this case) depends on the metal-ligand distance, these can be combined, and the remaining parameters for the E_{str} term can be determined (by a process of trial and error) by fitting the Morse function plus the CLFSE for a hypothetical Ni-N diatomic to the Harmonic functions reported by Hancock[15] for high spin Ni(II)-N species (Figure 3.3).

Figure 3.3.

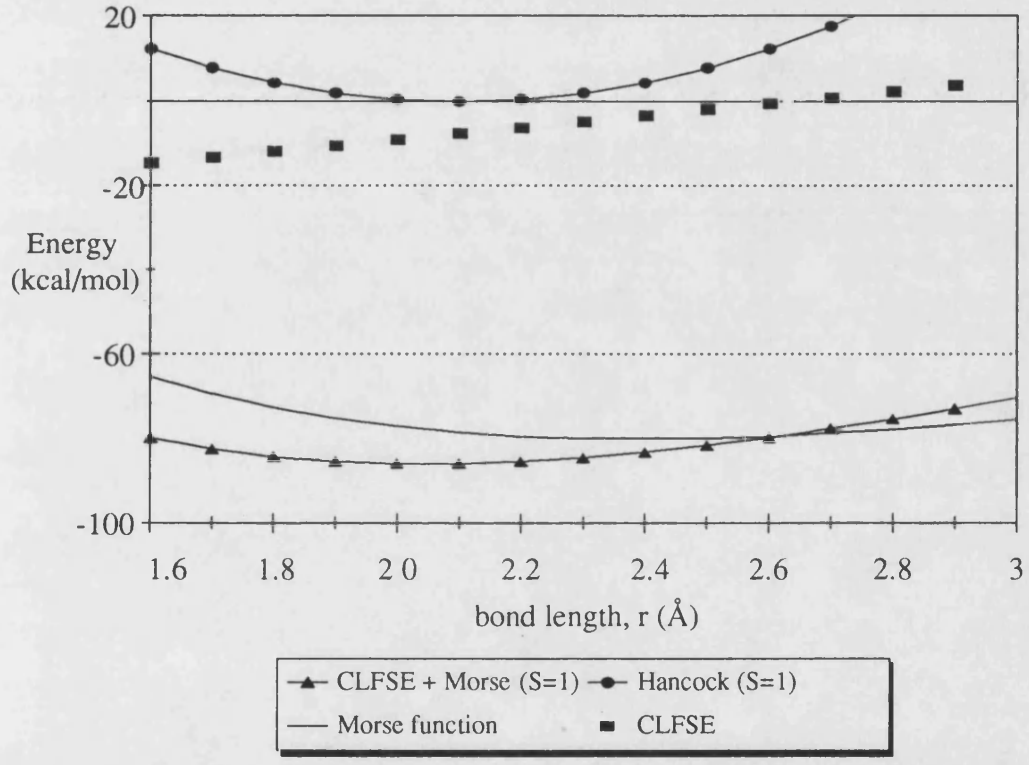

A similar approach can be followed for the low spin 4-coordinate Ni(II) complexes.

Consider a hypothetical NiN_4 low spin species. The d orbitals will split as shown in Figure 3.4 (overleaf).

Figure 3.4. Schematic diagram of d orbitals in NiN_4.

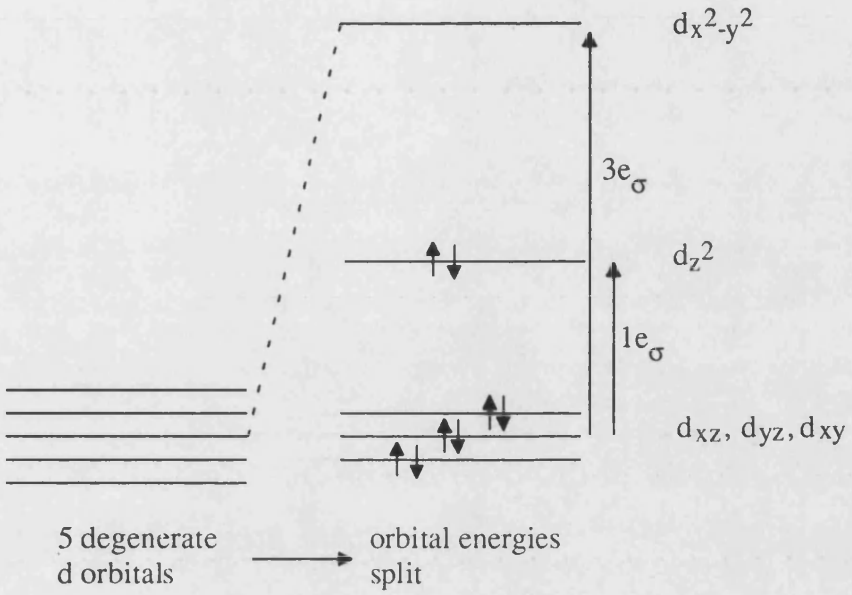

For d^8 low spin

$$BC = 1/5\ (4e_\sigma) \qquad (3.10)$$

Thus, the CLFSE is given by,

$$\begin{aligned} CLFSE &= 2[E(d_{xy}) - BC] + 2[E(d_{xz}) - BC] + 2[E(d_{yz}) - BC] + 2[E(d_z^2) - BC] \\ &\quad + 0[E(d_x^2\text{-}_y^2) - BC] \\ &= 2(0\text{-}4/5e_\sigma) + 2(0\text{-}4/5e_\sigma) + 2(0\text{-}4/5e_\sigma) + 2(1e_\sigma\text{-}4/5e_\sigma) + 0(3e_\sigma\text{-}4/5e_\sigma) \\ &= -4.4e_\sigma \end{aligned}$$

Therefore, for a hypothetical low spin diatomic Ni-N unit, the CLFSE is given by $-1.1e_\sigma$. Again, the remaining Morse function parameters may be determined from a plot of CLFSE and E_{str} vs bond length (Figure 3.5 overleaf).

Figure 3.5.

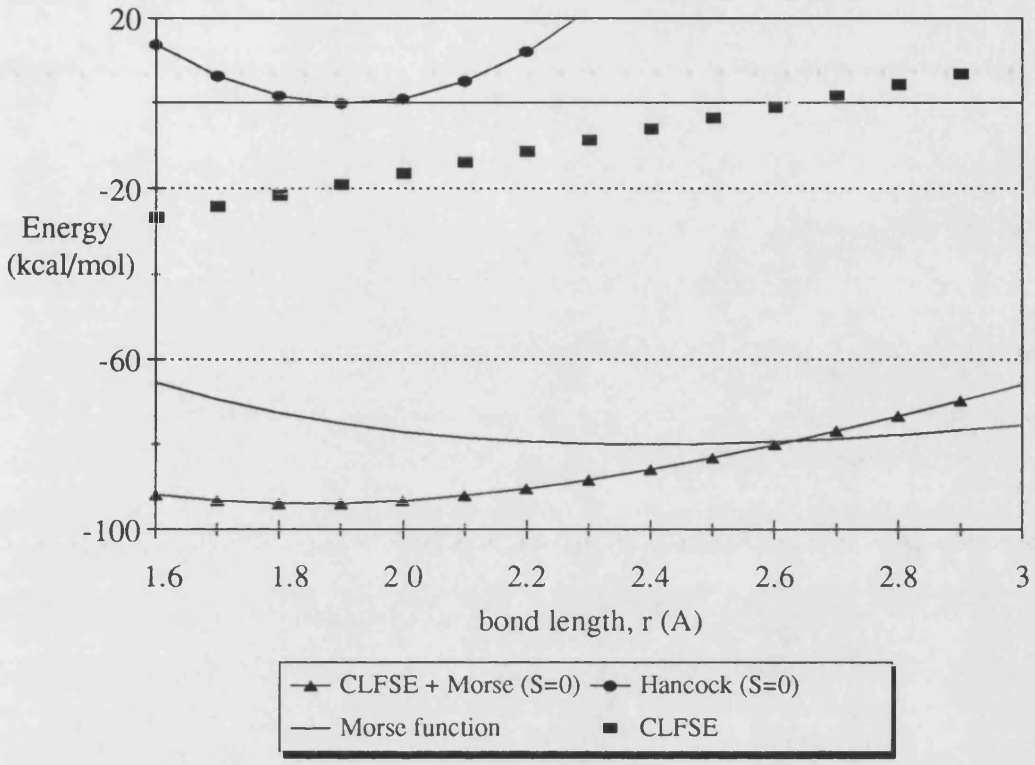

As from a CLFSE viewpoint, the only relevant difference between the high and low spin systems is the difference in d orbital occupation, it was possible to determine a single set of Morse parameters which, when combined with the CLFSE, approximately reproduce the minima of the harmonic functions of both high and low spin complexes.

3.5. Parameterisation of E_{bend}.

The L-M-L angle bend term is not parameterised using the conventional harmonic term. The CLFSE term implicitly contains an L-M-L angle bending contribution. However, certain d configurations have a zero CLFSE (e.g. high spin d^5), thus a general method is required. The 'unique labelling' problem[16] (mentioned in chapter 1) also needs to be avoided. Thus, 1,3 non-bonded interactions were employed. This approach had been successfully implemented in work by Comba[17]. The remainder of the angle bend terms are treated in the conventional way.

3.6. Parameterisation of E_{tors} and E_{vdw}.

The torsional term employed makes use of the normal cosine functions, with parameters involving the metal atom being set to zero. Apart from the 1,3 ligand-ligand terms, van der Waals interactions are only considered for atom pairs separated by more than three bonds.

A full listing of force field parameters used are given in the Appendix.

3.7. Computational Details.

A CLFSE/MM method was incorporated into an in-house MM software package[18], and using this program, the geometries of ten Ni(II) complexes were determined. All the calculations were run on a Dec Alpha 3000. The minimisation routine used a combination of steepest descent and conjugate gradient minimisers. In the calculation of the minimum energy structure, the first derivative of the energy was determined. When this value became less than a specified value of 0.001 then convergence was reached*.

3.8. Results.

The structures of six octahedral high spin and four planar low spin Ni(II) species were studied. All the structures, except $[Ni(NH_3)_6]^{2+}$, were obtained from the Cambridge Structural Database[19] and are displayed schematically in Figure 3.6 and 3.7 and listed in Table 3.1.

* The same minimiser and convergence criteria were used for all the Molecular Mechanics calculations reported in this thesis , unless otherwise specified. The calculations took anywhere between 1 and 90 minutes to run depending on the size of the molecule being studied.

Figure 3.6. High Spin Complexes.

I $[Ni(NH_3)_6]^{2+}$

Ni N H

II $[Ni(en)_3]^{2+}$

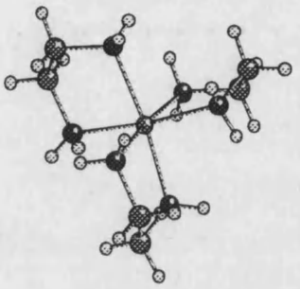

Ni N C H

III $[Ni(tn)_3]^{2+}$

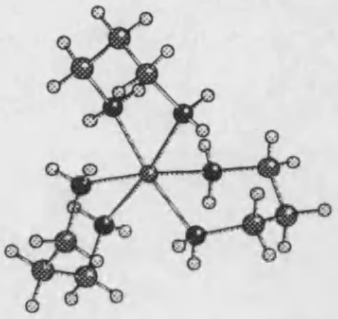

Ni N C H

IV $[Ni(dien)_2]^{2+}$

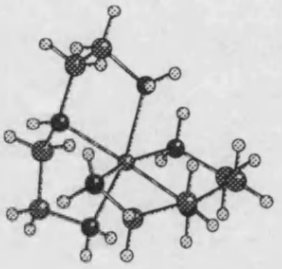

Ni N C H

V $[Ni(dptn)_2]^{2+}$

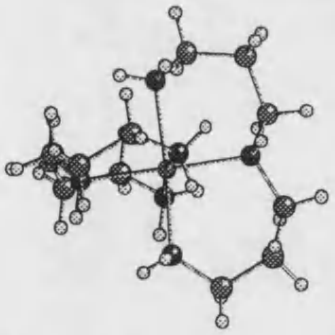

Ni N C H

VI $[Ni(tcn)_2]^{2+}$

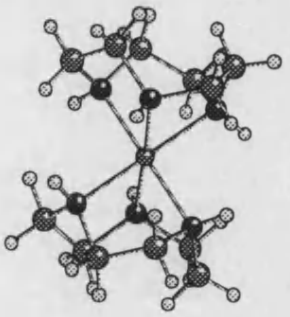

Ni N C H

Figure 3.7. Low Spin complexes.

VII $[Ni(en)_2]^{2+}$ **VIII** $[Ni(tmc)]^{2+}$

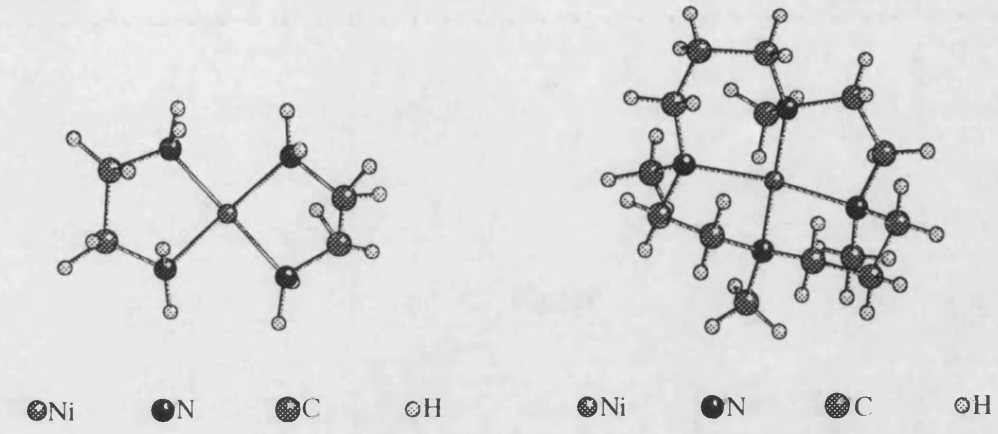

IX $[Ni(meso14ane)]^{2+}$ **X** $[Ni(B\text{-}12\text{-}ane\ N_4)]^{2+}$

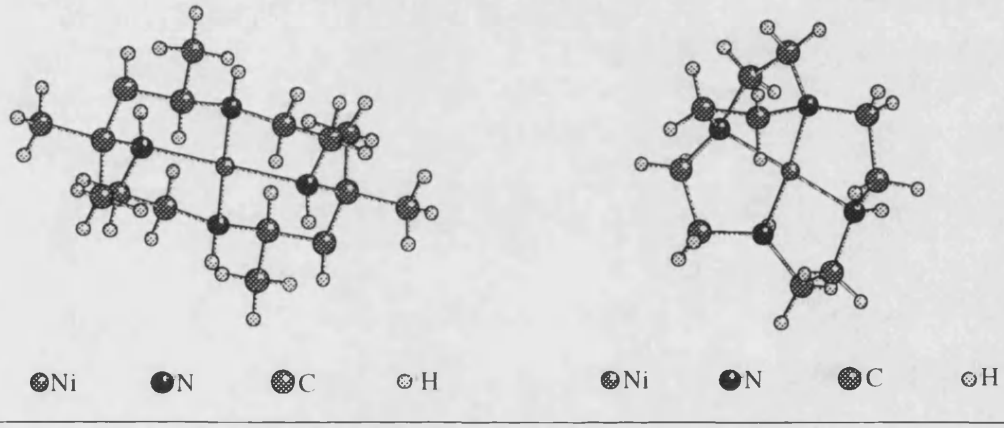

Table 3.1. Chemical Formulae, Full Ligand Name and Cambridge Structural Database Reference Codes for the Molecules shown in Figure 3.6 and 3.7.

Formula		Ligand name	CSD Refcode	Ref
I	$[Ni(NH_3)_6]^{2+}$			20
II	$[Ni(en)_3]^{2+}$	ethylenediamine	ENIACH	21
III	$[Ni(tn)_3]^{2+}$	1,3-diaminopropane	DAMPNI	22
IV	$[Ni(dien)_2]^{2+}$	diethylenetriamine	AEAMNI10	23
V	$[Ni(dptn)_2]^{2+}$	di(3-aminopropyl)amine	AMPRNI10	23
VI	$[Ni(tcn)_2]^{2+}$	1,4,7-triazacyclononane	BAZNNI	24
VII	$[Ni(en)_2]^{2+}$	ethylenediamine	EANBAG01	25
VIII	$[Ni(tmc)]^{2+}$	tetra-*N*-methylcyclam	DITMUO	26
IX	$[Ni(meso14ane)]^{2}$	[7R(S),14S(R)]-5,5,7,12,12,13-hexamethyl-1,4,8,11-tetraazacyclotetradecane	MAZNIA	27
X	$[Ni(B\text{-}12\text{-}ane\ N_4)]^{2+}$	1,4,7,10-tetraazabicyclo[8,2,2]tetradecane	GALZUO	6

3.8.1. High Spin Complexes.

The average observed and calculated bond lengths and angles for the six Ni(II) complexes are given in Table 3.2, and where possible, compared with the results from the conventional MM treatment of Hancock[15].

Table 3.2. Observed and Calculated Bond Lengths (Å) and Angles (°) Describing the Ni(II) Coordination Environment.

	$[Ni(NH_3)_6]^{2+}$ (I)			$[Ni(en)_3]^{2+}$ (II)			$[Ni(tn)_3]^{2+}$ (III)		
	calc	*obs*		calc	*obs*	Han	calc	*obs*	Han
Ni-N (Å)	2.12	*2.13*		2.11	*2.13*	2.12	2.12	*2.15*	2.15
average	90.0	*90.0*		81.1	*81.9*	84.3	85.5	*86.9*	85.1
N-Ni-N(°)	180.0	*180.0*		172.1	*171.8*	*	175.0	*175.8*	*

	$[Ni(dien)_2]^{2+}$ (IV)			$[Ni(dptn)_2]^{2+}$ (V)			$[Ni(tcn)_2]^{2+}$ (VI)		
	calc	*obs*	Han	calc	*obs*	Han	calc	*obs*	Han
Ni-N (Å)	2.04	*2.06*	2.05	2.15	*2.23*	2.20	2.08	*2.11*	2.09
	2.14	*2.15*	2.16	2.06	*2.15*	2.11			
average	81.8	*81.6*	82.9	90.0	*90.4*	91.2	82.0	*82.6*	82.6
N-Ni-N(°)	167.8	*167.3*	*	175.2	*176.4*	*	177.0	*177.1*	*

Individual and average root-mean-square (rms) errors for these parameters are given in the Supplementary Data, Table S3.1.

Overall, the performance of the CLFSE/MM method with respect to the metal coordination environment is at least as good as the conventional MM treatment. The average rms errors in bond lengths and bond angles are only 0.030 Å and 3.066 ° respectively. The worst agreement is for $[Ni(dptn)_2]^{2+}$ (**V**) where the average Ni-N rms error is 0.059 Å and the computed bond lengths are systematically too short by up to 0.09 Å.

* In this case, there was no value given in Hancock's work.

3.8.2. Low Spin Complexes.

The average observed and calculated bond lengths and angles for the four Ni(II) complexes are given in Table 3.3, and where possible, compared with the results from the conventional MM treatment of Hancock[15].

Table 3.3. Observed and Calculated Bond Lengths (Å) and Angles (°) Describing the Ni(II) Coordination Environment.

	$[Ni(en)_2]^{2+}$ (VII)			$[Ni(tmc)]^{2+}$ (VIII)		
	calc	*obs*	Han	calc	*obs*	Han
Ni-N (Å)	1.93	*1.92*	1.92	1.97	*1.98*	1.97
average N-Ni-N(°)	86.8 179.8	*86.4* *180.0*	88.5 180.0	90.6 167.3	*90.6* *168.6*	86.4 166.0

	[Ni(meso14ane)]$^{2+}$ (IX)			[Ni(B-12-aneN_4)]$^{2+}$ (X)		
	calc	*obs*	Han	calc	*obs*	Han
Ni-N (Å)	1.97	*1.96*	1.96	1.84	*1.87*	1.86
average N-Ni-N(°)	90.0 180.0	*90.0* *180.0*	90.0 180.0	89.6 168.8	*89.7* *169.1*	* *

Again, the results obtained from the CLFSE/MM method are at least as good as those calculated by Hancock[15], who used a conventional MM treatment. The average rms errors in bond lengths and bond angles for the Ni(II) coordination environment (displayed in Supplementary Data, Table S3.2), are 0.003 Å and 1.584 ° respectively.

The CLFSE/MM program has proved very successful in the calculation of the Ni(II) coordination sphere. An indication of the method's performance for the rest of the molecule including the Ni-N-C angles and the remaining 'organic' part of the molecule was obtained by computing the rms errors (Supplementary Data, Table S3.3). The 'organic' part is the remaining interactions involving the carbon chains connecting the ligand donor atoms. The interactions with hydrogen are excluded. The average rms error for the Ni-N-C angle is 2.622 ° while the average rms errors for the remaining

* In this case, there was no value given in Hancock's work.

bond lengths and angles (excluding any involving H) are 0.017Å and 1.755° respectively.

3.9. Discussion and Conclusions.

Ni(II) complexes can exhibit a wide variety of coordination numbers, the ones studied here being six- and four-coordinate. The six-coordinate complexes are all high spin and thus octahedral. The four-coordinate complexes studied here were all low spin square planar (however tetrahedral complexes of Ni(II) are known).

It has been suggested[28] that the planar geometries of low spin d^8 complexes can notionally be derived from a Jahn Teller distortion of the octahedral complex. In support of this, a calculation was carried out on a 'bare ligand', low spin, NiN_6 system. It was determined using the CLFSE/MM method that the $Ni\text{-}N_{ax}$ = 2.78 Å and the $Ni\text{-}N_{eq}$ = 1.90 Å. The axial bond length has been lengthened to such an extent, that it is suggested that it would be more energetically feasible for the axial ligands to be lost from the coordination sphere.

The aim of this work was to produce a transferable force field for both the paramagnetic and the diamagnetic systems of Ni(II). The advantage of this is that less parameterisation is needed, but the main advantage is the possible future application of being able to follow systems where the spin states change. As the CLFSE/MM method depends on d orbital occupancy, one could imagine following a spin crossover by progressively mixing the relevant sets of d orbital occupations. This will hopefully form the basis of future work.

By combining the CLFSE and Morse function for a Ni-N interaction, it was possible to elucidate a potential which could approximately reproduce the high and low spin Harmonic potentials in the vicinity of the minima. Thus, a single transferable force field for both the high and low spin systems was produced.

Overall, the agreement with experimental structures for the Ni(II) amine complexes is good. There is a sharp division between paramagnetic octahedral and diamagnetic planar geometries with the Ni-N distance being approximately 0.2 Å shorter for the latter.

The great success of the CLFSE/MM method is that only a single set of force field parameters were required to model both high and low spin systems, in contrast to conventional MM treatments.

3.10. Supplementary Data

Table S3.1. Rms Ni-N and N-Ni-N errors

structure		bond lengths rms difference / (Å)	bond angles rms difference / (°)
$[Ni(NH_3)_6]^{2+}$	I	-----	-----
$[Ni(en)_3]^{2+}$	II	0.002	1.526
$[Ni(tn)_3]^{2+}$	III	0.037	5.404
$[Ni(dien)_2]^{2+}$	IV	0.029	3.145
$[Ni(dptn)_2]^{2+}$	V	0.059	2.732
$[Ni(tcn)_2]^{2+}$	VI	0.025	2.523
average rms error		0.030	3.066

Table S3.2. Rms Ni-N and N-Ni-N errors

structure		bond lengths rms difference / (Å)	bond angles rms difference / (°)
$[Ni(en)_2]^{2+}$	VII	0.000	0.346
$[Ni(tmc)]^{2+}$	VIII	0.002	3.151
$[Ni(meso14ane)]^{2+}$	IX	0.000	0.695
$[Ni(B\text{-}12\text{-}aneN_4)]^{2+}$	X	0.009	2.144
average rms error		0.003	1.584

Table S3.3. Rms errors for rest of molecule (excluding H atoms).

	II	III	IV	V	VI
Metal Ni-N-C rms error (°)	1.908	3.248	1.146	1.682	2.484
'Organic' rms errors					
bond lengths (Å)	0.015	0.017	0.024	0.018	0.006
bond angles (°)	1.580	1.590	2.242	2.631	0.934

	VII	VIII	IX	X
Metal Ni-N-C rms error (°)	1.426	3.263	2.279	6.163
'Organic' rms errors				
bond lengths (Å)	0.017	0.014	0.013	0.027
bond angles (°)	0.800	1.769	1.548	2.700

3.11. References.

1. M. G. B. Drew, N. J. Jutson, P. C. H. Mitchell, R. J. Potter and D. Thompsett, *J. Chem. Soc., Faraday Trans,* 1993, **89**, 3963.
2. K. R. Adam, I. M. Atkinson, M. Antolovich, L. G. Brigden and L. F. Lindoy, *J. Mol. Struct.*, 1994, **323**, 223.
3. O. Q. Munro, J. C. Bradley, R. D. Hancock, H. M. Marques, F. Marsicano and P. W. Wade, *J. Am. Chem. Soc.*, 1992, **114,** 7218.
4. J. A. Shelnutt, C. J. Medforth, M. D. Berber, K. M. Barkigin and K. M. Smith, *J. Am. Chem. Soc.*, 1991, **113**, 4077.
5. K. R. Adam, M. Antolovich, L. G. Brigden and L. F. Lindoy, *J. Am. Chem. Soc.*, 1991, **113**, 3346.
6. R. D. Hancock, S. M. Dobson, A. Evers, P. W. Wade, M. P. Ngwenya, J. C. A. Boeyens and K. P. Wainwright, *J. Am. Chem. Soc.*, 1988, **110**, 2988.
7. G. J. McDougall, R. D. Hancock and J. C. A. Boeyens, *J. Chem. Soc., Dalton Trans,* 1978, 1438.
8. R. D. Hancock, G. J. McDougall and F. Marsicano, *Inorg. Chem.*, 1979, **18**, 2847.
9. M. G. B. Drew, D. A. Rice, S. B. Silong and P. C. Yates, *J. Chem. Soc., Dalton Trans,* 1986, 1081.
10. C. J. Medforth, K. M. Smith, M. Veyrat, M. Mazzanti, R. Ramasseul, J. C. Marchon, T. Takeuchi, W. A. Goddard and J. A. Shelnutt, *J. Am. Chem. Soc.*, 1995, **117**, 11085.
11. C. M. Kemp, *'The Cellular Ligand Field Stabilisation Energy, A New Term for Modelling Open Shell Transition Metal Systems'*, PhD Thesis, 1993.
12. I. Bertini, D. Gatteschi and A. Scozzofava, *Inorg. Chem.*, 1976, **15**, 203.
13. A. Bencini, C. Benelli and D. Gatteschi, *Inorg. Chem.*, 1983, **22**, 470.
14. A. B. P. Lever, I. M. Walker, P. J. McCarthy, K. B. Mertes, A. Jircitano and R. Sheldon, *Inorg. Chem.*, 1983, **22**, 70.
15. R. D. Hancock, *Prog. Inorg. Chem.*, 1989, **37**, 187.
16. V. S. Allured, C. M. Kelly, C. R. Landis, *J. Am. Chem. Soc.*, 1991, **113**, 1.
17. P. Comba, *Coord. Chem. Rev.*, 1993, **123**, 1.
18. In-house MM software was supplied by Dr. D. J. Osguthorpe, Molecular Graphics Unit, University of Bath.
19. Cambridge Structural Database, Version 4. Cambridge Crystallographic Centre, University Chemical Laboratory: Cambridge, 1994.
20. H. U. Hummel and F. Beiler, *Z. Anorg. Allg. Chem.*, 1988, **565**, 147.
21. R. E. Cramer, W. Van Doorne and J. T. Huneke, *Inorg. Chem.*, 1976, **15**, 529.
22. G. D. Andreetti, L. Cavalca and P. Sgarabotto, *Gazz. Chim. Ital.*, 1971, **101**, 494.
23. S. Biagini and M. Cannas, *J. Chem. Soc. (A)*, 1970, 2398.
24. L. J. Aompa and T. N. Margulis, *Inorg. Chim. Acta.*, 1978, **28**, L157.
25. R. Stomberg, *Acta. Chem. Scand.*, 1969, **23**, 3498.
26. T. W. Hambley, *J. Chem. Soc. Dalton Trans.*, 1986, 565.
27. T. Ito and K. Toriumi, *Acta. Cryst.*, 1981, **B37**, 88.
28. R. J. Deeth and M. A. Hitchman, *Inorg. Chem.*, 1986, **25**, 1225.
29. V. J. Burton, R. J. Deeth, C. M. Kemp and P. J. Gilbert, *J. Am. Chem. Soc.*, 1995, **117**, 8407.

Note: The results here are slightly different from those reported previously[29], as a slightly different force field has been used here. A full listing of force field parameters is given in the Appendix.

Chapter 4

Molecular Modelling of Cu(II) Amines.

4.1. Introduction.

The most common coordination numbers of Cu(II) are 4, 5 and 6[1]. The stereochemistry of the 6-coordinate complexes is dominated by the Jahn Teller effects, and tetragonally elongated structures are often observed. At the limit of tetragonal elongation , where the axial ligands are no longer bonded to the metal, a square planar environment is encountered. Four-coordinate complexes can also exhibit tetrahedral geometry, though these can also be subject to Jahn Teller distortions. Five-coordinate complexes can exhibit either trigonal bipyramidal (TBP) or square based pyramidal (SBP) structures, though the square based pyramidal stereochemistry is much more extensive. Some examples of the different geometries of Cu(II) complexes are shown in Table 4.1.

Table 4.1 Stereochemistries of Cu(II) species.

Coordination Number	Geometry	Example	Reference
4	square planar	$[Cu(en)_2]^{2+}$	a
		$[CuCl_4]^{2-}$	b
	distorted tetrahedral	$[CuCl_4]^{2-}$	b
5	TBP	$[Cu(bipy)_2NH_3]^{2+}$	c
	SBP	$[Cu(NH_3)_5]^{2+}$	d
6	distorted octahedral	$[Cu(en)_3]^{2+}$	e

a. V. Vrabel, J. Lokaj and J. Garaj, *Collect. Czech. Chem. Comm.*, 1983, **48**, 2893.
b. D. W. Smith, *Coord. Chem. Rev.*, 1976, **21**, 93.
c. F. S. Stephens, *J. Chem. Soc. Dalton Trans.*, 1972, 1350.
d. M. Sano, T. Maruo, Y. Masuda and H. Yamatara, *Inorg. Chem.*, 1984, **23**, 4466.
e. I. Bertini, P. Dapporto, D. Gatteschi and A. Scozzafava, *J. Chem. Soc. Dalton Trans.*, 1979, 1409.

Note: This chapter considers Cu(II) amine complexes only. All the 4-coordinate Cu(II) amines studied here were square planar, so any discussion , in this chapter, of 4-coordinate structures, will be restricted to the square planar geometry.

4.2. Distorted Octahedral Complexes.

The Jahn Teller theorem[2] states that a system with unevenly filled degenerate orbitals is unstable with respect to a geometric distortion which will remove the degeneracy.

Cu(II), having a d^9 configuration and thus an unevenly filled e_g set, is extremely susceptible to this type of distortion (Figure 4.1).

Figure 4.1. Schematic diagram of energies of Cu(II) d orbitals.

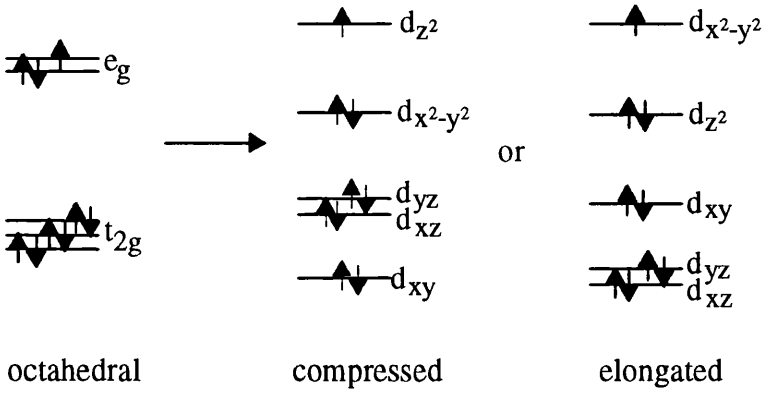

The distortion can be described by vibrational modes[3] Q_θ and Q_ε (Figure 4.2).

Figure 4.2. Two Jahn Teller active modes.

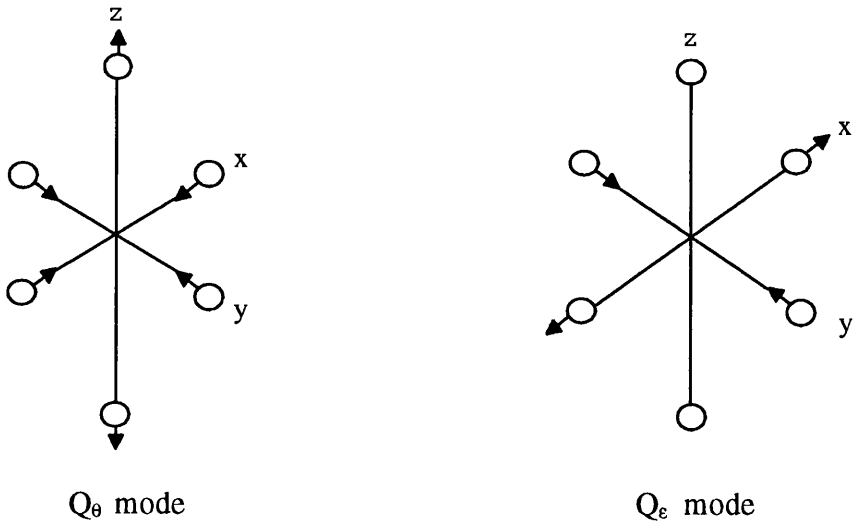

$$Q_\theta = 1/12^{1/2} (\delta x_1 + \delta x_2 + \delta y_3 + \delta y_4 - 2\delta z_5 - 2\delta z_6) \quad (4.1)$$

$$Q_\varepsilon = 1/2 (\delta x_1 + \delta x_2 - \delta y_3 - \delta y_4) \quad (4.2)$$

In Q_θ, if ligands move in by 1 unit and there are 4 ligands moving in, then the other 2 ligands must move out by 2 units each.

The driving force for the Jahn Teller distortion is the lowering of the energy of the complex due to the unequal occupancy of the split components of the e_g orbitals. Opposing this is the natural rise in energy when bonds are stretched or compressed. To a first approximation, this obeys the quadratic relationship of simple harmonic motion, (second term of equation 4.3)

$$U = U_0 + f/2(Q^2) - VQ \quad (4.3)$$

Here U is the total potential energy of the system, Q is the overall nuclear displacement, f is the vibrational stretching force constant, U_0 is the energy of the regular octahedral complex and V is a constant indicating the amount by which the energy is lowered due to the unequal occupancy of the d orbitals.

This can be shown diagramatically (Figure 4.3) by the Mexican hat potential.

Figure 4.3. The Mexican hat potential.

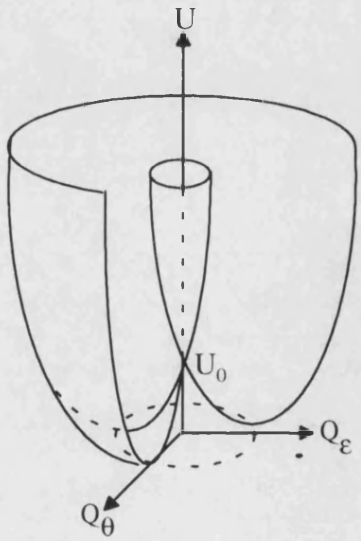

In this approximation a continuous set of energetically distorted structures along the circular valley is predicted, i.e. tetragonal elongation and compression are equally likely to occur.

However, experimentally, elongated geometries are usually observed[4]. It has been recognised that the addition of an anharmonic term to the vibrational potential and the extension of the electronic potential function to second order would destroy the equivalence of the two components, thus warping the Mexican hat potential. This warped potential then favours an elongated structure, agreeing with experiment.

4.3. Five-coordinate Cu(II) complexes.

The Cu(II) ion can form both trigonal bipyramidal (TBP) and square based pyramidal (SBP) structures[5]. As with many 5-coordinate systems, there is a delicate energy balance between the TBP and SBP geometries. A common distortion which takes place is an interconversion between the two stereochemistries (Figure 4.4).

Figure 4.4. Interconversion of TBP and SBP molecules.

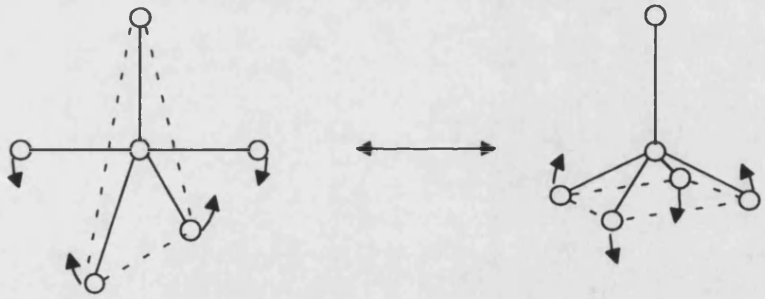

Despite this, the square based pyramidal stereochemistry of Cu(II) is much more frequently observed than the trigonal bipyramidal structure.

4.4. Four-coordinate Cu(II) complexes.

The amine complexes studied all showed square planar geometries. The d orbital energy diagram for these types of complexes can be derived from the octahedral shape by removal of two trans-axial ligands to infinity[6], as seen in Figure 4.5.

Figure 4.5. Distortion of octahedral system

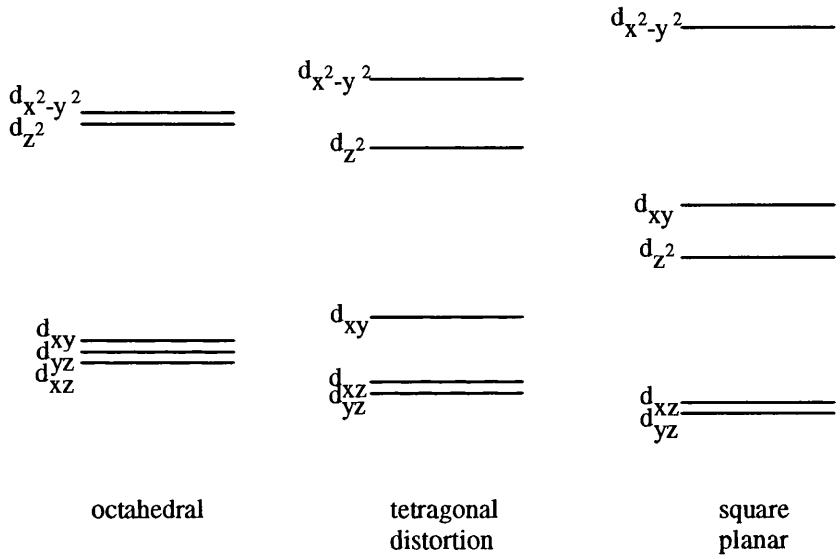

Thus, in this respect, the square planar geometry can be said to be at the limit of tetragonal elongation.

As described above, Cu(II) complexes exhibit a wide variety of stereochemistries. The aim of this study was to demonstrate the versatility of the CLFSE/MM method in being able to model the different structural properties of Cu(II) species using a single force field.

4.5. Theory.

The general form of the CLFSE/MM method is

$$E_{tot} = E_{str} + E_{bend} + E_{tors} + E_{vdw} + CLFSE \qquad (4.4)$$

The terms in equation 4.4 refer to the bond stretch, angle bend, torsional, non bonding and CLFSE interactions respectively, and have been described in chapters 1 and 2.

In order to generate the tetragonal structures exhibited by the 6-coordinate systems, the computational method must be able to account for the ligand field stabilisation which drives these distortions. This is where the CLFSE/MM strategy surpasses other conventional MM treatments[7-10], in that it can automatically generate the elongated geometry of a Jahn Teller active system[†].

Consider a hypothetical 'bare ligand' d^9 system, CuN_6, where N is a σ donor only. The orbital diagram is shown in Figure 4.6.

Figure 4.6.

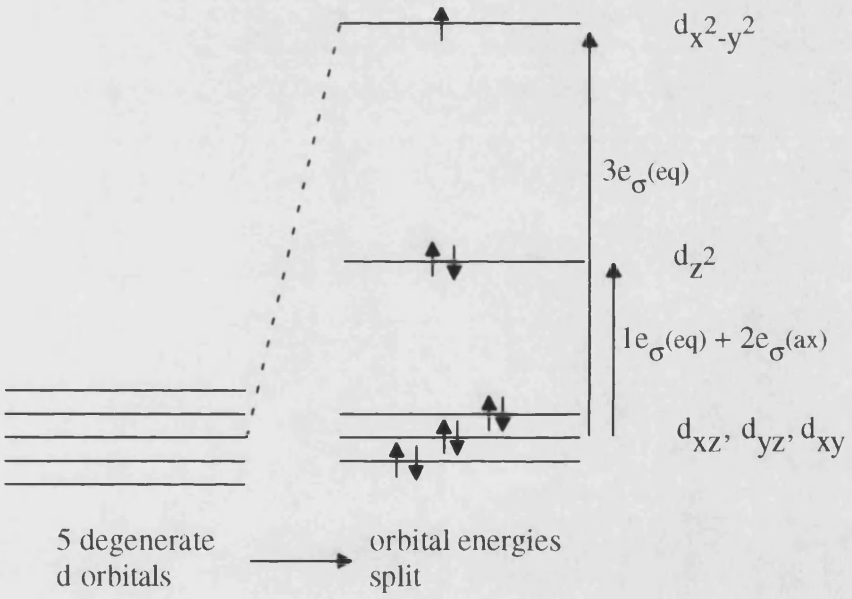

Thus, BC would be given by

$$BC = 1/5\ (4e_\sigma(eq) + 2e_\sigma(ax)) \qquad (4.5)$$

[†] Conventional MM treatments of Cu(II) species have not been discussed in this chapter, as they were thoroughly discussed in chapter 1.

and the CLFSE would then be

$$\begin{aligned}CLFSE &= 2[E(d_{xy}) - BC] + 2[E(d_{xz}) - BC] + 2[E(d_{yz}) - BC] + 2[E(d_z^2) - BC] \\ &\quad + 1[E(d_{x^2-y^2}) - BC]\end{aligned}$$

$$\begin{aligned}&= 2[0-4/5e_\sigma(eq)-2/5e_\sigma(ax)] + 2[0-4/5e_\sigma(eq)-2/5e_\sigma(ax)] + 2[0-4/5e_\sigma(eq)-2/5e_\sigma(ax)] \\ &\quad + 2[1e_\sigma(eq)+2e_\sigma(ax)-4/5e_\sigma(eq)-2/5e_\sigma(ax)] + 1[3e_\sigma(eq)-4/5e_\sigma(eq)-2/5e_\sigma(ax)]\end{aligned}$$

$$= -11/5e_\sigma(eq) + 2/5e_\sigma(ax)$$

So for a single equatorial interaction the CLFSE contribution would be

$$-11/20\ e_\sigma(eq)$$

and for a single axial interaction the CLFSE contribution would be given by

$$+2/10\ e_\sigma(ax)$$

This can be illustrated, as shown in Figure 4.7.

Figure 4.7. Plot of CLFSE+E_{str} Energy vs Bond Length, for CuN_6 System.

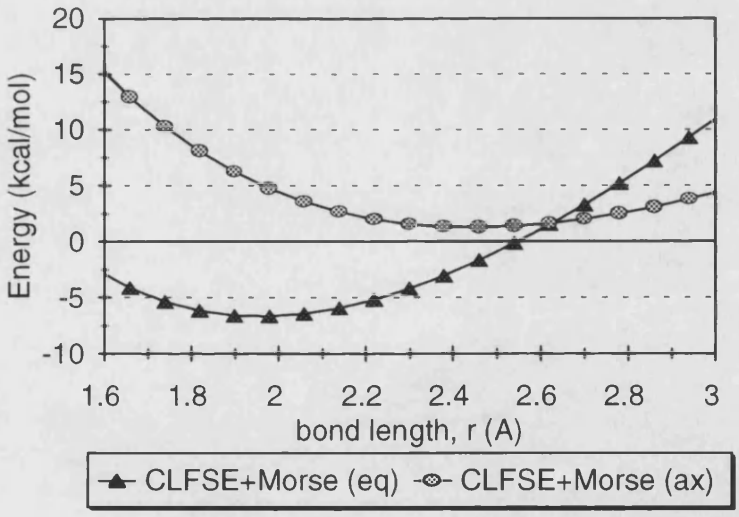

Two minima are exhibited, one for the axial interaction at ≈2.45 Å and the other for the equatorial bond distance at ≈1.96 Å. Thus, the CLFSE term is capable of reproducing the tetragonal elongation of the Jahn Teller active systems.

For the d^9 complexes, a linear function for the e_σ dependence with bond length was chosen. It is recognised that the use of a linear function for the e_σ values of copper complexes is a relatively poor approximation to the empirically observed variation[11]. However, the aim here was to reproduce the structures so that the actual values of the CLF parameters are irrelevant.

4.6. Results and Discussion

The structures of five 6-coordinate, three 5-coordinate and seven 4-coordinate Cu(II) amine species were studied. All the structures, except $[Cu(NH_3)_6]^{2+}$, were obtained from the Cambridge Structural Database[12] and are displayed schematically in Figure 4.8 and listed in Table 4.1.

Figure 4.8. Schematic diagram of Cu(II) complexes studied.

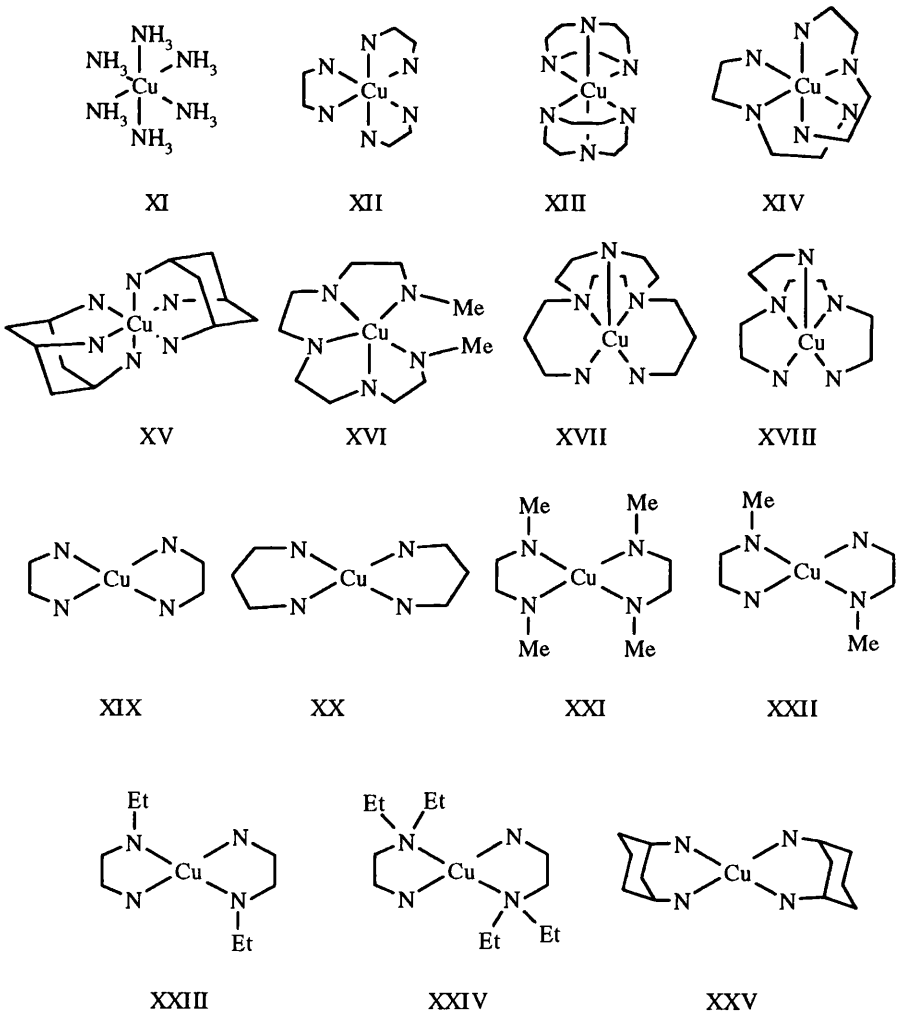

Table 4.1. Chemical Formulae, Full Ligand Names and Cambridge Structural Database Reference Codes for the Molecules shown in Figure 4.8.

	Formula	Ligand Name	Ref Code	Ref
XI	$[Cu(NH_3)_6]^{2+}$	ammine		13
XII	$[Cu(en)_3]^{2+}$	ethylenediamine	CUENCL	14
XIII	$[Cu(tcn)_2]^{2+}$	1,4,7-triazacyclononane	DUSJAC01	15
XIV	$[Cu(dien)_2]^{2+}$	diethylenetriamine	ETACUB	16
XV	$[Cu(tach)_2]^{2+}$	triaminocyclohexane	TACCUP	17
XVI	$[Cu(papd)]^{2+}$	2,5,8,11,14-pentaazapentadecane	LATSII	18
XVII	$[Cu(apt)]^{2+}$	1,4-di(3-aminopropyl)-1,4,7-triazacyclononane	JIBZUP	19
XVIII	$[Cu(adt)]^{2+}$	N,N-bis(2aminoethyl)diethylenetriamine)	TENCUB	20
XIX	$[Cu(en)_2]^{2+}$	ethylenediamine	CEDHAU	21
XX	$[Cu(tn)_2]^{2+}$	1,3-diaminopropane	DAPRCU	22
XXI	$[Cu(dmed)_2]^{2+}$	(N,N-dimethylaminoethyl)amine	DMEDCU	23
XXII	$[Cu(med)_2]^{2+}$	N-methylethylenediamine	CMENOX	24
XXIII	$[Cu(nen)_2]^{2+}$	N-ethylethylenediamine	ETEACU	25
XXIV	$[Cu(deen)_2]^{2+}$	N,N-diethylethylenediamine	CEFBEU	26
XXV	$[Cu(chn)_2]^{2+}$	1,3-diaminocyclohexane	CHXCUA	27

The average calculated and observed bond lengths and angles for the Cu(II) coordination sphere are given in Tables 4.2, 4.3 and 4.4[⊗].

Table 4.2. Observed and Calculated Bond Lengths (Å) and Angles (°) for the 6-coordinate Cu(II) environment.

	$[Cu(NH_3)_6]^{2+}$ (XI)		**$[Cu(en)_3]^{2+}$ (XII)**		**$[Cu(tcn)_2]^{2+}$ (XIII)**	
	calc	*obs*	calc	*obs*	calc	*obs*
Cu-N (Å)	2.48	*2.45*	2.46	*2.49*	2.30	*2.34*
	2.04	*2.15*	2.45	*2.33*	2.28	*2.30*
			2.03	*2.11*	2.14	*2.08*
			1.97	*2.09*	1.96	*2.06*
			2.02	*2.06*	2.12	*2.05*
			1.96	*1.91*	1.96	*2.05*
average	90.0	*90.0*	79.6	*80.7*	80.8	*81.3*
N-Cu-N (°)	180.0	*180.0*	169.8	*168.9*	177.0	*178.2*

	$[Cu(dien)_2]^{2+}$ (XIV)		**$[Cu(tach)_2]^{2+}$ (XV)**	
	calc	*obs*	calc	*obs*
Cu-N (Å)	2.43	*2.46*	2.28	*2.35*
	2.39	*2.35*	2.01	*2.07*
	2.13	*2.13*		
	2.09	*2.07*		
	2.07	*2.04*		
	1.95	*2.03*		
average	80.3	*80.6*	88.9	*87.0*
N-Cu-N (°)	163.6	*166.1*		

[⊗] Calculated values are only compared with those observed values which could be obtained from either the literature or the Cambridge Structural Database.

Table 4.3. Observed and Calculated Bond Lengths (Å) and Angles (°) for the 5-coordinate Cu(II) environment.

	$[Cu(papd)]^{2+}$ (XVI)		**$[Cu(apt)]^{2+}$ (XVII)**		**$[Cu(adt)]^{2+}$ (XVIII)**	
	calc	*obs*	calc	*obs*	calc	*obs*
Cu-N (Å)	1.96	*2.01*	2.03	*2.03*	1.95	*2.01*
	2.01	*2.03*	2.03	*2.06*	2.18	*2.09*
	2.37	*2.16*	2.32	*2.25*	2.39	*2.09*
	2.00	*2.02*	2.08	*2.08*	2.08	*2.04*
	2.13	*2.09*	1.97	*2.03*	2.05	*2.01*
N-Cu-N (°)	85.4	*84.5*	90.6	*90.3*	83.4	*86.4*
	110.9	*104.9*	102.1	*101.6*	108.5	*116.7*
	114.5	*111.8*	78.4	*81.5*	76.6	*83.2*
	169.4	*167.8*	175.4	*172.9*	130.9	*128.3*
	86.4	*85.1*	85.6	*86.3*	81.9	*86.2*
	78.7	*84.9*	79.7	*84.0*	113.1	*113.1*
	86.3	*84.4*	92.7	*87.8*	85.6	*84.1*
	141.3	*140.2*	170.1	*173.2*	165.4	*169.6*
	103.8	*108.0*	91.7	*105.2*	116.2	*105.0*
	96.0	*99.6*	91.5	*94.9*	98.1	*96.3*

Table 4.4. Observed and Calculated Bond Lengths (Å) and Angles (°) for the 4-coordinate Cu(II) environment.

	$[Cu(en)_2]^{2+}$ (XIX)		**$[Cu(tn)_2]^{2+}$ (XX)**		**$[Cu(dmed)_2]^{2+}$ (XXI)**		**$[Cu(med)_2]^{2+}$ (XXII)**	
	calc	*obs*	calc	*obs*	calc	*obs*	calc	*obs*
Cu-N (Å)	2.03	*2.02*	2.01	*2.04*	2.05	*2.06*	2.00	*2.01*
							2.04	*2.06*
average	84.3	*84.1*	86.9	*86.7*	84.9	*85.3*	85.3	*85.9*
N-Cu-N (°)	180.0	*180.0*	180.0	*180.0*	169.2	*180.0*	180.0	*180.0*

	$[Cu(nen)_2]^{2+}$ (XXIII)		**$[Cu(deen)_2]^{2+}$ (XXIV)**		**$[Cu(chn)_2]^{2+}$ (XXV)**	
	calc	*obs*	calc	*obs*	calc	*obs*
Cu-N (Å)	2.00	*2.01*	1.96	*2.01*	1.99	*2.02*
	2.04	*2.03*	2.08	*2.08*		
average	85.3	*85.0*	85.8	*84.9*	86.3	*87.6*
N-Cu-N (°)	180.0	*180.0*	180.0	*180.0*	180.0	*180.0*

Before discussing the results, the experimental structures to which the computed structures are compared must be considered.

Copper(II) complexes are notoriously 'plastic'[28]. This means that a range of structures are possible which have similar energies and the final 'observed' solid-state structure

may depend critically on relatively subtle crystal packing forces. As an example, consider TBP and SBP coordination.

In TBP symmetry the d^9 copper systems exhibit two short axial contacts and three medium equatorial distances. Whereas, the SBP symmetry yields four short equatorial bonds and a quite long apical contact[29]. The CLFSE/MM calculations reflect this behaviour for a hypothetical CuN_5 system. For the TBP structure, the optimised axial and equatorial distances are 1.88 Å and 2.28 Å respectively, while the SBP system has an apical distance of 2.48 Å and equatorial distances of 2.01 Å. The energies of the two isomers are very similar, the C_{4v} system being 2 kcal/mol lower in energy.

Experimentally, five-coordinate Cu(II) species frequently display intermediate and variable structures[30]. If the metal coordination environment is fixed at that observed crystallographically, and the ligand is minimised, then an estimate of the strain energy difference between the 'in crystal' and 'in vacuo' structures can be obtained. The 'in crystal' energy is, as expected, slightly higher but only by 1.4 kcal/mol for $[Cu(papd)]^{2+}$ (**XVI**), 2.8 kcal/mol for $[Cu(apt)]^{2+}$ (**XVII**) and 2.4 kcal/mol for $[Cu(adt)]^{2+}$ (**XVIII**). Thus, the calculated structures may not be in excellent agreement with the observed structures but this is not energetically significant. The surrounding lattice has some effect on the structure of the molecule, so unless these are explicitly included in the calculation, one can not expect to get exact agreement with the solid state structures. The extension of the CLFSE/MM model to simulate the crystal packing forces is beyond the scope of this thesis, but, no doubt, will form the basis of future work.

The 6-coordinate complexes are also sensitive to lattice effects. For example, $[Cu(tach)_2]^{2+}$ (**XV**) with ClO_4^- counterions yields a typical elongated geometry ($Cu\text{-}N_{(ax)}$ = 2.353 Å, $Cu\text{-}N_{(eq)}$ = 2.071 Å)[17] while the nitrate salt has virtually equal Cu-N contacts ($Cu\text{-}N_{(ax)}$ = 2.173 Å, $Cu\text{-}N_{(eq)}$ = 2.164 Å)[17]. This latter structure is an artefact of the X-ray diffraction experiment as the d-d spectra of both salts are essentially identical.

Dynamic Jahn Teller effects could also play a large role in the structure of a 6-coordinate d^9 system. Different structures may be observed where the molecule may occupy more than one minimum on the warped Mexican Hat potential energy surface[31].

The CuN_6 species studied here all show tetragonal elongation. The solid state structures that they are compared with, are ones which show the largest tetragonal distortion (Table 4.2).

Four-coordinate complexes are less plastic being at the limit of tetragonal elongation, and are easier to model, (as shown by the number of other Molecular Mechanics applications[32-36]). However, lattice effects can still influence the observed geometry. For example, the conformations of the cyclohexane ring in $[Cu(chn)_2]^{2+}$ (XXV)[28] induce a 6° variation of the ligand bite angle from about 93° for the nitrate salt to 87° for the bromide compound (Figure 4.9).

Figure 4.9. Molecular structures from X-ray structural analyses of two forms of $[Cu(chn)_2]^{2+}$ showing the variation of the N-Cu-N bite angle.

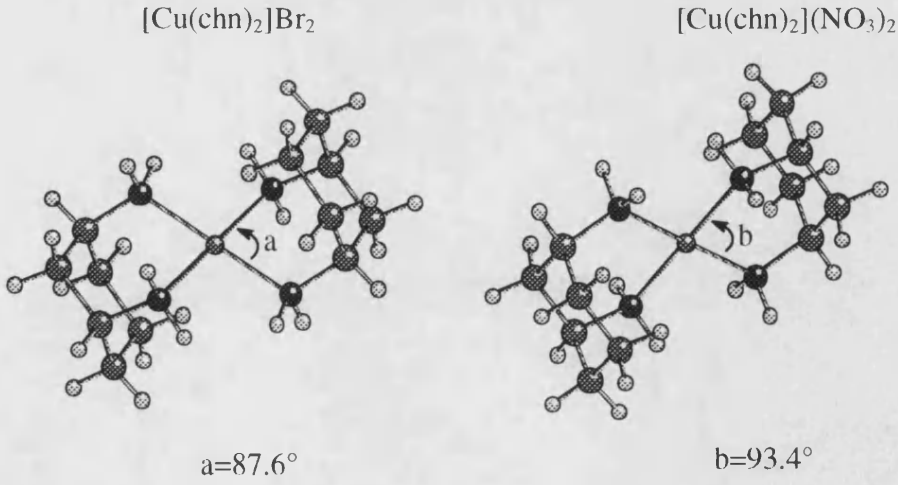

Overall, therefore, care is required when making comparisons between computed and 'observed' structures.

Despite the 'flexibility' of the Cu(II) systems, the CLFSE/MM approach still provides satisfactory structures (Tables 4.2, 4.3 and 4.4). A full table of rms errors is given in the Supplementary Data, Tables S4.1 and S4.2.

All the four-coordinate complexes resemble the experimental structures to a high degree of accuracy, the worst case being for $[Cu(deen)_2]^{2+}$ (**XXIV**) where the Cu-N distance for the unsubstituted nitrogen is underestimated by 0.05 Å. However, all the other Cu-N distances are in excellent agreement, the maximum deviation being only 0.03 Å.

A mixed performance is shown by the 5-coordinate complexes, ranging from reasonable for $[Cu(apt)_2]^{2+}$ (**XVII**) to apparently quite poor for $[Cu(adt)_2]^{2+}$ (**XVIII**) and $[Cu(papd)_2]^{2+}$ (**XVI**). This apparently poor agreement between theory and experiment is attributed to the subtle, yet critical, effects of crystal packing.

The six-coordinate species are relatively well treated and all exhibit tetragonal elongation. Given the large experimental errors associated with $[Cu(NH_3)_6]^{2+}$ (**XI**) and the apparent uncertainty regarding its existence[37], the data in Table 5.2 should be considered as illustrative. The other computed complexes are rather more symmetrical than the experimental data. For example, the $Cu\text{-}N_{(ax)}$ distances in $[Cu(en)_3]^{2+}$ (**XII**) are calculated to be almost identical at 2.46 Å and 2.45 Å, while the observed values differ by 0.16 Å. Packing forces could be attributed to this, or, alternatively, the 'observed' solid state structure may represent contributions from more than one minimum of the Mexican hat potential energy surface.

4.7. Conclusion

The complexes of Cu(II) are probably the hardest to determine using conventional Molecular Mechanics, the distorted geometries often requiring external constraints to force the molecule along a particular coordinate.

The CLFSE/MM scheme, however, appears to be the first general empirical method for modelling a variety of Cu(II) geometries, and thus represents a significant advance in Molecular Mechanics methodology.

The calculated 4-coordinate complexes are in excellent agreement with experiment. The pentacoordinated systems are apparently poorly treated. However, this reflects the high 'flexibility' of systems of this type. It was also shown that even though the structural agreement is poor, the difference between the 'in crystal' and 'in vacuo' structures did not differ energetically by more than 2.8 kcal/mol. Thus, this reflects the delicate energy balance between the different geometries of the five coordinate complexes.

The CLFSE/MM method is the first Molecular Mechanics strategy to be able to reproduce the stereochemical activity of the d electrons. For example, consider the energy levels of the d orbitals in Cu(II) five-coordinate systems.

Figure 4.10. Illustration of d orbital energies of Cu(II) five-coordinate systems.

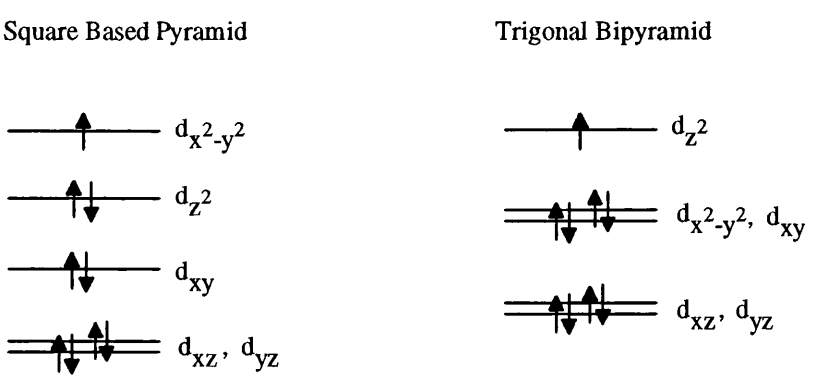

In the square based pyramid, there is a 'hole' in the $d_{x^2-y^2}$ orbital. This results in the ligands which interact directly with this orbital, i.e. the equatorial ligands, being pulled in towards the metal. Whereas, in the trigonal bipyramid, the 'hole' being in the d_{z^2} orbital, results in the axial ligands being compressed. This is reflected in the calculations on the 'bare ligand' systems, CuN_5. Here the trigonal bipyramidal structure gives compressed axial distances of 1.88 Å , while the equatorial distance is

2.28 Å, while the square based pyramid gave an apical distance of 2.48 Å and equatorial distances of 2.01 Å.

Using the CLFSE/MM strategy, Jahn Teller effects of the 6-coordinate complexes are automatically generated. These results suggest a possible future application of the CLFSE/MM approach, being used to study static versus dynamic Jahn Teller effects in distorted systems. To do this, the crystal lattice effects would need to be included. The energy of an elongated and compressed geometry would need to be determined, and then the energy difference between the two would then be related to whether or not a static or dynamic influence would occur.

Note: The results in this chapter differ slightly from results previously reported[38]. This is because a new force field to that previously reported has been used. A full listing of the force field is given in the Appendix.

4.8. Supplementary Data *

Table S4.1. Rms Cu-N and N-Cu-N errors

structure		bond lengths rms difference / (Å)	bond angles rms difference / (°)
$[Cu(NH_3)_6]^{2+}$	XI	-----	-----
$[Cu(en)_3]^{2+}$	XII	0.079	4.694
$[Cu(tcn)_2]^{2+}$	XIII	0.068	1.851
$[Cu(dien)_2]^{2+}$	XIV	0.041	4.393
$[Cu(tach)_2]^{2+}$	XV	0.065	-----
$[Cu(papd)]^{2+}$	XVI	0.100	4.292
$[Cu(apt)]^{2+}$	XVII	0.043	5.120
$[Cu(adt)]^{2+}$	XVIII	0.145	5.419
$[Cu(en)_2]^{2+}$	XIX	0.002	0.163
$[Cu(tn)_2]^{2+}$	XX	0.032	3.696
$[Cu(dmed)_2]^{2+}$	XXI	0.000	6.307
$[Cu(med)_2]^{2+}$	XXII	0.016	0.492
$[Cu(nen)_2]^{2+}$	XXIII	0.000	0.245
$[Cu(deen)_2]^{2+}$	XXIV	0.035	0.736
$[Cu(chn)_2]^{2+}$	XXV	0.032	0.980
average rms error		0.047	2.953

Table S4.2. Rms errors for rest of molecule (excluding H atoms).

	XII	XIII	XIV	XV	XVI
Metal Cu-N-C rms error (°)	6.279	3.760	3.525	4.639	2.661
'Organic' rms errors					
bond lengths (Å)	-----	0.016	0.014	-----	0.017
bond angles (°)	-----	2.449	2.165	-----	1.649

	XVII	XVIII	XIX	XX	XXI
Metal Cu-N-C rms error (°)	2.715	2.304	1.436	1.098	2.968
'Organic' rms errors					
bond lengths (Å)	0.025	0.034	0.057	0.008	0.011
bond angles (°)	2.813	3.489	1.956	0.339	2.153

	XXII	XXIII	XXIV	XXV
Metal Cu-N-C rms error (°)	1.034	2.350	4.022	3.353
'Organic' rms errors				
bond lengths (Å)	0.012	0.016	0.019	0.014
bond angles (°)	2.016	2.309	1.331	1.755

* Vacancies in the tables occur due to insufficient experimental data being available.

4.9. References.

1. F. A. Cotton and G. Wilkinson, *'Advanced Inorganic Chemisty'* 4th edition, John Wiley and Sons, 1980.
2. I. B. Bersuker, *'The Jahn Teller Effect and Vibronic Interactions in Modern Chemistry'*, Plenum Press, 1983.
3. R. J. Deeth and M. A. Hitchman, *Inorg. Chem.*, 1986, **25**, 1225.
4. J. H. Ammeter, H. B. Burgi, E. Gamp, V. Meyer-Sandrin and W. P, Jenson, *Inorg. Chem.*, 1979, **18**, 733.
5. B. J. Hathaway and D. E. Billing, *Coord. Chem. Rev.*, 1970, **5**, 143.
6. D. Nicholls, *'Complexes and 1st Row Transition Elements'*, Macmillan Education Ltd., 1987.
7. T. N. Doman, T. K. Hollis and B. Bosnich, *J. Am. Chem. Soc.*, 1995, **117**, 1352.
8. J. Gao and L. Shao, *J. Phys. Chem.*, 1994, **98**, 13772.
9. F. Weisemann, S. Teipel, B. Krebs and U. Howler, *Inorg. Chem.*, 1994, **33**, 1891
10. P. Comba, T. W. Hambley and M. Stöhle, *Helv. Chim. Acta.*, 1995, **78**, 2042.
11. R. J. Deeth and M. Gerloch, *Inorg. Chem.*, 1984, **23**, 3846.
12. Cambridge Structural Database, Version 4. Cambridge Crystallographic Data Centre, University Chemical Laboratory, Cambridge, 1994.
13. T. Distler and P. A. Vaughan, *Inorg. Chem.*, 1967, **6**, 126.
14. I. Bertini, P. Dapporto, D. Gatteschi and A. Scozzafava, *J. Chem. Soc. Dalton Trans.*, 1979, 1409.
15. J. H. Ammeter, H. B. Burgi, E. Gamp, V. Meyer-Sandrin and W. P. Jensen, *Inorg. Chem.*, 1979, **18**, 733.
16. P. Chaudhuri, K. Oder, K. Weighardt, J. Weiss, J. Reedijk, W. Hinrichs, J. Wood, A. Ozarowski, H. Stratemaier and D. Reinen, *Inorg. Chem.*, 1986, **25**, 2951.
17. F. S. Stephens, *J. Chem. Soc.*, 1969, 2233.
18. D. G. Fortier and A. M. McAuley, *J. Chem. Soc. Dalton Trans.*, 1991, 101.
19. M. Cannas, A. Cristini and G. Marongiu, *Inorg. Chim. Acta.*, 1976, **19**, 241.
20. T. H. Lu, T. H. Tahirov, C. K. Bin, C. D. Hsaio, Y. L. Liu, J. C. Lee and C. S. Chung, *Acta Cryst. C. (Cr. Str. Comm.)*, 1993, **49**, 1747.
21. V. Vrabel, J. Lokaj and J. Garaj, *Collect. Czech. Chem. Comm.*, 1983, **48**, 2893.
22. A. Pajunen, *Suom. Kemistil B*, 1969, **42**, 15.
23. A. Pajunen, *Suom. Kemistil B*, 1969, **42**, 261.
24. A. Walsh and B. J. Hathaway; *J. Chem. Soc. Dalton Trans.*, 1984, 15.
25. I. Grenthe, P. Paoletti, M. Sandstrom and S. Glikberg, *Inorg. Chem.*, 1979, **18**, 2687.
26. R. Hamalainen, *Suom. Kemistil B*, 1973, **46**, 237.
27. K. Kamisawa, K. Matsumoto, S. Ooi, R. Saito and Y. Kidani, *Bull. Chem. Soc. Jpn.*, 1981, **54**, 1072.
28. J. Gazo, I. B. Bersuker, J. Garaj, M. Kabesova, J. Kohout, H. Langfelferova, M. Melnik, M. Serator and F. Valach, *Coord. Chem. Rev.*, 1976, **19**, 253.
29. R. J. Deeth and M. Gerloch, *Inorg. Chem.*, 1985, **24**, 4490.
30. W. D. Harrison, D. M. Kennedy, M. Power, R. Sheahan and B. J. Hathaway, *J. Chem. Soc., Dalton Trans.*, 1981, 1556.
31. D. Reinen and C. Freibel, *Struct. Bond.* 1979, **37**, 1.
32. T. V. Timofeevan. J. H. Lii and N. L. Allinger, *J. Am. Chem. Soc.*, 1994, **7**, 591.
33. J. Gao, *J. Phys. Chem.*, 1992, **96**, 537.
34. I. H. Hillier, B. Waszkowycz, N. Gensmantel and D. W. Payling, *J. Chem. Soc., Perkin Trans. 2*, 1991, 225.
35. R. V. Stanton, D. S., Hartsough and K. M. Marz Jr., *J. Comp. Chem.*, 1995, **16**, 113.
36. R. D. Hancock, *J. Chem. Soc., Chem. Comm.*, 1996, 1301.
37. See discussion in V. J. Burton and R. J. Deeth, *J. Chem. Soc., Chem. Comm.*, 1995, 573.
38. V. J. Burton, R. J. Deeth, C. M. Kemp and P. J. Gilbert, *J. Am. Chem. Soc.*, 1995, **117**, 8407.

Chapter 5

Molecular Modelling of Mixed Ligand Systems.

5.1. Introduction.

This study describes the extension of the force field for the CLFSE/MM treatment of transition metal complexes, to incorporate potentially π donor ligands. Complexes of Cu(II), Ni(II) and Co(III) with various combinations of σ-bonding amine plus π-bonding imine and chloride ligands have been calculated. As Cl ligands have now been incorporated into the scheme, an obvious complex to investigate would be $[NiCl_4]^{2-}$. This molecule exhibits tetrahedral stereochemistry. Until now, the four-coordinate complexes studied have all been square planar. Thus, a discussion of how the CLFSE treats these two different geometries of the four-coordinate species will be reported.

5.2. Theory.

The general form of the CLFSE/MM method is,

$$E_{tot} = E_{str} + E_{bend} + E_{tors} + E_{vdw} + CLFSE \qquad (5.1)$$

The terms in equation 5.1 refer to the bond stretch, angle bend, torsional, non bonding and CLFSE interactions respectively, and have been described in chapters 1 and 2.

The CLFSE for a d^n system (as defined previously) is given by equation 5.2.

$$CLFSE = \sum_{n} \rho(d_i)E(d_i) \qquad (5.2)$$

where $\rho(d_i)$ = the occupation number

$E(d_i)$ = the energy of the orbital d_i

The d orbital energies are expressed in terms of the Cellular Ligand Field (CLF) parameters e_λ (where $\lambda = \sigma$, πx or πy)[1,2] which are in turn expressed as a function of the M-L distance, r. For simple σ-bonding-only ligands like amines ($e_{\pi x} = e_{\pi y} = 0$), a linear dependence of e_σ vs r was chosen (equation 5.3).

$$e_\sigma = a_0 + a_1 r \qquad (5.3)$$

In equation 5.3, a_0 and a_1 are empirically derived constants and the resulting values for e_σ are not required to reproduce the d-d spectrum. Similar expressions can be used for e_π.

5.2.1. Modelling π-bonding ligands.

Consider an octahedral complex ML_6, where L is a σ bonding only ligand. The ligand field splitting parameter 10Dq or Δ_{oct} is given by:

$$\Delta_{oct} = 3e_\sigma \qquad (5.4)$$

If L was in fact a π bonding ligand also then Δ_{oct} would be given by

$$\Delta_{oct} = 3e_\sigma + 4e_\pi \qquad (5.5)$$

Depending on whether the ligand was a π donor or a π acceptor determines whether e_π is positive or negative and whether Δ_{oct} decreases or increases relative to solely σ donor ligands. Likewise, the stabilisation energy is either decreased or increased with respect to σ donor only ligands.

However, when considering the CLFSE alone, it is required that shortening and strengthening a given M-L bond should be energetically favourable - i.e. be associated with an increasingly negative CLFSE. Such is the case for σ bonding. However, since the π-symmetry d orbitals are lower in energy than the global barycentre, increasing e_π

pushes the d_π orbitals up which tends to reduce the magnitude of the CLFSE. Of course, the values of a_0 and a_1 in equation 5.3 could be adjusted such that e_σ changes fast enough to counteract the increase in e_π but, given the empirical nature of MM, this is an unnecessary complication and no bond length dependence is required for e_π.

Setting a_1 to zero for π interactions gives fixed e_π values. Thus, the e_π values can still contribute to the L-M-L angle bending as well as to the torsional potential for rotations about the M-L bond, providing, in the latter case, that $e_{\pi x} \neq e_{\pi y}$.

The contribution to the torsional potential will be discussed now, and the contribution to the angle bend will be discussed later, in section 5.2.1.2.

5.2.1.1. e_π Contribution to Torsional Potential

Consider a hypothetical d^1 ML_6 system where L is a σ and π donor, but $e_{\pi x} \neq e_{\pi y}$, and $e_{\pi y} = 0$. The orbitals which will destabilise the d orbitals of π symmetry, i.e. make a contribution to $e_{\pi x}$ are illustrated in Figure 5.1.

Figure 5.1. Illustration of orbitals which will destabilise the d orbitals of π symmetry for the hypothetical ML_6 system.

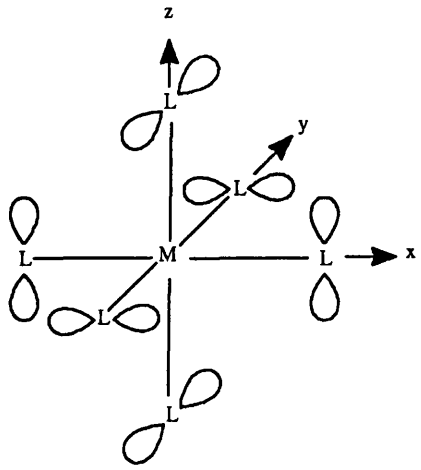

The energy level diagram for this d^1 system is illustrated in Figure 5.2 overleaf.

Figure 5.2. Energy level diagram of d orbitals in ML_6 system.

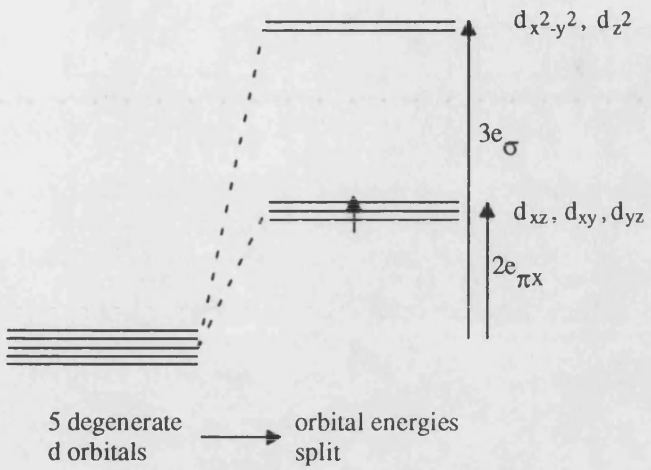

The BC is given by

$$BC = 6/5\ e_\sigma + 6/5\ e_{\pi x} \qquad (6.6)$$

Thus the CLFSE is given by

$$CLFSE = 2\ e_{\pi x} - BC$$
$$= -6/5\ e_\sigma + 4/5\ e_{\pi x} \qquad (6.7)$$

However, if the ligand on the y axis was rotated through 90 °, as shown in Figure 5.3,

Figure 5.3. Illustration of orbitals of π symmetry after rotation of the ligand on the y axis.

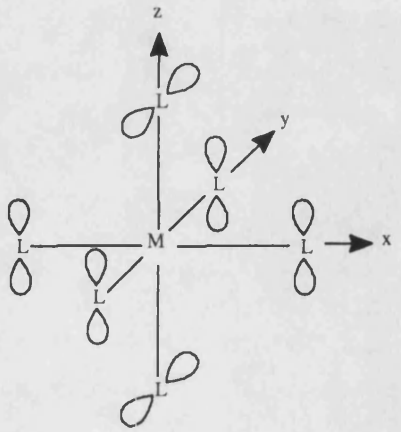

then the energy level diagram becomes (Figure 5.4)

Figure 5.4. Energy level diagram after rotation of ligands on the y axis.

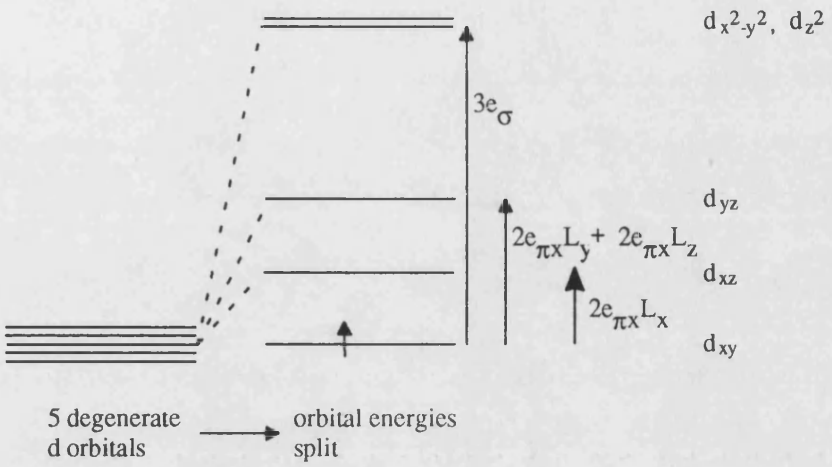

Thus the BC remains the same, but the CLFSE becomes

$$\text{CLFSE} = 1(0 - \text{BC})$$
$$= -6/5\ e_\sigma - 6/5\ e_{\pi x} \qquad (5.8)$$

Therefore, the energies of the d orbitals and thus the CLFSE, respond to rotations about the M-L vector. However, the lack of any distance dependence gives these d functions their own barycentre such that, if these 't_{2g}' orbitals each contain the same number of electrons, rotation about the M-L bond cannot affect the overall CLFSE. This is the case for low spin d^6 Co(III), high spin d^8 Ni(II) and d^9 Cu(II). Hence, a σ-bonding-only model is sufficient for these configurations even though the ligands have a π-bonding capability. The same will not be true for complexes where the d_π functions are not symmetrically filled as for d^1 (shown above), d^2, d^6 (high spin) and d^7 (high spin).

Investigations as to whether the magnitude of any π effects is large enough to significantly influence calculated structures in these types of complexes is beyond the

scope of this thesis. However, it will no doubt form the basis of future work in this area.

5.2.1.2. e_π Contribution to Angular Potential.

As discovered in the last section for low spin d^6 Co(III), high spin d^8 Ni(II) and d^9 Cu(II), the parameterisation of e_π does not seem to be necessary. Before this concept is accepted completely, it is necessary to investigate the effect of π bonding to the L-M-L contribution.

Calculations of hypothetical ML_4 systems, where M has a d^8 or d^9 configuration, using just e_σ to parameterise the CLFSE term, always yields a square planar geometry. However, investigation as to whether π bonding will influence the modelling of tetrahedral over square planar geometry, i.e. whether π bonding will favour a L-M-L angle of $\approx$ 109 ° or L-M-L angle of $\approx$ 180 °, needs to be considered.

Consider $[NiCl_4]^{2-}$. Experimentally, this is observed to be tetrahedral in shape[3] and the Cl ligands are both σ and π donors. The CLFSE for a d^8 tetrahedral complex can be calculated by consideration of the following.

For a tetrahedral complex, where the ligands were σ and π donors, the energy level diagram for the d orbitals is shown below.

Figure 5.5. Diagram to show the energy levels of d orbitals in d^8 tetrahedral complex.

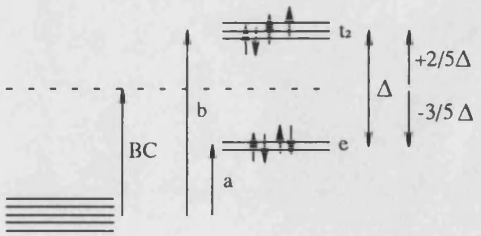

$\Delta = 4/9\,\Delta_{oct}$

$\Delta_{oct} = 3e_\sigma - 4e_\tau$

$\Delta = 12/9\,e_\sigma - 16/9\,e_\pi$

BC is given by

$$BC = 1/5\ (4e_\sigma + 8e_\pi) \qquad (5.9)$$

In tetrahedral symmetry there is no easy way of assigning the energies of the e or t_2 set, given by a and b respectively. In the hand calculation of CLFSE, a and b need to be assigned.

$$a = BC - 3/5\ \Delta \qquad (5.10)$$

$$b = BC + 2/5\ \Delta \qquad (5.11)$$

Then, the CLFSE is given by

$$\begin{aligned} CLFSE &= 4(a - BC) + 4(b - BC) \\ &= 4a + 4b - 8BC \\ &= -4/5\Delta \\ &= -48/45\ e_\sigma + 64/45\ e_\pi \end{aligned} \qquad (5.12)$$

Compare this with a square planar geometry. As π interactions are now being considered the energy level diagram of the d orbitals is now illustrated in Figure 5.6.

Figure 5.6. Diagram to show the energy levels of d orbitals in d^8 square planar complex.

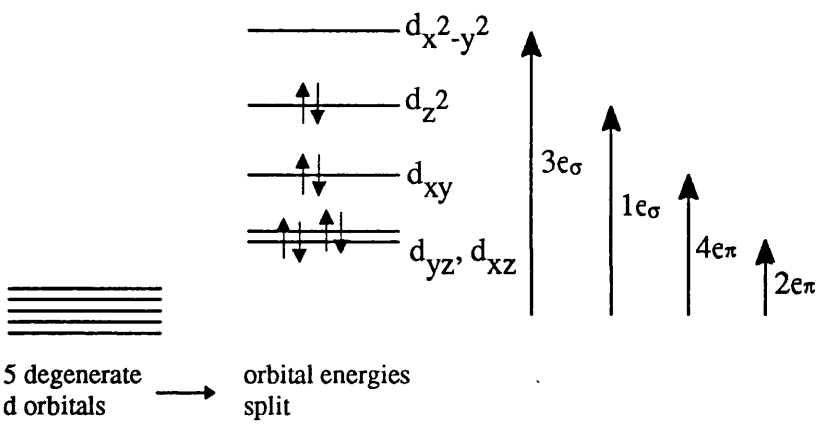

BC is given by

$$BC = 4/5\ e_\sigma + 8/5\ e_\pi \qquad (5.13)$$

Then the CLFSE is given by

$$\begin{aligned} CLFSE &= 4(2e_\pi\text{-}BC) + 2(4e_\pi\text{-}BC) + 2(1e_\sigma\text{-}BC) + 0(3e_\sigma\text{-}BC) \\ &= -22/5e_\sigma + 16/5e_\pi \\ &= -198/45e_\sigma + 144/45e_\pi \end{aligned} \qquad (5.14)$$

From a comparison of equation 5.12 and 5.14, it can be seen that the CLFSE will always favour a square planar structure, provided $e_\sigma > e_\pi$, as is found empirically. If equation 5.12 and 5.14 are equated, and e_π/e_σ is allowed to equal R, then R = 15/8 implying that e_π must be nearly twice the magnitude of e_σ to favour tetrahedral coordination. However, if e_π is larger than e_σ then the d orbital energy level diagram for a tetrahedral complex would be inverted with the e set being of higher energy than the t_2 set. This leads to a change in ground state.

Thus, e_π can, in principle, play a role in determing L-M-L angles. However, for any reasonable value of this parameter, then this effect is minor. In the particular case of the balance between tetrahedral and square planar complexes, an unreasonably large value of e_π is required to ensure tetrahedral geometry. This would also then be accompanied by a change in ground state. Therefore, the inclusion of π interactions does not assist in the modelling of a tetrahedral structure.

From the above discussions it seems that the extra parameterisation of an e_π term in the molecular modelling for low spin d^6 Co(III), high spin d^8 Ni(II) and d^9 Cu(II) species is unnecessary. Thus, the CLFSE term, in the following calculations, was paramaterised with an e_σ dependence on bond length only.

5.3. Computational Details.

The in-house Molecular Mechanics program DOMMINO[4] was used to compute the structures of the 28 compounds displayed schematically in Figure 5.7 and listed in Table 5.1. The latter also gives the ligand abbreviations and their full names. Initial structures used for minimisation were obtained from the Cambridge Structural Database (CSD).[5]

Table 5.1. Chemical formulae, full ligand names and Cambridge Structural Database (CSD) reference codes for the molecules shown in Figure 6.7.

No.	Formula	Ligand name	CSD Refcode	Ref.
XXVI	$Co(NH_3)_6$		EDTACO	6
XXVII	$Co(en)_3$	ethylenediamine	ENCOPN	7
XXVIII	$Co(tn)_3$	1,3-diaminopropane	COTNCL	8
XXIX	$Co(dptn)_2$	di-3-aminopropyl(-amine)	BOKYEF	9
XXX	$Co(en)_2Cl_2$-cis	ethylenediamine	CENCOC	10
XXXI	$Co(en)_2Cl_2$-trans	ethylenediamine	CENCOS	11
XXXII	$Co(metn)_2Cl_2$	2-Methyl-1,3-propanediamine	CAWPOF	12
XXXIII	$Ni(mesoane)Cl_2$	meso-((7R(S),14S(R)-5,5,7,12,12,14-hexamethyl-1,4,8,11-tetra-azacyclotetradecane N',N'',N''',N'''')	MAZNIB	13
XXXIV	$Ni(taz)Cl_2$	1,4,8,11-tetra-azacyclotetradecane	TAZDNC01	14
XXXV	$Ni(15\text{-ane})Cl_2$	1,4,8,12-tetra-azacyclopentadecane	DITVEH*	14
XXXVI	$Ni(dit)Cl_2$	1,5,9,13-tetra-azacyclohexadecane	DITVIL	14
XXXVII	$Ni(tact)Cl_2$	1,4,7,10-tetra-azacyclotetradecane	BOZZIZ	15
XXXVIII	$Ni(pypz)_2$	2,6-bis(Pyrazol-1-yl-methyl)pyridine-N,N'N''	FILYOO	16
XXXIX	$Ni(imid)_6$	Imidazole	HIMZNI	17
XL	$Ni(bipy)_3$	2,2'-Bipyridyl	BPYNIS	18
XLI	$Ni(terpy)_2$	2,2',2''-Terpyridyl	BIKJUA	19
XLII	$Ni(dipa)_2$	Di-2-pyridylmethanamine	JUNCOK	20
XLIII	$Ni(pyraz)_2$	pyrazole	PYZNIN	21
XLIV	$Cu(mepy)_3$	2-(Aminomethyl)pyridine-N,N'	SITBUS	22
XLV	$Cu(dipa)_2$	Di-2-pyridylmethanamine	JUNDAX	23
XLVI	$Cu(bipy)_3$	2,2'-Bipyridyl	TBPYCU	24
XLVII	$Cu(pzme)_2$	tris(Pyrazol-1-yl)methane-N,N',N''	SUHCAZ	25
XLVIII	$Cu(imid)_6$	Imidazole	IMZCUN	26
XLIX	$Cu(terpy)_2$	2,2',2''-Terpyridyl	SIBWEF	27
L	$Cu(bipy)_2NH_3$	2,2'-Bipyridyl	ABPYCU	28
LI	$Cu(imid)_4$	Imidazole	TIMZCU	29
LII	$Cu(aepy)_2$	2-(2-Aminoethyl)pyridine	CUAEPP10	30
LIII	$Cu(bipy)_2$	2,2'-Bipyridyl	BPYCUP	31

* The experimental data was not taken from the Cambridge Database but from the paper referenced.

Figure 5.7. Schematic diagrams of the complexes used in this study

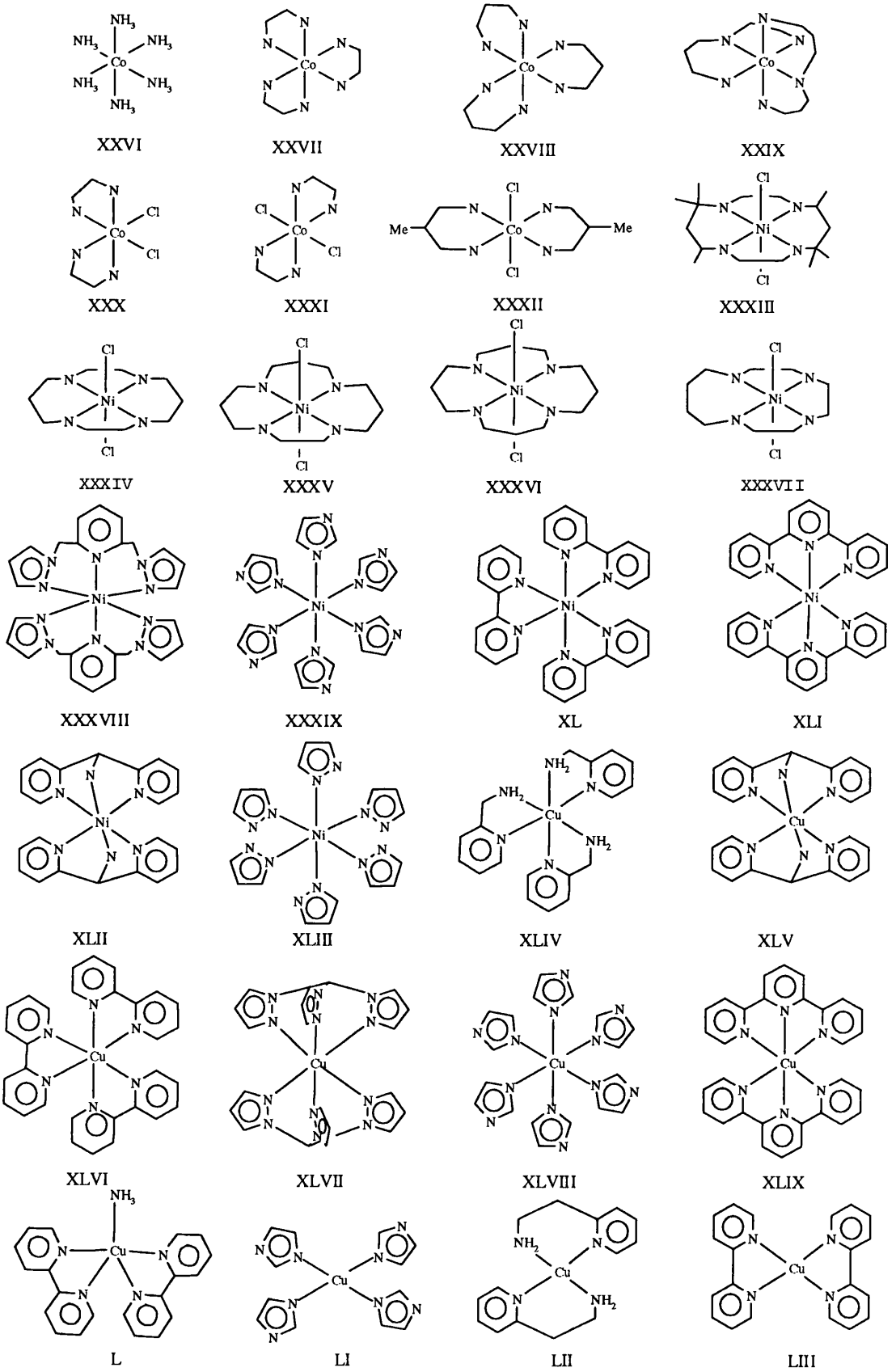

5.4. Results and Discussion.

The complexes shown in Figure 5.1 have been divided into several related sets which are discussed in turn below. The 'organic' part of the molecule is the carbon skeleton which connects between donor atoms or groups.

5.4.1. Co(III) Amine Complexes: XXVI-XXIX

Low spin d^6 Co(III) complexes have a well-defined octahedral stereochemistry which is relatively straightforward to treat within a conventional MM scheme.[32, 33] CLFSE/MM parameters were developed for Co-N_{amine} firstly to show the behaviour of conventional force fields can easily be mimicked and secondly for use with the mixed amine/chloro complexes described later.

The observed and calculated Co-N bond lengths and N-Co-N angles are given in Table 5.2 and, where possible, compared with the results from the treatment of Hancock.[33]♦ The rms errors for these data and for the M-N-C and 'organic' part of the molecule (excluding any features involving hydrogen) are placed in the Supplementary Data, Tables S5.1 and S5.2. Overall, the performance of the CLFSE/MM method with respect to the metal coordination environment is at least as good as conventional MM. The average rms errors in metal-ligand bond lengths and angles are only 0.018Å and 2.3° respectively.

Table 5.2. Observed and calculated bond lengths (Å) and angles (°) for six-coordinate Co(III) amine complexes. (See Figure 5.7 for structural diagrams.) Where appropriate, comparisons with the work of Hancock[33] are made.

	$[Co(NH_3)_6]^{3+}$ (XXVI)			$[Co(en)_3]^{3+}$ (XXVII)		
	calc	*obs*	Hancock	calc	*obs*	Hancock
Co -N	1.96	*1.96*	1.96	1.96	*1.96*	1.96
av N-Co-N	90.0	*90.0*	90.0	90.0	*90.6*	88.0
	179.8	*179.7*		176.0	*175.6*	
	$[Co(tn)_3]^{3+}$ (XXVIII)			$[Co(dptn)_2]^{3+}$ (XXIX)		
	calc	*obs*	Hancock	calc	*obs*	Hancock
Co -N	1.99	*1.98*	1.99	1.99	*2.00*	1.97
				2.02	*2.04*	2.04
av N-Co-N	90.0	*90.0*	94.7	90.0	*90.1*	94.5
	178.6	*177.8*		*176.9*	*174.6*	

♦ In Tables 5.2 and 5.3 some values have been omitted, as experimentally observed data is not readily available.

5.4.2. Mixed Chloro/Amine Complexes [MN_4Cl_2], M = Co(III), Ni(II): XXX-XXXVII

The usefulness of the CLFSE/MM method depends on its ability to treat mixed-ligand systems. As a first step, parameters for mono-atomic chloride have been developed and merged with the existing metal-amine force field. The average observed and calculated M-L bond lengths and angles for the [MN_4Cl_2] complexes shown in Figure 5.7 are given in Table 5.3. An indication of the performance for the rest of the molecule is give in Supplementary Data, Tables S5.3 and S5.4, where rms errors for the M-N-C angles and the remaining 'organic' bond lengths and angles are presented.

Table 5.3. Observed and calculated bond lengths (Å) and angles (°) for six-coordinate Co(III) and Ni(II) MN_4Cl_2 amine/chloride complexes. (See Figure 5.7 for structural diagrams.) All complexes are trans unless otherwise marked.

	cis - $[Co(en)_2Cl_2]^+$ (XXX)		**trans - $[Co(en)_2Cl_2]^+$ (XXXI)**		**$[Co(metn)_2Cl_2]^+$ (XXXII)**	
	calc	*obs*	calc	*obs*	calc	*obs*
Co-Cl	2.25	*2.26*	2.27	*2.24*	2.25	*2.27*
Co-N	1.96	*1.97*	1.95	*1.95*	1.97	*2.00*
Cl-Co-Cl	89.5	*93.1*	180.0	*178.3*	180.0	-----
Cl-Co-N	90.4 177.4	*89.5* *178.1*	90.0 180.0	*90.,0* *178.2*		
N-Co-N	89.6 177.1	*90.0* *178.1*	90.0	*90.7*	88.3 91.7	*88.1* *89.9*

	$[Ni(mesoane)Cl_2]$ (XXXIII)		**$[Ni(taz)Cl_2]$ (XXXIV)**	
	calc	*obs*	calc	*obs*
Ni-Cl	2.56	*2.56*	2.50	*2.51*
Ni-N	2.06 2.02	*2.10* *2.06*	2.02	*2.07*
N-Ni-Cl	90.0	*90.0*	90.0	*90.0*
N-Ni-N	90.0 180.0	*90.0* *180.0*	90.0 180.0	*90.0* *180.0*
Cl-Ni-Cl	179.9	*180.0*	180.0	*180.0*

Table 5.3(cont)

	[Ni(15-ane)Cl_2] (XXXV)		[Ni(dit)Cl_2] (XXXVI)		[Ni(tact)Cl_2] (XXXVII)	
	calc	*obs*	calc	*obs*	calc	*obs*
Ni-Cl	2.50	*2.50*	2.52	*2.54*	2.53	*2.55*
			2.44	*2.43*		
Ni-N	2.07	*2.10*	2.28	*2.21*	2.02	*2.06*
	2.13	*2.12*	2.16	*2.19*	2.04	*2.08*
			2.13	*2.14*		
			2.13	*2.14*		
N-Ni-Cl	90.0		90.0	*90.1*	90.1	*90.1*
N-Ni-N	90.1		89.9	*90.0*	90.7	*90.7*
	173.7		173.2	*172.8*	163.1	*161.7*
Cl-Ni-Cl	176.1		174.3	*172.9*	177.3	*177.6*

Calculated structures are in good agreement with experimental geometries. The overall M-L and L-M-L rms errors for all 8 complexes are 0.025Å and 1.4° respectively with the worst case being for [Ni(taz)Cl_2] (**XXXIV**) where the Ni-N bond lengths are computed to be 0.05A too short.

An interesting feature of these complexes is the interplay between the M-Cl and M-N bonds. For the Co(III) species, there is not much variation (either calculated or observed) in the Co-Cl and Co-N distances but for the Ni(II) species, the observed Ni-Cl bonds vary by up to 0.09Å. The computed Ni-Cl lengths correlate well with experiment both for the trans species where both Ni-Cl bonds are essentially the same, and for [Ni(dit)Cl_2] (**XXXVI**) where they differ by 0.09Å. The latter feature is due to the configuration of the skeletal structure.[14] Two of the carbon atoms are disposed close to one of the axial coordination sites, causing steric hindrance which results in the lengthening of one axial bond. Overall, the CLFSE/MM scheme appears to give a good description of the reported synergism[34] that exists between the axial monodentate ligand and the in-plane macrocyclic ligand. However, it should be noted that the bond length changes which Ito et al.[34] base their arguments on are only of the order of a few hundredths of an Ångstrom which are barely significant. Nevertheless, the d-electron term in the CLFSE/MM method provides a 'through bond' connection and appears to be the first MM-based approach capable of reproducing these subtle structural effects.

The Ni-Cl parameters do not, however, reproduce the structures of $[NiCl_n]^{2-n}$ (n = 4, 6) and generate bonds which are too long. The computed Ni-Cl distances in complexes **XXXIII** to **XXXVII** are between 2.48 and 2.56Å. These values should be compared with the notional 'strain free' Ni-Cl contact of 2.39Å computed using only the Morse function and the CLFSE. The longer values found for the macrocyclic species reflect the intramolecular interactions between the axial chlorides and the ring systems. Such interactions are absent for $[NiCl_n]^{2-n}$ (n = 4, 6) and bond lengths close to the 'strain free' value result. However, the experimental Ni-Cl distance in, for example, $[NiCl_4]^{2-}$ is 2.26 Å.[3] The present force field requires some further tuning, possibly by including electrostatic interactions (this is discussed later).

5.4.3. Ni(II) and Cu(II) Imine and Mixed Amine/Imine Complexes: XXXVIII - LIII

Unsaturated nitrogen donor ligands are extremely important in coordination chemistry. For example, metalloproteins often bind transition metals, especially Cu(II), via the imidazole groups on histidine side chains. The observed and calculated metal-ligand bond lengths and angles are reported for six $Ni(II)N_6$ complexes (Table 5.4), six 6-coordinate Cu(II) complexes (Table 5.5) and one 5-coordinate Cu(II) plus three 4-coordinate Cu(II) complexes (Table 5.6). As before, the relevant rms errors for these data and for the remaining 'organic' parts of the molecules have been placed in the Supplementary Data (Tables S5.5 - S5.8).

Table 5.4. Observed and calculated bond lengths (Å) and angles (°) for six-coordinate Ni(II) imine complexes. (See Figure 5.7 for structural diagrams.)

	$[Ni(pypz)_2]^{2+}$ (XXXVIII)		$[Ni(imid)_6]^{2+}$ (XXXIX)		$[Ni(bipy)_3]^{2+}$ (XL)	
	calc	*obs*	calc	*obs*	calc	*obs*
$Ni\text{-}N_{py}$	2.15	*2.16*			2.08	*2.09*
$Ni\text{-}N_{pz}$	2.07	*2.08*	2.10	*2.13*		
av N-Ni-N	90.0	*90.0*	90.0	*90.2*	90.0	*90.2*
	177.2	*177.7*	180.0	*180.0*	175.4	*169.7*
	$[Ni(terpy)_2]^{2+}$ (XLI)		$[Ni(dipa)_2]^{2+}$ (XLII)		$[Ni(pyraz)_6]^{2+}$ (XLIII)	
	calc	*obs*	calc	*obs*	calc	*obs*
$Ni\text{-}N_{py}$	2.14	*2.13*	2.10	*2.11*		
	1.99	*2.02*				
$Ni\text{-}N_{am}$			2.12	*2.11*		
$Ni\text{-}N_{pz}$					2.11	*2.13*
av N-Ni-N	90.6	*90.4*	90.0	*90.0*	90.0	*90.0*
	166.7	*163.2*	180.0	*180.0*	180.0	*180.0*

Table 5.5. Observed and calculated bond lengths (Å) and angles (°) for six-coordinate Cu(II) complexes.

	$[Cu(mepy)_3]^{2+}$ (XLIV)		$[Cu(dipa)_2]^{2+}$ (XLV)		$[Cu(bipy)_3]^{2+}$ (XLVI)	
	calc	*obs*	calc	*obs*	calc	*obs*
$Cu\text{-}N_{am}$	1.93	*2.05*	1.99	*2.02*		
	2.01	*2.01*				
	2.09	*2.04*				
$Cu\text{-}N_{py}$	2.05	*2.06*	2.05	*2.02*	2.36	*2.45*
	2.45	*2.44*	2.51	*2.54*	2.36	*2.23*
	2.47	*2.42*			1.98	*2.03*
					1.96	*2.03*
					1.98	*2.03*
					2.00	*2.03*
N-Cu-N	173.0	*166.4*	71.2	*72.2*	79.7	*78.2*
	91.4	*96*	82.9	*86.4*	84.7	*101.6*
	95.4	*89.5*	108.8	*107.8*	99.0	*99.5*
	101.3	*96.1*	97.0	*93.6*	96.3	*92.4*
	82.5	*73*	80.9	*79.8*	92.0	*91.6*
	93.0	*90.1*	108.9	*107.8*	99.0	*99.1*
	91.2	*103.9*	99.1	*100.2*	96.2	*94.4*
	73.1	*80.5*	97.1	*93.6*	88.3	*73.9*
	93.5	*94.3*	99.1	*100.2*	88.1	*94.1*
	71.6	*75.2*	71.2	*72.2*	85.1	*93.6*
	172.2	*163.8*	82.9	*86.4*	91.9	*92.2*
	91.8	*95.8*	80.9	*79.8*	80.0	*80.4*
	94.1	*94.2*	180.0	*180.0*	178.4	*174.8*
	156.8	*159.6*	180.0	*180.0*	175.9	*174.2*
	104.0	*98.1*	180.0	*180.0*	176.3	*165.6*
	$[Cu(pzme)_2]^{2+}$ (XLVII)		$[Cu(imid)_6]^{2+}$ (XLVIII)		$[Cu(terpy)_2]^{2+}$ (XLIX)	
	calc	*obs*	calc	*obs*	calc	*obs*
$Cu\text{-}N_{pz}$	1.99	*2.00*	2.04	*2.01*		
	1.99	*2.00*	2.04	*2.01*		
	2.01	*2.03*	2.06	*2.05*		
	2.01	*2.03*	2.06	*2.02*		
	2.41	*2.36*	2.51	*2.59*		
	2.41	*2.36*	2.51	*2.59*		
$Cu\text{-}N_{py}$					1.83	*1.98*
					1.83	*1.98*
					2.27	*2.18*
					2.27	*2.18*
					2.27	*2.18*
					2.27	*2.18*
N-Cu-N	84.5	86.1	87.8	88.3	82.6	78.9
	79.7	81.5	92.1	92.1	85	87.8
	100.3	98.5	92.1	91.7	97.1	100.6
	95.4	93.9	87.9	87.9	97.5	96
	180	180	89.5	91.4	82.5	78.2
	85.5	86.8	92.1	92.1	97.3	96.8
	94.6	93.2	87.9	88.6	97.6	108.3
	180	180	90.5	91.4	97.2	97
	95.5	93.9	90.5	88.3	97.7	102.3
	180	180	87.9	88.6	84.1	89.2
	94.3	93.2	92.1	91.7	82.6	77.4
	100.3	95.5	89.5	87.9	82.6	77.5
	84.5	86.8	180	180	165.1	157.1
	79.7	81.5	180	180	165.1	154.9
	85.5	86.1	180	180	179.7	174.2

Table 5.6. Observed and calculated bond lengths (Å) and angles (°) for five- and four-coordinate Cu(II) complexes

	$[Cu(bipy)_2NH_3]^{2+}$ (L)		$[Cu(imid)_4]^{2+}$ (LI)		$[Cu(aepy)_2]^{2+}$ (LII)		$[Cu(bipy)_2]^{2+}$ (LIII)	
	calc (SQP)	*obs (TBP)*	calc	*obs*	calc	*obs*	calc	*obs*
$Cu\text{-}N_{am}$	2.05	*2.05*			1.97	*2.01*		
$Cu\text{-}N_{py}$	1.96	*2.05*			2.00	*2.02*	2.19	*1.97*
	1.96	*1.98*					2.19	*1.99*
	1.99	*2.11*					1.82	*1.99*
	2.36	*2.07*					1.82	*2.03*
$Cu\text{-}N_{pz}$			2.03	*2.01*				
N-Cu-N	88.6	92.7	90.0	88.4	87.6	86.6	86.5	83.6
	179.5	129.5	90.0	88.4	87.6	86.6	94.5	102.3
	92.1	122.3	90.0	91.6	92.4	93.4	125.7	160.9
	92.8	91.5	90.0	91.6	92.4	93.4	177.7	151.1
	80.3	79.4	180.0	180.0	180.0	180.0	94.5	102.4
	90.8	98.0	180.0	180.0	180.0	180.0	86.5	81.3
	176.9	175.8						
	96.7	108.3						
	88.1	97.9						
	87.8	79.6						

N_{am} is an amine N
N_{pz} is N in a five membered ring
N_{py} is N in a six membered ring

The Ni(II) complexes (Table 5.4) are all in good agreement with the observed structures, the worst cases being for $[Ni(terpy)_2]^{2+}$ (**XLI**) where a Ni-N bond length is calculated 0.03Å too short and for $[Ni(bipy)_3]^{2+}$ (**XL**) where the trans N-Ni-N angle is calculated some 5° too large. However, the average rms errors for complexes **XXXVIII** - **XLIII** are only 0.011Å and 2.4° for Ni-N distances and N-Ni-N angles respectively.

As found previously,[35] the CLFSE/MM model automatically generates tetragonal distortions for six-coordinate Cu(II) complexes (Table 5.5). Tetragonal elongations are predicted except for $[Cu(terpy)_2]^{2+}$ (**XLIX**) which is computed to have a compressed geometry. Although room temperature crystallographic studies apparently yield a compressed structure as well,[27,36] (see Table 5.5) variable temperature Electron Spin Resonance measurements indicate that this is a result of a dynamic Jahn Teller effect and that the true low-temperature coordination geometry is tetragonally

elongated.[27] The CLFSE/MM model predicts the wrong sense of distortion. The Ni(II) analogue shows a pronounced tetragonal compression which is imposed by the rigid terpy ligand. Although the CLFSE alone favours an elongated structure, it is apparently not sufficient to overcome the ligand's tendency to compress the structure.

For the remaining CuN_6 species, the magnitudes of the elongations are reproduced quite well. Given the 'plasticity' of Cu(II) complexes, perfect agreement should not be expected since relatively small crystal packing forces can significantly alter the relative equatorial and axial bond lengths. To first order, if the equatorial distance changes by δx, then the axial bond should change by $-2\delta x$[37]. Relative to experiment, therefore, it is expected and found that if the Cu-N_{eq} distance is computed to be smaller than observed, the Cu-N_{ax} contact is longer than experiment. This pattern is found for $[Cu(imid)_6]^{2+}$ (**XLVIII**), $[Cu(dipa)_2]^{2+}$ (**XLV**) and $[Cu(pzme)_2]^{2+}$ (**XLVII**). The observed and calculated elongations are about the same for $[Cu(mepy)_3]^{2+}$ (**XLIV**). For $[Cu(bipy)_3]^{2+}$ (**XLVI**), there is an apparent asymmetry in the observed Cu-N_{ax} distances while theory gives identical bond lengths. However, the average observed Cu-N_{ax} contact is only 0.02Å shorter than the calculated value.

The orientation of the planes of these unsaturated ligands is also expected to be affected by crystal packing. For example, the observed $[Cu(imid)_6]^{2+}$ structure shows tilting of the axial ligand about the Cu-N bond in order that the H of the ligand may take part in H bonding with the O of the NO_3^- counter ion.[26] This tilting was not reproduced by the Molecular Mechanics calculation as interactions of the complex with counter ions, and other crystal packing forces, have yet to be included.

For the five coordinate case (Table 5.6), the calculated structure displays square based pyramidal geometry whereas the observed structure is approximately trigonal bipyramidal. The counter ion for the experimental structure is $[BF_4]^-$, and there is apparently hydrogen bonding between the F of the $[BF_4]^-$ and the H on the ammonia.[28] Experimentally, five coordinate Cu(II) complexes frequently display intermediate and variable structures from near trigonal bipyramidal to near square pyramidal with quite dramatic effects on the Cu-L distances. This is shown, for example, by complexes of

the type $[Cu(2,2'\text{-bipyridyl})_2X]^{n+}$.[38,39] Previous observations[35] demonstrated that the CLFSE/MM model favours a square pyramidal symmetry but that the analogous trigonal bipyramidal complex has a very similar energy. If the surrounding lattice was explicitly included in the calculations then better agreement between calculated and observed structures would be expected.

Planar four coordinate d^9 species are usually less plastic than five- and six-coordinate complexes since the former are at the limit of tetragonal elongation. Thus, one would expect this class of Cu(II) complex to give the best agreement between the calculated and observed structures. This is indeed the case for $[Cu(imid)_4]^{2+}$ (**LI**) and $[Cu(aepy)_2]^{2+}$ (**LII**) where the maximum Cu-N deviation from the observed bond length is only 0.03 Å (Table 5.6). However, for $[Cu(bipy)_2]^{2+}$ (**LIII**) very poor agreement is found. Experimentally, the complex displays distorted tetrahedral geometry,[31] whereas the calculated structure is nearer a square plane. Thus, a way of modelling 4-coordinate complexes which do not exhibit square planar stereochemistry, needs to be addressed.

For d^9 species, there is a balance between the ligand-ligand repulsions, which favour a tetrahedral structure, and the d-electron stabilisation energy which favours planar coordination. The latter dominates in the present CLFSE/MM force field. For example, a sample calculation for $[CuCl_4]^{2-}$ yields a D_{4h} structure. Experimentally, $[CuCl_4]^{2-}$ usually has a flattened tetrahedral D_{2d} geometry[40] and various ab initio quantum chemical calculations have confirmed this as the lowest energy structure in the gas phase.[41] However, the energy difference between tetrahedral and planar coordination is very small and the latter is observed with a suitable choice of countercation. As mentioned earlier the CLFSE favours square planar geometry. One way of inducing a tetrahedral geometry would be to include π bonding. This was discussed earlier and found to be unacceptable. Another method could be to increase the non-bonding repulsion term. When computing the structure of $[CuCl_4]^{2-}$, tetrahedral geometry can be forced by increasing the 1,3-non-bonding repulsive term, but very large values (an approximately 20-fold increases over the used value - see Appendix) for the van der Waals parameters are required. An alternative method is to

include 1,3 (and 1,2) electrostatic interactions. This latter course is favoured since it was recognised that ultimately, an electrostatic energy term should be included into the strain energy expression.

An illustrative calculation[42] for $[CuCl_4]^{2-}$ with a Cu charge of 0.5 and Cl charges of -0.7 yields a D_{2d} symmetry with the large Cl-Cu-Cl angle of 142° and shows that electrostatic interactions can distort the structure in the desired way. Preliminary results for $[Cu(bipy)_2]^{2+}$ show that charges on Cu and N also distort the structure away from planarity and, as shown in Figure 5.8, corrects the discrepancy between theory and experiment.

Figure 5.8. Comparison of $[Cu(bipy)_2]^{2+}$, calculated with and without charges.

Observed Structure[31]

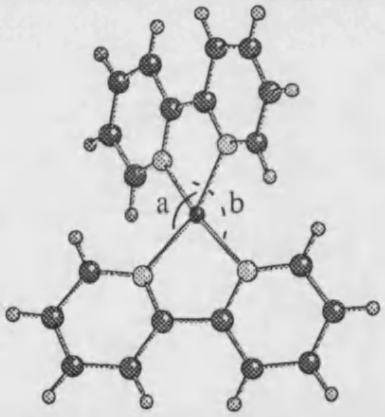

Cu - N (Å) 1.97, 1.99, 1.99, 2.03
a = 160.9° , b = 151.1°

Calculated Structure (No Charges)	Calculated Structure (Charges Included)
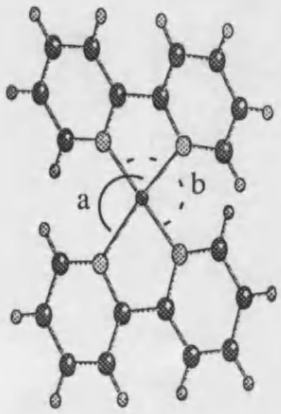	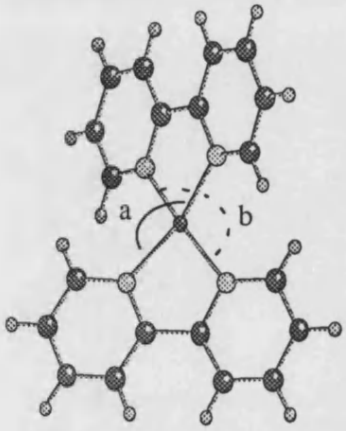
Cu - N (Å) 1.82, 2.19, 1.82, 2.19 a = 177.7° , b = 125.7°	Cu - N (Å) 1.99, 2.03, 1.99, 2.03 a = 164.2°, b = 152.5°

Thus, the inclusion of electrostatic interactions seems to be the most reasonable method for inducing a non planar stereochemistry for 4-coordinate complexes.

5.5. Conclusions

The CLFSE/MM method has successfully been extended to mixed ligand complexes of Co(III), Ni(II) and Cu(II). As a preliminary step, calculations on simple amine complexes of Co(III) showed that the CLFSE/MM scheme can readily reproduce the performance of conventional MM methods. Then mixed amine/chloro complexes of Co(III) and Ni(II) were considered.

Chloride ligands are potential π-donors. However, an analysis of the CLFSE shows that for such ligands, the increasingly positive value of e_π associated with a shorter, stronger M-L bond can give a less negative CLFSE. The π-interaction works against σ-bonding which is opposite to the desired behaviour. Thus, a fixed value of e_π could be used. This could still, in principle, influence the rotation about the M-L vector but not for d^8, d^9 and low spin d^6 configurations since the d_π orbitals maintain their own barycentre and are symmetrically occupied for these configurations. Also, the effect of π interactions on the L-M-L angle potential is small unless $e_\pi > e_\sigma$ for d^8 systems. This is unreasonable as it is not empirically observed and also causes a change in ground state. It is simplest, therefore, to retain the σ-only implementation of the CLFSE.

The calculated structures for the eight chloro/amine MN_4Cl_2 complexes are in good agreement with experiment with the average rms error in M-L distances and L-M-L angles of less that 0.03 Å and 3 ° respectively. The CLFSE term provides the 'through bond' communication between axial and equatorial ligands in the Ni(II) macrocyclic complexes such that the synergism observed experimentally is reproduced. The CLFSE/MM model is the first MM-based approach capable of treating this relatively subtle effect.

Calculations for imine and amine/imine $Ni(II)N_6$ complexes are also in good agreement with experiment. In general, slightly poorer absolute agreement was found for

comparable Cu(II) systems but, given the plasticity of the Cu(II) coordination sphere, this result is not surprising. Jahn-Teller elongated structures are computed automatically for five of the six CuN_6 species and two of the three four-coordinate complexes have the required planar geometries. The three remaining systems, $[Cu(bipy)_2(NH_3)]^{2+}$, $[Cu(terpy)_2]^{2+}$ and $[Cu(bipy)_2]^{2+}$ are not treated as well.

For five-coordinate species, it has already been noted[35] that the CLFSE/MM scheme favours square pyramidal coordination although a trigonal bipyramidal structure is very close in energy. Crystal packing forces are sufficiently large that any structure between these two extremes may be observed. For $[Cu(bipy)_2(NH_3)]^{2+}$, the experimental structure happens to be near trigonal bipyramidal so the discrepancy between the modelling and experiment is not significant. In contrast, the force field is not properly balanced for $[Cu(terpy)_2]^{2+}$ and predicts a compressed octahedral geometry. The Ni(II) analogue is also compressed. Evidently, the ligand is able to overcome the tetragonal elongation favoured by the CLFSE. Finally, $[Cu(bipy)_2]^{2+}$ is calculated to be too flat. A simple treatment of $[CuCl_4]^{2-}$ shows that explicit inclusion of 1,3 and 1,2 electrostatic interactions can force the geometry towards the observed flattened tetrahedral structure and sample calculations for $[Cu(bipy)_2]^{2+}$ show the same behaviour. The ability to model charge effects is highly desirable anyway and the inclusion of an electrostatic term into the force field will be the basis of the next chapter.

5.6. Supplementary Data

Table S5.1. Rms Co-N and N-Co-N errors

structure		bond lengths rms difference / (Å)	bond angles rms difference / (°)
$[Co(NH_3)_6]^{3+}$	XXVI	0.007	0.571
$[Co(en)_3]^{3+}$	XXVII	0.010	2.926
$[Co(tn)_3]^{3+}$	XXVIII	0.027	1.655
$[Co(dptn)_2]^{3+}$	XXIX	0.029	4.064
average rms error		0.018	2.304

Table S5.2. Rms errors for rest of molecule (excluding H atoms).

	XXVII	XXVIII	XXIX
Metal Co-N-C rms error (°)	0.986	1.733	2.332
'Organic' rms errors			
bond lengths (Å)	0.006	0.011	0.015
bond angles (°)	1.116	2.873	1.558

Table S5.3

structure		bond lengths rms difference / (Å)	bond angles rms difference / (°)
$[Co(en)_2Cl_2\text{-(cis)}]^+$	XXX	0.019	1.664
$[Co(en)_2Cl_2\text{-(trans)}]^+$	XXXI	0.018	1.215
$[Co(metn)_2Cl_2]^+$	XXXII	------	------
[Ni(mesoane)Cl_2]	XXXIII	0.006	1.339
[Ni(taz)Cl_2]	XXXIV	0.041	1.849
[Ni(15-ane)Cl_2]	XXXV	------	-----
[Ni(dit)Cl_2]	XXXVI	0.033	1.201
[Ni(tact)Cl_2]	XXXVII	0.034	1.079
average rms error		0.025	1.391

Table S5.4

	XXX	XXXI			
Metal Co-N-C rms error (°)	1.355	1.337			
'Organic' rms errors					
bond lengths (Å)	0.045	0.015			
bond angles (°)	2.703	1.308			
	XXXIII	XXXIV	XXXV	XXXVI	XXXVII
Metal Ni-N-C rms error (°)	2.673	0.618	------	2.464	1.265
'Organic' rms errors					
bond lengths (Å)	0.015	0.003	------	0.0.15	0.030
bond angles (°)	1.339	1.141	------	2.195	3.011

Table S5.5

structure		bond lengths rms difference / (Å)	bond angles rms difference / (°)
$[Ni(pypz)_2]^{2+}$	XXXVIII	0.010	2.715
$[Ni(imid)_6]^{2+}$	XXXIX	0.027	0.626
$[Ni(bipy)_3]^{2+}$	XL	0.012	4.194
$[Ni(terpy)_2]^{2+}$	XLI	0.009	2.368
$[Ni(dipa)_2]^{2+}$	XLII	0.008	1.899
$[Ni(pyraz)_6]^{2+}$	XLIII	0.020	2.584
$[Cu(mepy)_3]^{2+}$	XLIV	0.057	6.240
$[Cu(dipa)_2]^{2+}$	XLV	0.030	1.956
$[Cu(bipy)_3]^{2+}$	XLVI	0.077	6.747
$[Cu(pzme)_2]^{2+}$	XLVII	0.037	1.453
$[Cu(imid)_6]^{2+}$	XLVIII	0.050	0.944
$[Cu(terpy)_2]^{2+}$	XLIX	0.118	5.585
$[Cu(bipy)_2am]^{2+}$	L	0.163	19.448
$[Cu(imid)_4]^{2+}$	LI	0.022	1.306
$[Cu(aepy)_2]^{2+}$	LII	0.030	0.816
$[Cu(bipy)_2]^{2+}$	LIII	0.201	18.732

Table S5.6

	XXXVIII	XXXIX	XL	XLI	XLII	XLIII
Metal Ni-N-C rms error (°)	3.413	1.793	1.288	2.908	2.855	0.100
'Organic' rms errors						
bond lengths (Å)	0.006	0.024	0.026	0.062	0.028	0.010
bond angles (°)	3.316	1.965	1.804	3.906	1.395	0.564

Table S5.7

	XLIV	XLV	XLVI	XLVII	XLVIII	XLIX
Metal Cu-N-C rms error (°)	2.456	3.004	5.703	1.771	5.502	5.088
'Organic' rms errors						
bond lengths (Å)	0.027	0.036	0.036	0.020	0.033	0.027
bond angles (°)	2.045	1.852	2.485	1.816	2.230	1.937

Table S5.8

	L	LI	LII	LIII
Metal Cu-N-C rms error (°)	5.832	1.734	5.280	3.193
'Organic' rms errors				
bond lengths (Å)	0.272	0.033	0.027	0.053
bond angles (°)	2.781	1.734	2.330	3.193

5.7. References.

1. M. Gerloch, '*Magnetism and Ligand Field Analysis*' Cambridge University Press, New York, 1983.
2. M. Gerloch, J. H. Harding and R. G. Wolley, *Struct. and Bonding*, 1981, **46**, 1.
3. P. B. Hitchcock, K. R. Seddon and T. Welton, *J. Chem. Soc. Dalton Trans.*, 1993, 2639.
4. DOMMINO is based on molecular mechanics software kindly supplied by Dr D. J. Osguthorpe, Molecular Graphics Unit, University of Bath and modified to include the CLFSE contribution.
5. Cambridge Structural Database, Version 4. Cambridge Crystallographic Data Centre, University Chemical Laboratory, Cambridge, 1994.
6. E. O. Schlemper, *J.Cryst. Mol. Struct.*, 1977, **7**, 81.
7. E. N. Duesler and K. N. Raymond, *Inorg. Chem*, 1971, **10**, 1486.
8. R. Nagao and F. Marumo, Y. Saito, *Acta. Cryst. Sect. B*, 1973, **29**, 2438.
9. T. W. Hambley, G. H. Searle and M. R. Snow, *Aust. J. Chem.*, 1982, **35**, 1285.
10. K. Matsumoto, S. Ooi and H. Kuroya, *Bull. Chem. Soc. Jpn.*, 1970, **43**, 3801.
11. A. S. Foust and V. Janickis, *Inorg. Chem.*, 1980, **19**, 1048.
12. J. D. Mather, R. E. Tapscott and C. F. Campana, *Inorg. Chim. Acta.*, 1983, **73**, 235.
13. T. Ito and K. Toriumi, *Acta Cryst. Sect. B*, 1981, **37**, 88.
14. T. Ito, M. Kato and H. Ito, *Bull. Chem. Soc. Jpn.*, 1984, **57**, 2641.
15. M. Sugimoto, J. Fugita, H. Ito, K. Toriumi and T. Ito, *Inorg. Chem.*, 1983, **22**, 955.
16. A. A. Watson, D. A. House and P. J. Steel, *Inorg. Chim. Acta*, 1987, **130**, 167.
17. J. P. Konopelski, C. W. Reimann, C. R. Hubbard, A. D. Mighell and A. Santoro, *Acta Cryst. Sect. B*, 1976, **32**, 2911.
18. A. Wada, N. Sakabe and J. Tanaka, *Acta Cryst. Sect. B.*, 1976, **32** 1121.
19. M. I. Arriortua, T. Rojo, J. M. Amigo, G. Germain and J. P. Declercq, *Bull. Soc. Chim. Belg.*, 1982, **91**, 337.
20. P. V. Bernhardt, P. Comba, A. Mahu-Rickenbach, S. Stebler, S. Steiner, K. Varnagy and M. Zehnder, *Inorg Chem.*, 1992, **31**, 4194.
21. C. W. Reinann, A. Santoro and A. D. Mighell, *Acta Cryst. Sect. B*, 1970, **26**, 521.
22. A. W. Maverick, M. L. Ivie and F. R. Fronczek, *J. Coord. Chem.*, 1990, **21**, 315.
23. P. V. Bernhardt, P. Comba, A. Mahu-Rickenbach, S. Stebler, S. Steiner, K. Varnagy and M Zehnder, *Inorg Chem.*, 1992, **31**, 4194.
24. O. P. Anderson, *J. Chem. Soc. Dalton Trans.*, 1972, 2597.
25. T. Astley, J. M. Gulbis, M. A. Hitchman and E. R. T. Tiekink, *J. Chem. Soc. Dalton Trans*, 1993, 509.
26. D. L. McFadden, A. T. McPhail, C. D. Garner and F. E. Mabbs, *J. Chem Soc Dalton Trans.*, 1975, 263.
27. J. V. Folgado, W. Henke, R. Allmann, H. Stratmeier, D. Beltran-Porter, T. Rojo and D. Reinen, *Inorg. Chem.*, 1990, **29**, 2035.
28. F. S. Stephens, *J. Chem. Soc. Dalton Trans.*, 1972, 1350.
29. G. Fransson and B. K. S. Lundberg, *Acta Chem. Scand.*, 1972, **26**, 3969.
30. D. L. Lewis and D. J. Hodgson, *Inorg. Chem.*, 1974, **13**, 143.
31. H. Nakai, *Bull. Chem. Soc. Jpn.*, 1971, **44**, 2412.
32. P. Comba and T. W. Hambley, *Molecular Modelling of Inorganic Compounds*, VCH, Weinheim, Germany, 1995.
33. R. D. Hancock, *Prog. Inorg. Chem.*, 1989, **37**, 187.
34. T. Ito, M. Kato and H. Ito, *Bull. Chem. Soc. Jpn.*, 1984, **57**, 1556.
35. V. J. Burton, R. J. Deeth, C. M. Kemp and P. J. Gilbert, *J. Am. Chem. Soc.*, 1995, **117**, 8407.
36. M. I. Arriortua, T. Rojo, J. M. Amigo, G. Germain and J. P. Declerdq, *Acta Cryst.*, 1982, **B38**, 1323.
37. R. J. Deeth and M. A. Hitchman, *Inorg. Chem.*, 1986, **25**, 1225.
38. W. D. Harrison, D. M. Kennedy, M. Power, R. Sheahen and B. J. Hathaway, *J. Chem. Soc.*, 1963, 1556.
39. G. A. Barely, B. F. Hoskins and C. H. C. Kennard, *J. Chem. Soc.*, 1963, 5691.
40. K. E. Halvarson, C. Patterson and R. D. Willett, *Acta Cryst.*, 1990, **B46**, 508.

41. P. D. Sheen, *'A Hybrid DFT/MM Model for Transition Metal Systems'*, PhD Thesis, 1995, Bath University; K. Waizumi, H. Masuda, H. Einaga and N. Fukushima, *Chem. Lett.*, 1993, 1145.
42. Other parameters for $[CuCl_4]^{2-}$ calculation: Cu-Cl Morse function D_0 = 80.0 kcal mol^{-1}, r_e = 2.05 , α = 0.45; van der Waals A = 49496.2, B = 1154.4; CLFSE e_σ

Chapter 6

Molecular Modelling Including Electrostatic Interactions

6.1. Introduction

The concept of net atomic charges in molecules is important as it greatly enhances the understanding of the chemistry of complexes. For example, net atomic charges can be used as an indication of reactivity of atomic sites in molecules. They can also be used as an aid in the understanding of molecular dipole moments, and for interaction energy calculations in crystals.

If the lattice or solvent effects, or any other intermolecular interactions were to be considered then the electrostatic interactions of these molecules becomes important. Thus, it would seem more 'chemically reasonable' that electrostatics should be included in a Molecular Mechanics force field for determining structures.

Electrostatic interactions are usually modelled by assigning point charges to the atoms and then the Coulombic energy, E_{el}, is calculated using equation (6.1).

$$E_{el} = q_i q_j / \varepsilon r_{ij} \qquad (6.1)$$

where q_i is the charge on atom i, q_j is the charge on atom j, ε is the dielectric constant and r_{ij} is the distance between atom i and atom j.

The problem that arises when electrostatics are included is that there is no simple or accurate method of empirically calculating these point charges. In many cases, i.e. for small molecules, organic and inorganic, Coulombic terms have not been included explicitly. They are taken account of by means of the other functions. For example, the electrostatic attraction between a metal and a coordinated ligand may be simply modelled as part of the bonding interaction between the two. This type of method has been shown, in most cases[1-3], not to be detrimental to the modelling.

However, in biological systems where there are many long range interactions, the electrostatic contribution becomes more important, and electrostatic terms are routinely employed in models for biological macromolecules[4].

Point charges on atoms have been estimated using quantum mechanical calculations[5], for example ab initio and semi empirical methods can be used[6], but these can be very time consuming. The accuracy of these point charges has also been questioned[7], but they have been used successfully. It should be noted that no great chemical significance should be placed on the point charges used. For example, consider the charges derived from quantum mechanical calculations. The charges may depend upon the conformation of molecule used, the basis set chosen in the calculation, and also for very large molecules it is only practical to do quantum mechanics calculations on fragments and then to 'patch' these together.

The estimation of the dielectric constant also creates some challenges. The dielectric can be employed as either a constant value or it can be distance dependent. The constant dielectric is what has been classically used, whereas the distance dependent dielectric has been introduced to allow the charges to 'respond' to the environment. The importance of this distance dependent dielectric has been illustrated by Warshel[8], who has shown that the effective dielectric constant for short range ionic interaction in water is smaller than the bulk dielectric and increases (roughly linearly) with charge separation. Hall et al.[9] have compared different force fields for modelling polypeptides, and they discovered that the best method was one which included a distance dependent dielectric.

In the modelling of transition metal complexes, assigning a point charge to a metal atom itself is important. Pauling's electroneutrality principle[10] shows that it would be incorrect to assign a full formal charge, so partial charges should be employed. Hambley[11] has successfully modelled the binding of cis-platin to DNA using a charge of 0.5 for the Pt. Tueting et al.[12] have shown in the modelling of cobalt bleomycin, that a change in charge on the cobalt from +3 to +1 had a significant effect on the conformation of the molecule. It has also been shown in this work (chapter 5) that

including charges on the metal and directly coordinating ligands has an important consequence on the minimum energy structure obtained.

For example, consider high spin $[NiCl_4]^{2-}$. The d orbital diagram is shown in Figure 6.1.

Figure 6.1. d Orbital diagram for $[NiCl_4]^{2-}$

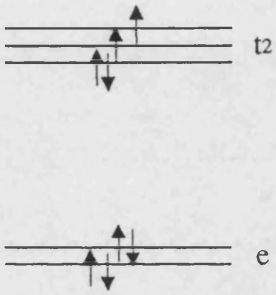

Due to the uneven filling of the t_2 set, one would expect a Jahn Teller distortion to take place[13]. However, from experimentally determined structures[14-18] a tetrahedron is observed.

A force field including parameters for Ni and Cl atoms has already been developed within DOMMINO (chapter 5), so a calculation of the structure of $[NiCl_4]^{2-}$ was easily carried out. However, a square planar structure was determined. It was not until point charges were assigned, +0.9 and -0.7 to Ni and Cl respectively, and the force field was modified slightly so that $D_0 = 120$, $r_0 = 2.52$Å and $\alpha = 0.45$, that the following structure was obtained (figure 6.2).

Fig. 6.2. Calculated $[NiCl_4]^{2-}$ structure, including charges.

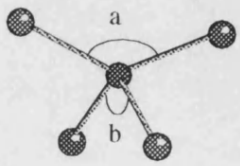

a = 134.0 ° and b = 109.1°

Here, the Ni-Cl bond lengths are 2.26 Å, 2.26 Å, 2.31 Å, 2.31 Å, and selected Cl-Ni-Cl bond angles are shown in the diagram. Thus, even with the inclusion of charges, there is a deviation from experimental structures where the average Ni-Cl distance is 2.25 Å and Cl-N-Cl angle is 109.5 °. The calculated structure also displays a distortion from a tetrahedron. However, the average calculated Cl-Ni-Cl angle is 109.5 °, thus, it can be speculated that this is perhaps some Jahn Teller effect, as tetrahedral Ni(II) is in principle subject to this. This distortion is not observed experimentally, but this may be due to vibronic coupling of different vibrations or maybe crystal packing effects. Calculations also show that the tetrahedral geometry has E_{tot} = -108.87 kcal/mol compared to -111.12 kcal/mol of the minimised structure. Thus, it could be speculated that some kind of dynamic Jahn Teller effect is possible, the calculated energy difference of 2.25 kcal/mol being an upper bound in the interconversion barrier.

Another consideration where the inclusion of charges has proved to be important was in the geometry determination of $[Cu(bipy)_2]^{2+}$ (see previous chapter).

It was because of these considerations that the determination of a transferable force field which included an electrostatic term for all the Ni(II) and Cu(II) systems, was carried out.

Therefore, in this study, the calculation of geometries of the previous Ni(II), Cu(II) amine systems, Ni(II) and Cu(II) imine systems has been repeated, but this time the force field has been extended to include electrostatic terms on the metal and directly coordinating ligand. The charges on the other atoms were not included as this was a preliminary study to investigate whether a transferable force field could be developed to include an electrostatic potential.

6.2. Theory

The general form for the total strain energy is,

$$E_{tot} = E_{str} + E_{bend} + E_{tor} + E_{vdw} + CLFSE + E_{el} \qquad (6.2)$$

The terms in equation 6.2 refer to the bond stretching, angle bending, torsional, non-bonding, CLFSE, and electrostatic interactions, respectively. The first six terms have been described elsewhere[1] and the E_{el} term is given in equation 6.3.

$$E_{el} = q_i q_j / r_{ij} \qquad (6.3)$$

Readers may note that the dielectric constant term has not been included in the calculation of E_{el}, this is because that the in house program DOMMINO[20] was initially written with the intention that all complexes with all solvent molecules would be modelled. Thus, as the medium in which the molecule is in is explicitly included in the calculations, i.e. all the interactions between the solute and the solvent are taken account of, then it is not necessary for a dielectric constant to be defined.

In the calculations carried out here, a dielectric constant was not categorically expressed, even though solvent molecules were omitted from the calculations. Thus, it may be assumed that $\varepsilon = 1$. This is necessary so as to ensure that the units of E_{el} may be expressed in terms of kcal/mol.

However, if one required the incorporation of a dielectric constant in this program, then it could be inserted implicitly by letting the value of q_i, for example, be given by

$$q_i = q_i'/\sqrt{\varepsilon} \qquad (6.4)$$

and similarly,

$$q_j = q_j'/\sqrt{\varepsilon} \qquad (6.5)$$

then in the program

$$E_{el} = q_i q_j / r_{ij} = q_i'/\sqrt{\varepsilon} \times q_j'/\sqrt{\varepsilon} \times 1/r_{ij} = q_i' q_j' / \varepsilon r_{ij} \qquad (6.6)$$

After analysis of other Molecular Mechanics procedures which include electrostatics[11], and discussion with T. W. Hambley, arbitrary values for q_i and q_j were chosen in these studies. It is also worth noting that as long as the force field as a whole is able to determine the molecular properties required, then the individual components (e.g. electrostatics) need have no physical relevance themselves.

6.3. Computational Details

The in-house Molecular Mechanics program DOMMINO was used to compute the structures of 46 compounds displayed schematically in Figure 6.3 and listed in Table 6.1.

Table 6.1

	Formula	Ligand name	CSD Refcode
I	$[Ni(NH_3)_6]^{2+}$		
II	$[Ni(en)_3]^{2+}$	ethylenediamine	ENIACH
III	$[Ni(tn)_3]^{2+}$	1,3-diaminopropane	DAMPNI
IV	$[Ni(dien)_2]^{2+}$	diethylenetriamine	AEAMNI10
V	$[Ni(dptn)_2]^{2+}$	di(3-aminopropyl)amine	AMPRNI10
VI	$[Ni(tcn)_2]^{2+}$	1,4,7-triazacyclononane	BAZNNI
VII	$[Ni(en)_2]^{2+}$	ethylenediamine	EANBAG01
VIII	$[Ni(tmc)]^{2+}$	tetra-*N*-methylcyclam	DITMUO
IX	$[Ni(meso14ane)]^{2}$	[7R(S),14S(R)]-5,5,7,12,12,13-hexamethyl-1,4,8,11-tetraazacyclotetradecane	MAZNIA
X	$[Ni(B\text{-}12\text{-}ane\ N_4)]^{2+}$	1,4,7,10-tetraazabicyclo[8,2,2]tetradecane	GALZUO
XI	$[Cu(NH_3)_6]^{2+}$		
XII	$[Cu(en)_3]^{2+}$	ethylenediamine	CUENCL
XIII	$[Cu(tcn)_2]^{2+}$	1,4,7-triazacyclononane	DUSJAC01
XIV	$[Cu(dien)_2]^{2+}$	diethylenetriamine	ETACUB
XV	$[Cu(tach)_2]^{2+}$	triaminocyclohexane	TACCUP
XVI	$[Cu(papd)]^{2+}$	2,5,8,11,14-pentaazapentadecane	LATSII
XVII	$[Cu(apt)]^{2+}$	1,4-di(3-aminopropyl)-1,4,7-triazacyclononane	JIBZUP
XVIII	$[Cu(adt)]^{2+}$	N,N-bis(2aminoethyl)diethylenetriamine)	TENCUB
XIX	$[Cu(en)_2]^{2+}$	ethylenediamine	CEDHAU
XX	$[Cu(tn)_2]^{2+}$	1,3-diaminopropane	DAPRCU
XXI	$[Cu(dmed)_2]^{2+}$	(N,N-dimethylaminoethyl)amine	DMEDCU
XXII	$[Cu(med)_2]^{2+}$	N-methylethylenediamine	CMENOX
XXIII	$[Cu(nen)_2]^{2+}$	N-ethylethylenediamine	ETEACU
XXIV	$[Cu(deen)_2]^{2+}$	N,N-diethylethylenediamine	CEFBEU
XXV	$[Cu(chd)_2]^{2+}$	1,3-diaminocyclohexane	CHXCUA
XXXIII	$[Ni(mesoane)Cl_2]$	meso-((7R(S),14S(R)-5,5,7,12,12,14-hexamethyl-1,4,8,11-tetra- azacyclotetradecane N',N'',N''',N'''')	MAZNIB
XXXIV	$[Ni(taz)Cl_2]$	1,4,8,11-tetra-azacyclotetradecane	TAZDNC01
XXXV	$Ni(15\text{-}ane)Cl_2]$	1,4,8,12-tetra-azacyclopentadecane	DITVEH
XXXVI	$[Ni(dit)Cl_2]$	1,5,9,13-tetra-azacyclohexadecane	DITVIL
XXXVII	$[Ni(tact)Cl_2]$	1,4,7,10-tetra-azacyclotetradecane	BOZZIZ
XXXVIII	$[Ni(pypz)_2]^{2+}$	2,6-bis(Pyrazol-1-yl-methyl)pyridine-N,N'N''	FILYOO
XXXIX	$[Ni(imid)_6]^{2+}$	Imidazole	HIMZNI
XL	$[Ni(bipy)_3]^{2+}$	2,2'-Bipyridyl	BPYNIS
XLI	$[Ni(terpy)_2]^{2+}$	2,2',2''-Terpyridyl	BIKJUA
XLII	$[Ni(dipa)_2]^{2+}$	Di-2-pyridylmethanamine	JUNCOK
XLIII	$[Ni(pyraz)_2]^{2+}$	pyrazole	PYZNIN
XLIV	$[Cu(mepy)_3]^{2+}$	2-(Aminomethyl)pyridine-N,N'	SITBUS
XLV	$[Cu(dipa)_2]^{2+}$	Di-2-pyridylmethanamine	JUNDAX
XLVI	$[Cu(bipy)_3]^{2+}$	2,2'-Bipyridyl	TBPYCU
XLVII	$[Cu(pzme)_2]^{2+}$	tris(Pyrazol-1-yl)methane-N,N',N''	SUHCAZ
XLVIII	$[Cu(imid)_6]^{2+}$	Imidazole	IMZCUN
XLIX	$[Cu(terpy)_2]^{2+}$	2,2',2''-Terpyridyl	SIBWEF
L	$[Cu(bipy)_2NH_3]^{2+}$	2,2'-Bipyridyl	ABPYCU
LI	$[Cu(imid)_4]^{2+}$	Imidazole	TIMZCU
LII	$[Cu(aepy)_2]^{2+}$	2-(2-Aminoethyl)pyridine	CUAEPP10
LIII	$[Cu(bipy)_2]^{2+}$	2,2'-Bipyridyl	BPYCUP

Figure 6.3. A schematic diagram of the complexes studied

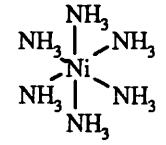

I

II

III

IV

V

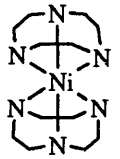

VI

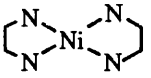

VII

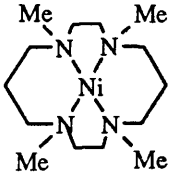

VIII

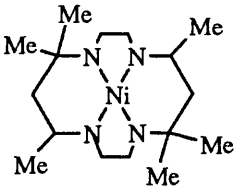

IX

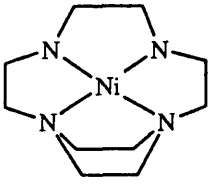

X

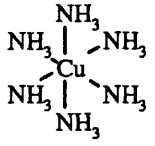

XI

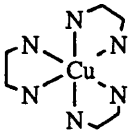

XII

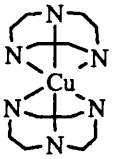

XIII

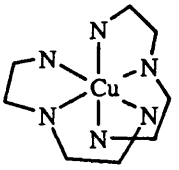

XIV

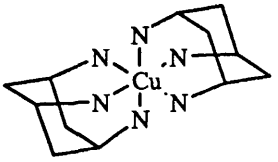

XV

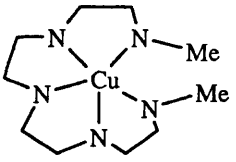

XVI

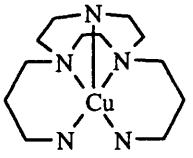

XVII

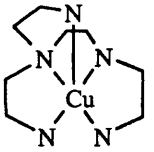

XVIII

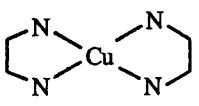

XIX

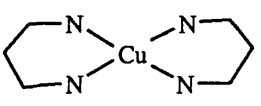

XX

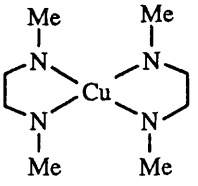

XXI

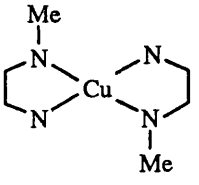

XXII

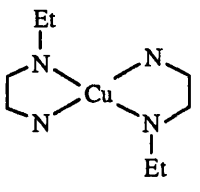

XXIII

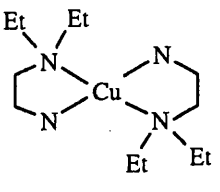

XXIV

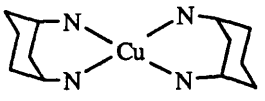

XXV

Figure 6.3 (cont)

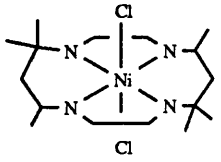

XXXIII

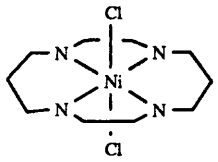

XXXIV

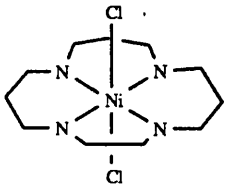

XXXV

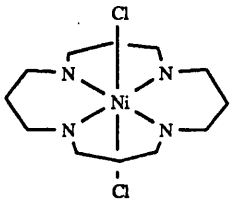

XXXVI

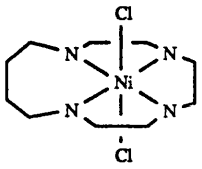

XXXVII

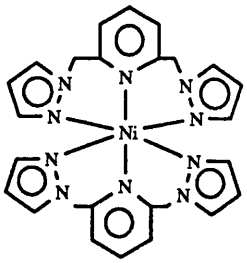

XXXVIII

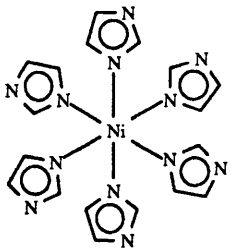

XXXIX

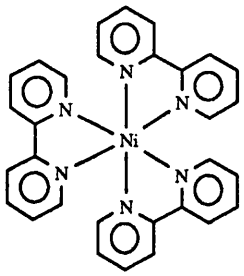

XL

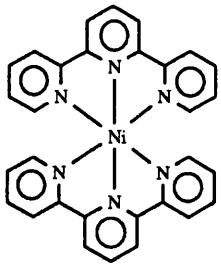

XLI

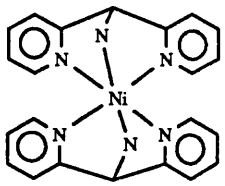

XLII

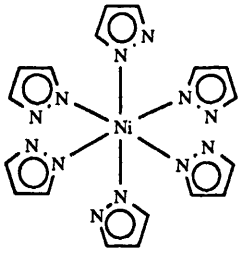

XLIII

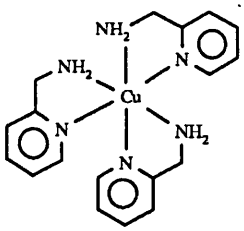

XLIV

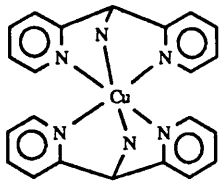

XLV

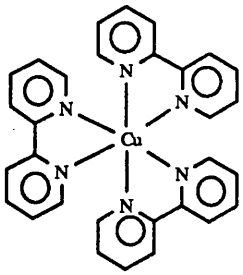

XLVI

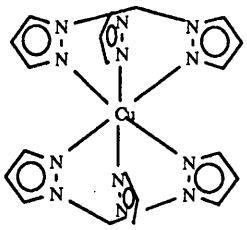

XLVII

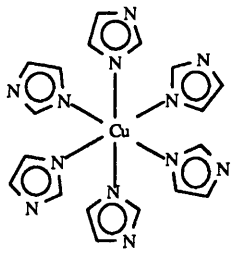

XLVIII

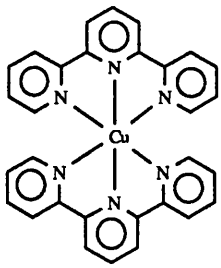

XLIX

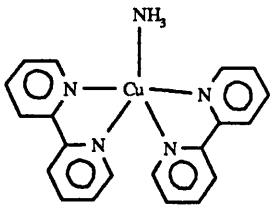

L

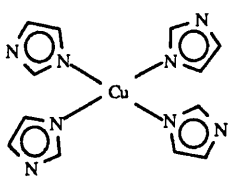

LI

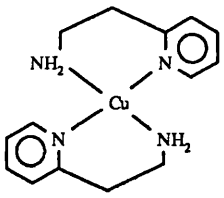

LII

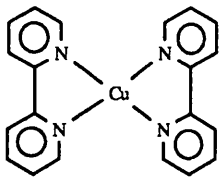

LIII

Table 6.1 also gives the ligand abbreviations and their full names. Initial structures used for minimisation were obtained from the Cambridge Structural Database[21] (where relevant).

A full listing of the force field parameters are given in the Appendix.

6.4. Results and Discussion.

The complexes shown in Figure 6.3 have been divided into several related sets which are discussed in turn below. The 'organic' connections between donor atoms or groups are generally some linkage of saturated carbon atoms.

6.4.1. Ni(II) Amine Complexes I-X

For the ten Ni(II) complexes, the average observed and calculated bond lengths and angles are given in Table 6.2 and where possible compared with the results from the conventional Molecular Mechanics treatment of Hancock[22].

Table 6.2

	$[Ni(NH_3)_6]^{2+}$ (I)		$[Ni(en)_3]^{2+}$ (II)			$[Ni(tn)_3]^{2+}$ (III)		
	calc	*obs*	calc	*obs*	Han	calc	*obs*	Han
Ni-N (Å)	2.15	*2.13*	2.14	*2.13*	2.12	2.15	*2.15*	2.15
average	90.0	*90.0*	90.2	*81.9*	84.3	85.5	*86.9*	85.1
N-Ni-N (°)	180.0	*180.0*	171.6	*171.8*		175.1	*175.8*	

	$[Ni(dien)_2]^{2+}$ (IV)			$[Ni(dptn)_2]^{2+}$ (V)			$[Ni(tcn)_2]^{2+}$ (VI)		
	calc	*obs*	Han	calc	*obs*	Han	calc	*obs*	Han
Ni-N (Å)	2.07	*2.06*	2.05	2.17	*2.23*	2.20	2.10	*2.11*	2.09
	2.17	*2.15*	2.16	2.10	*2.15*	2.11			
average	83.0	*81.6*	82.9	89.3	*90.4*	91.2	82.1	*82.6*	82.6
N-Ni-N (°)	166.9	*167.3*		176.0	*176.4*		177.4	*177.1*	

Table 6.2 (cont)

	$[Ni(en)_2]^{2+}$ (VII)			$[Ni(tmc)]^{2+}$ (VIII)		
	calc	*obs*	Han	calc	*obs*	Han
Ni-N (Å)	1.91	*1.92*	1.92	1.95	*1.98*	1.97
average N-Ni-N (°)	86.8 179.7	*86.4* *180.0*	88.5 180.0	90.7 167.1	*90.6* *168.6*	86.4 166.0
	$[Ni(meso14ane)]^{2+}$ (IX)			$[Ni(B\text{-}12\text{-}aneN_4)]^{2+}$ (X)		
	calc	*obs*	Han	calc	*obs*	Han
Ni-N (Å)	1.96	*1.96*	1.96	1.83	*1.87*	1.86
average N-Ni-N (°)	90.0 180.0	*90.0* *180.0*	90.0 180.0	89.8 170.9	*89.7* *169.1*	

The rms errors for these data and for the M-N-C and 'organic' part of the molecule (excluding and terms which include hydrogen) have been placed in the Supplementary Data, Tables S6.1 and S6.2.

When considering the metal coordination environment, the performance of the CLFSE/MM method with charges remains at least as good as conventional Molecular Mechanics. The rms errors in bond lengths and bond angles are only 0.021 Å and 2.968 ° respectively.

As with previous work[1], a transferable force field has been achieved for both high and low spin Ni(II) complexes.

6.4.2. Cu(II) Amine Complexes XI-XXV

In this study the structures of five 6-coordinate (**XI-XV**), three 5-coordinate (**XVI-XVIII**) and seven 4-coordinate (**XIX-XXV**) Cu(II) complexes were determined. The average observed and calculated bond lengths and angles are given in Tables 6.3, 6.4 and 6.5, and the rms errors for these data, and for the M-N-C and 'organic' part of the molecules is given in the Supplementary Data, Tables S6.3 and S6.4.

Table 6.3

	$[Cu(NH_3)_6]^{2+}$ (XI)		$[Cu(en)_3]^{2+}$ (XII)		$[Cu(tcn)_2]^{2+}$ (XIII)	
	calc	*obs*	calc	*obs*	calc	*obs*
Cu-N (Å)	2.58	*2.45*	2.48	*2.49*	2.34	*2.34*
	2.13	*2.15*	2.48	*2.33*	2.34	*2.30*
			2.17	*2.11*	2.17	*2.08*
			2.17	*2.09*	2.06	*2.06*
			2.13	*2.06*	2.18	*2.05*
			2.12	*1.91*	2.06	*2.05*
average						
N-Cu-N (°)	90.0	*90.0*	75.8	*80.7*	78.6	*81.3*
	180.0	*180.0*	167.5	*168.9*	178.4	*178.2*

	$[Cu(dien)_2]^{2+}$ (XIV)		$[Cu(tach)_2]^{2+}$ (XV)	
	calc	*obs*	calc	*obs*
Cu-N (Å)	2.46	*2.46*	2.36	*2.35*
	2.41	*2.35*	2.09	*2.07*
	2.25	*2.13*		
	2.25	*2.07*		
	2.12	*2.04*		
	2.06	*2.03*		
average				
N-Cu-N (°)	77.1	*80.6*	87.8	*87.0*
	159.6	*166.1*		

Table 6.4

	$[Cu(papd)]^{2+}$ (XVI)		$[Cu(apt)]^{2+}$ (XVII)		$[Cu(adt)]^{2+}$ (XVIII)	
	calc	*obs*	calc	*obs*	calc	*obs*
Cu-N (Å)	2.01	*2.01*	2.03	*2.03*	1.99	*2.01*
	2.05	*2.03*	2.09	*2.06*	2.23	*2.09*
	2.38	*2.16*	2.26	*2.25*	2.34	*2.09*
	2.02	*2.02*	2.07	*2.08*	2.08	*2.04*
	2.19	*2.09*	2.07	*2.03*	2.07	*2.01*
average						
N-Cu-N (°)	836.	*84.5*	91.3	*90.3*	83.5	*86.4*
	114.9	*104.9*	110.7	*101.6*	111.3	*116.7*
	114.6	*111.8*	80.5	*81.5*	78.2	*83.2*
	165.2	*167.8*	116.9	*172.9*	128.2	*128.3*
	84.8	*85.1*	84.1	*86.3*	80.8	*86.2*
	78.4	*84.9*	80.6	*84.0*	113.2	*113.1*
	83.2	*84.4*	93.2	*87.8*	83.9	*84.1*
	136.5	*140.2*	175.2	*173.2*	164.3	*169.6*
	108.5	*108.0*	96.2	*105.2*	115.3	*105.0*
	99.0	*99.6*	91.8	*94.9*	99.7	*96.3*

Table 6.5

	$[Cu(en)_2]^{2+}$ (XIX)		$[Cu(tn)_2]^{2+}$ (XX)		$[Cu(dmed)_2]^{2+}$ (XXI)		$[Cu(med)_2]^{2+}$ (XXII)	
	calc	*obs*	calc	*obs*	calc	*obs*	calc	*obs*
Cu-N (Å)	2.04	*2.02*	2.03	*2.04*	2.05	*2.06*	2.01 2.05	*2.01* *2.06*
average N-Cu-N (°)	83.1 180.0	*84.1* *180.0*	87.0 180.0	*86.7* *180.0*	84.3 169.6	*85.3* *180.0*	84.1 179.9	*85.9* *180.0*
	$[Cu(nen)_2]^{2+}$ (XXIII)		$[Cu(deen)_2]^{2+}$ (XXIV)		$[Cu(chn)_2]^{2+}$ (XXV)	
	calc	*obs*	calc	*obs*	calc	*obs*
Cu-N (Å)	2.01 2.05	*2.01* *2.03*	1.98 2.08	*2.01* *2.08*	2.01	*2.02*
average N-Cu-N (°)	84.2 180.0	*85.0* *180.0*	84.7 180.0	*84.9* *180.0*	86.4 180.0	*87.6* *180.0*

When comparing the calculated and observed bond lengths for the six- and five-coordinate complexes, then it may be observed that there is not as good agreement, as in the case of the Ni(II) complexes. However, as noted in Chapter 4 copper(II) complexes are notoriously 'plastic'[23], i.e. that relatively subtle changes in crystal packing forces may have a critical influence on the geometry of the complex[24].

Thus, unless the calculations explicitly include the effects of the surrounding lattice, one cannot expect to get exact agreement.

The six-coordinate complexes are also subject to Jahn Teller distortions. It can be seen that tetragonally elongated structures have automatically been calculated for four out of the five complexes. The worst case is for the $[Cu(dien)_2]^{2+}$ where a rhombic structure has been determined.

The four-coordinate species, being at the limit of tetragonal elongation, are less 'plastic' and thus the calculated structures are a good reproduction of the observed structures. The worst case being $[Cu(dmed)_2]^{2+}$ which shows excellent agreement for the Cu-N distances (observed 2.06 Å , calculated 2.05 Å), but the bond angles are underestimated by approximately 10°, the structure being slightly distorted from square planar.

6.4.3. Mixed Chloro/Amine Complexes [Ni(II)N_4Cl_2]

Table 6.6 shows the comparison of observed and calculated bond length and bond angles for the five Ni(II) complexes studied, **XXXIII-XXXVII**. The Supplementary Data, Table S6.5 and S6.6 display the rms errors for the M-N-C angles and the 'organic' part of the molecule.

Table 6.6

	[Ni(mesoane)Cl_2] (XXXIII)		[Ni(taz)Cl_2] (XXXIV)	
	calc	*obs*	calc	*obs*
Ni-Cl	2.53	*2.56*	2.51	*2.51*
Ni-N	2.10	*2.10*	2.06	*2.07*
	2.06	*2.06*		
N-Ni-Cl	90.0	*90.0*	90.0	*90.0*
N-Ni-N	90.0	*90.0*	90.0	*90.0*
	180.0	*180.0*	180.0	*180.0*
Cl-Ni-Cl	179.9	*180.0*	180.0	*180.0*

	[Ni(15-ane)Cl_2] (XXXV)		[Ni(dit)Cl_2] (XXXVI)		[Ni(tact)Cl_2] (XXXVII)	
	calc	*obs*	calc	*obs*	calc	*obs*
Ni-Cl	2.47	*2.50*	2.46	*2.54*	2.52	*2.55*
			2.40	*2.43*		
Ni-N	2.11	*2.10*	2.31	*2.21*	2.05	*2.06*
	2.18	*2.12*	2.17	*2.19*	2.08	*2.08*
			2.21	*2.14*		
			2.21	*2.14*		
N-Ni-Cl	90.0		90.1	*90.1*	90.1	*90.1*
N-Ni-N	90.1		9.0	*90.0*	90.6	*90.7*
	174.1		174.5	*172.8*	163.2	*161.7*
Cl-Ni-Cl	178.5		175.8	*172.9*	174.5	*177.6*

Excellent agreement between experimentally observed structures and the computationally determined structures is achieved, the rms errors in bond lengths and angles being only 0.029 Å and 1.332° respectively.

It should be noted that the force field which has calculated $[NiCl_4]^{2-}$ to have an average Ni-Cl bond length of 2.29 Å (compared with an experimental Ni-Cl average of 2.25 Å) can also compute Ni-Cl distances in complexes **XXXIII-XXXVII** between 2.40 and 2.53 Å. For the NiN_4Cl_2 species, the longer values of the Ni-Cl bond, reflects the intramolecular interactions between the axial Cl and the ring systems, whereas the Ni-Cl distance in $[NiCl_4]^{2-}$ represents the notional 'strain free' Ni-Cl contact.

Thus, by inclusion of electrostatic interactions, a transferable force field for Ni-Cl, which had previously been unobtainable[19], has been achieved.

6.4.4. Ni(II) and Cu(II) Imine and Mixed Amine/Imine Complexes: XXXVIII-LIII

Six Ni(II)N_6 complexes, six 6-coordinate Cu(II) species, one 5-coordinate plus three 4-coordinate Cu(II) compounds have been structurally determined. The observed and calculated metal-ligand bond lengths and ligand-metal-ligand angles have been reported, for all of these, in Tables 6.7, 6.8 and 6.9 respectively. As before, relevant rms errors for these data and the remaining 'organic' part of the molecule, are in the Supplementary Data, Tables S6.7-S6.10.

Table 6.7

	$[Ni(pypz)_2]^{2+}$ (XXXVIII)		$[Ni(imid)_6]^{2+}$ (XXXIX)		$[Ni(bipy)_3]^{2+}$ (XL)	
	calc	*obs*	calc	*obs*	calc	*obs*
Ni-N_{py}	2.19	*2.16*			2.12	*2.09*
Ni-N_{pz}	2.10	*2.08*	2.13	*2.13*		
av N-Ni-N	90.0	*90.0*	90.0	*90.2*	90.1	*90.2*
	178.4	*177.7*	180.0	*180.0*	173.7	*169.7*

	$[Ni(terpy)_2]^{2+}$ (XLI)		$[Ni(dipa)_2]^{2+}$ (XLII)		$[Ni(pyraz)_6]^{2+}$ (XLIII)	
	calc	*obs*	calc	*obs*	calc	*obs*
Ni-N_{py}	2.18	*2.13*	2.12	*2.11*		
	2.03	*2.02*				
Ni-N_{am}			2.13	*2.11*		
Ni-N_{pz}					2.13	*2.13*
av N-Ni-N	90.7	*90.4*	90.3	*90.0*	90.0	*90.0*
	165.6	*163.2*	180.0	*180.0*	180.0	*180.0*

Table 6.8

	$[Cu(mepy)_3]^{2+}$ (XLIV)		$[Cu(dipa)_2]^{2+}$ (XLV)		$[Cu(bipy)_3]^{2+}$ (XLVI)	
	calc	*obs*	calc	*obs*	calc	*obs*
$Cu\text{-}N_{am}$	2.20	*2.05*	2.01	*2.02*		
	2.01	*2.01*				
	2.05	*2.04*				
$Cu\text{-}N_{py}$	2.20	*2.06*	2.19	*2.02*	2.42	*2.45*
	2.48	*2.44*	2.49	*2.54*	2.42	*2.23*
	2.46	*2.42*			2.12	*2.03*
					2.09	*2.03*
					2.06	*2.03*
					2.09	*2.03*
N-Cu-N	171.7	*166.4*	73.5	*72.2*	77.6	*78.2*
	94.1	*96.0*	82.1	*86.4*	90.1	*101.6*
	92.9	*89.5*	106.5	*107.8*	96.2	*99.5*
	94.9	*96.1*	98.0	*93.6*	90.3	*92.4*
	74.3	*73.0*	79.5	*79.8*	91.	*91.6*
	92.1	*90.1*	106.5	*107.8*	96.4	*99.1*
	94.1	*103.9*	100.2	*100.2*	95.7	*94.4*
	79.8	*80.5*	97.9	*93.6*	84.8	*73.9*
	99.7	*94.3*	100.2	*100.2*	96.4	*94.1*
	72.1	*75.2*	73.5	*72.2*	92.8	*93.6*
	167.9	*163.8*	82.1	*86.4*	92.7	*92.2*
	93.4	*95.8*	79.4	*79.8*	78.	*80.4*
	99.4	*94.2*	180.0	*180.0*	170.7	*174.8*
	162.7	*159.6*	180.0	*180.0*	173.4	*174.2*
	96.7	*98.1*	180.0	*180.0*	173.8	*165.6*
	$[Cu(pzme)_2]^{2+}$ (XLVII)		$[Cu(imid)_6]^{2+}$ (XLVIII)		$[Cu(terpy)_2]^{2+}$ (XLIX)	
	calc	*obs*	calc	*obs*	calc	*obs*
$Cu\text{-}N_{pz}$	2.09	*2.00*	2.08	*2.01*		
	2.09	*2.00*	2.08	*2.01*		
	1.97	*2.03*	2.08	*2.05*		
	1.97	*2.03*	2.08	*2.02*		
	2.44	*2.36*	2.55	*2.59*		
	2.44	*2.36*	2.55	*2.59*		
$Cu\text{-}N_{py}$					1.95	*1.98*
					1.95	*1.98*
					2.36	*2.18*
					2.36	*2.18*
					2.36	*2.18*
					2.36	*2.18*
N-Cu-N	84.1	*86.1*	90.0	*88.3*	79.7	*78.9*
	81.5	*81.5*	90.2	*92.1*	91.0	*87.8*
	98.5	*98.5*	90.0	*91.7*	100.1	*100.6*
	96.0	*93.9*	89.8	*87.9*	93.0	*96*
	180.0	*180.0*	90.9	*91.4*	79.6	*78.2*
	85.1	*86.8*	90.2	*92.1*	100.0	*96.8*
	94.9	*93.2*	89.1	*88.6*	100.6	*108.3*
	180.0	*180.0*	90.9	*91.4*	93.1	*97*
	95.9	*93.9*	90.0	*88.3*	100.6	*102.3*
	180.0	*180.0*	89.1	*88.6*	90.3	*89.2*
	94.5	*93.2*	90.0	*91.7*	79.7	*77.4*
	98.4	*95.5*	89.8	*87.9*	79.7	*77.5*
	85.1	*86.8*	180.0	*180.0*	157.3	*157.1*
	81.6	*81.5*	180.0	*180.0*	159.3	*154.9*
	84.0	*86.1*	180.0	*180.0*	179.6	*174.2*

Table 6.9

	$[Cu(bipy)_2NH_3]^{2+}$ (L)		$[Cu(imid)_4]^{2+}$ (LI)		$[Cu(aepy)_2]^{2+}$ (LII)		$[Cu(bipy)_2]^{2+}$ (LIII)	
	calc	*obs*	calc	*obs*	calc	*obs*	calc	*obs*
$Cu\text{-}N_{am}$	2.35	*2.05*			1.99	*2.01*		
$Cu\text{-}N_{py}$	1.92	*2.05*			2.05	*2.02*	1.96	*1.97*
	1.92	*1.98*					1.96	*1.99*
	2.23	*2.11*					2.08	*1.99*
	2.22	*2.07*					2.08	*2.03*
$Cu\text{-}N_{pz}$			1.97	*2.01*				
N-Cu-N	90.6	92.7	90.0	88.4	87.6	86.6	87.0	83.6
	121.1	129.5	90.0	88.4	87.6	86.6	97.0	102.3
	119.5	122.3	90.0	91.6	92.4	93.4	163.9	160.9
	90.7	91.5	90.0	91.6	92.4	93.4	151.2	151.1
	84.5	79.4	180.0	180.0	180.0	180.0	97.0	102.4
	94.8	98.0	180.0	180.0	180.0	180.0	87.0	81.3
	178.7	175.8						
	119.4	108.3						
	94.9	97.9						
	84.5	79.6						

N_{am} is amine N
N_{pz} is N in a five membered ring
N_{py} is N in a six membered ring

Good agreement is illustrated for all of the Ni(II) complexes (Table 6.7), the worst case being $[Ni(terpy)_2]^{2+}$, (**XLI**), where the Ni-N bond length is overestimated by 0.05 Å. Overall, the average rms errors for **XXXVIII-XLIII** are only 0.016 Å and 1.921° for the Ni-N distances and N-Ni-N angles respectively.

On analysis of the results for the six-coordinate Cu(II) complexes, (Table 6.8), it can be seen that the Jahn Teller distortion had been predicted in all cases. However, for $[Cu(mepy)_3]^{2+}$ a rhombic structure has been determined. Also, for $[Cu(terpy)_2]^{2+}$, a compressed structure has been calculated. The experimental structure also appears to be compressed in the solid state. However, low temperature Electron Spin Resonance measurements indicate that the true structure is in fact tetragonally elongated. This has been discussed previously[19], and it was hoped that the inclusion of the electrostatic terms would have been sufficient to overcome the rigidity of the terpy ligand which tends to compress the structure. However, this has obviously not been successful.

The charges included in the calculation were only those of the Cu and the N, thus extension of this force field to include charges on all atoms may then be able to reproduce the structure of $[Cu(mepy)_3]^{2+}$ and $[Cu(terpy)_2]^{2+}$ more accurately.

The five-coordinate complex $[Cu(bipy)_2NH_3]^{2+}$ displays an approximately trigonal bipyramidal (TBP) structure, in agreement with experiment. In previous calculations[19], a square based pyramidal (SBP) geometry was ascertained. Thus, the inclusion of the Coulombic term, in this case, has obviously favoured the TBP formation over the SBP. This is also supported by calculations (including charges) on 'bare' ligand systems of CuN_5. Here the SBP structure is calculated to have Cu-N_{ax} = 2.76 Å, Cu-N_{eq} = 2.30 Å and energy = 137.17 kcal/mol, whereas the TBP structure is calculated to have Cu-N_{ax} = 2.17 Å, Cu-N_{eq} = 2.57 Å and energy = 135.24 kcal/mol. Thus, it can be seen that the stereochemical activity of the d electrons is still reproduced, and the delicate energy balance between the two stereochemistries is also maintained by the inclusion of charges. However, the TBP geometry is calculated to be at a slightly lower energy than the SBP.

The 4-coordinate complexes are very well reproduced. Here the incorporation of charges has allowed the distortion from square planar to be observed for the $[Cu(bipy)_2]^{2+}$ while the $[Cu(imid)_4]^{2+}$ and the $[Cu(aepy)_2]^{2+}$ remain rigorously square planar. The average rms errors for the Cu-N bond lengths and N-Cu-N angles are 0.04 Å and 2.137 ° respectively.

6.5. Conclusions

The CLFSE/MM method has successfully been extended to include an electrostatic term in its force field. As a preliminary step, charges for only the direct coordination sphere of the metal were included.

The calculated geometries for Ni(II) amines, Cu(II) amines and Ni(II)N_4Cl_2 complexes were in good agreement with experiment, the inclusion of charges to the force field

having no adverse effect on the determination of structures relative to the previous force field.

The structures of the imine and imine/amine Ni(II)N_6 complexes are also modelled accurately. The Cu(II) coordination sphere, exhibiting 'plasticity', does not have such good reproducibility. However the Jahn Teller elongations for four of the six CuN_6 species were automatically generated. The five-coordinate complex was well treated, and two of the three 4-coordinate geometries exhibited the required square planar geometry. The structure of $[Cu(bipy)_2]^{2+}$ correctly displayed the observed distorted structure. This leaves only two structures, $[Cu(mepy)_3]^{2+}$ and $[Cu(terpy)_2]^{2+}$, where an improvement of the force field is desired.

Overall, the inclusion of an electrostatic term to the MM/CLFSE method had proved most successful. The extension of this force field to incorporate charges for all atoms, as opposed to charges on just the metal and directly coordinating ligands, would be the next natural progression.

6.6. Supplementary Data

Table S6.1. Rms Ni-N and N-Ni-N errors

structure		bond lengths rms difference / (Å)	angles rms difference / (°)
$[Ni(NH_3)_6]^{2+}$	I	-----	-----
$[Ni(en)_3]^{2+}$	II	0.017	5.600
$[Ni(tn)_3]^{2+}$	III	0.023	5.444
$[Ni(dien)_2]^{2+}$	IV	0.029	4.751
$[Ni(dptn)_2]^{2+}$	V	0.034	1.924
$[Ni(tcn)_2]^{2+}$	VI	0.008	2.350
$[Ni(en)_2]^{2+}$	VII	0.010	0.876
$[Ni(tmc)]^{2+}$	VIII	0.057	2.300
$[Ni(meso14ane)]^{2+}$	IX	0.0000	1.064
$[Ni(B\text{-}12\text{-}aneN_4)]^{2+}$	X	0.009	2.401
average rms error		0.021	2.968

Table S6.2. Rms errors for rest of molecule (excluding H atoms).

	II	III	IV	V	VI
Metal					
Ni-N-C	1.628	2.598	1.266	1.886	1.026
rms error (°)					
'Organic' rms errors					
bond lengths (Å)	0.017	0.017	0.022	0.017	0.020
angles (°)	1.117	1.860	2.148	2.695	2.102

	VII	VIII	IX	X
Metal				
Ni-N-C				
rms error (°)	1.500	3.569	2.019	5.744
'Organic' rms errors				
bond lengths (Å)	0.017	0.014	0.015	0.027
angles (°)	0.600	1.848	1.687	2.734

Table S6.3. Rms Cu-N and N-Cu-N errors

structure		bond lengths rms difference / (Å)	angles rms difference / (°)
$[Cu(NH_3)_6]^{2+}$	XI	-----	-----
$[Cu(en)_3]^{2+}$	XII	0.117	3.241
$[Cu(tcn)_2]^{2+}$	XIII	0.065	2.187
$[Cu(dien)_2]^{2+}$	XIV	0.107	4.945
$[Cu(tach)_2]^{2+}$	XV	-----	-----
$[Cu(papd)]^{2+}$	XVI	0.059	5.454
$[Cu(apt)]^{2+}$	XVII	0.023	5.120
$[Cu(adt)]^{2+}$	XVIII	0.132	4.874
$[Cu(en)_2]^{2+}$	XIX	0.003	0.816
$[Cu(tn)_2]^{2+}$	XX	0.014	0.248
$[Cu(dmed)_2]^{2+}$	XXI	0.000	6.150
$[Cu(med)_2]^{2+}$	XXII	0.000	1.470
$[Cu(nen)_2]^{2+}$	XXIII	0.001	0.653
$[Cu(deen)_2]^{2+}$	XXIV	0.002	0.168
$[Cu(chn)_2]^{2+}$	XXV	0.001	0.898
average rms error		0.040	2.786

Table S6.4. Rms errors for rest of molecule (excluding H atoms).

	XII	XIII	XIV	XV	XVI
Metal					
Cu-N-C					
rms error (°)	6.502	4.050	4.100	-----	2.341
'Organic' rms errors					
bond lengths (Å)	-----	0.017	0.035	-----	0.020
angles (°)	-----	2.354	2.612	-----	1.779

	XVII	XVIII	XIX	XX	XXI
Metal					
Cu-N-C					
rms error (°)	6.294	2.337	1.492	2.316	2.373
'Organic' rms errors					
bond lengths (Å)	0.024	0.036	0.057	0.009	0.013
angles (°)	2.980	2.845	2.110	0.581	2.721

	XXII	XXIII	XXIV	XXV
Metal				
Cu-N-C				
rms error (°)	1.194	1.173	3.404	1.802
'Organic' rms errors				
bond lengths (Å)	0.014	0.016	0.019	0.016
angles (°)	2.723	2.618	1.639	1.777

Table S6.5. Rms Ni-L and L-Ni-L errors (where L = N, Cl)

structure		bond lengths rms difference / (Å)	angles rms difference / (°)
[Ni(mesoane)Cl_2]	XXXIII	0.017	0.544
[Ni(taz)Cl_2]	XXXIV	0.008	1.424
[Ni(15-ane)Cl_2]	XXXV	------	-----
[Ni(dit)Cl_2]	XXXVI	0.068	1.770
[Ni(tact)Cl_2]	XXXVII	0.021	1.593
average rms error		0.029	1.332

Table S6.6. Rms errors for rest of molecule (excluding H atoms).

	XXXIII	XXXIV	XXXV	XXXVI	XXXVII
Metal					
Ni-N-C					
rms error (°)	2.550	0.541	------	3.088	1.643
'Organic' rms errors					
bond lengths (Å)	0.015	0.005	------	0.015	0.030
angles (°)	1.702	0.828	------	2.017	3.103

Table S6.7. Rms M-N and N-M-N errors

structure		bond lengths rms difference / (Å)	angles rms difference / (°)
$[Ni(pypz)_2]^{2+}$	XXXVIII	0.024	2.501
$[Ni(imid)_6]^{2+}$	XXXIX	0.006	0.600
$[Ni(bipy)_3]^{2+}$	XL	0.032	2.414
$[Ni(terpy)_2]^{2+}$	XLI	0.018	1.861
$[Ni(dipa)_2]^{2+}$	XLII	0.017	1.503
$[Ni(pyraz)_6]^{2+}$	XLIII	0.000	2.645
$[Cu(mepy)_3]^{2+}$	XLIV	0.087	4.057
$[Cu(dipa)_2]^{2+}$	XLV	0.102	2.336
$[Cu(bipy)_3]^{2+}$	XLVI	0.094	5.518
$[Cu(pzme)_2]^{2+}$	XLVII	0.081	1.218
$[Cu(imid)_6]^{2+}$	XLVIII	0.050	1.341
$[Cu(terpy)_2]^{2+}$	XLIX	0.153	3.363
$[Cu(bipy)_2am]^{2+}$	L	0.191	4.896
$[Cu(imid)_4]^{2+}$	LI	0.041	1.306
$[Cu(aepy)_2]^{2+}$	LII	0.025	0.816
$[Cu(bipy)_2]^{2+}$	LIII	0.054	4.288
average rms error		0.061	2.541

Table S6.8. Rms errors for rest of molecule (excluding H atoms).

	XXXVIII	XXXIX	XL	XLI	XLII	XLIII
Metal						
Ni-N-C						
rms error (°)	3.504	1.506	1.376	3.010	1.679	0.158
'Organic' rms errors						
bond lengths (Å)	0.010	0.019	0.027	0.058	0.029	0.010
angles (°)	3.356	1.984	1.821	3.946	1.229	0.540

Table S6.9. Rms errors for rest of molecule (excluding H atoms).

	XLIV	XLV	XLVI	XLVII	XLVIII	XLIX
Metal						
Cu-N-C						
rms error (°)	1.631	3.611	4.926	1.691	5.522	4.766
'Organic' rms errors						
bond lengths (Å)	0.035	0.011	0.039	0.017	0.033	0.029
angles (°)	1.906	1.760	2.697	1.729	2.223	2.332

Table S6.10. Rms errors for rest of molecule (excluding H atoms).

	L	LI	LII	LIII
Metal				
Cu-N-C				
rms error (°)	5.332	2.048	5.593	3.737
'Organic' rms errors				
bond lengths (Å)	0.033	0.033	0.029	0.056
angles (°)	2.386	1.726	2.283	3.464

6.7. References

1. V. J. Burton, R. J. Deeth, C. M. Kemp and P. J. Gilbert, *J. Am. Chem. Soc.*, 1995, **117**, 8407.
2. P. V. Bernhardt and P. Comba, *Inorg. Chem.*, 1992, **31**, 2638.
3. T. W. Hambley, C. J. Hawkins, J. A. Palmer and M. R. Snow, *Aust. J. Chem.*, 1981, **34**, 45.
4. S. J. Weiner, P. A. Kollman, D. A. Case, E. Singh, C. Ghio and S Proteta, *J. Am. Chem. Soc.*, 1984, **106**, 765.
5. S. Cox and D. E. Williams, *J. Comp. Chem.*, 1981, **2**, 304.
6. R. J. Abraham, L. Griffiths and P. Loftus, *J. Comp. Chem.*, 1982, **3**, 407.
7. R. J. Abraham and B. Hudson, *J. Comp. Chem.*, 1985, **6**, 173.
8. A. Warshel, *J. Phys. Chem.*, 1979, **83**, 1640.
9. D. Hall and N. Pevitt, *J. Comp. Chem.*, 1984, **5**, 441.
10. L. Pauling, *J. Chem. Soc.*, 1948, 1461.
11. T. W. Hambley, *Inorg. Chem.*, 1991, **30**, 937.
12. J. L. Tueting, K. L. Spence and M. Zimmer, *J. Chem. Soc., Dalton Trans.*, 1994, 551.
13. D. Reinen, M. Atanasov, G. S. Nikolov and F. Steffens, *Inorg. Chem.*, 1988, **27**, 1678.
14. P. B Hitchcock, K. R. Seddon and T. Welton, *J. Chem Soc., Dalton Trans.*, 1993, 2639.
15. M. K. Cooper, J. M. Downes, P. A. Duckworth and E. R. T. Tiekink, *Aust . J. Chem.*, 1992, **45**, 595.
16. J. A. Albanese, D. L. Staley, A. L. Rheingold and J. L. Burmeister, *Acta Cryst., C (Cr. Str. Comm.)*, 1989, **45**, 1128.
17. G. D. Stucky, J. B. Folkers and T. J. Kistenmacher, *Acta Cryst.* 1967, **23**, 1064.
18. P. Pauling, *Inorg. Chem.*, 1966, **5**, 1498.
19. R. J. Deeth and V. J. Paget, submitted to *J. Chem. Soc., Dalton Trans.*
20. In-house MM software supplied by Dr. D. J. Osguthorpe, Molecular Graphics Unit, University of Bath, and edited by Dr. R. J. Deeth, Inorganic Computational Chemistry Group, Warwick University.
21. Cambridge Structural Database, Version 4. Cambridge Crystallographic Data Centre, University Chemical Laboratory: Cambridge, 1994.
22. R. D. Hancock, *Prog. Inorg. Chem.*, 1989, **37**, 187, and references therein.
23. J. Gazo, I. B. Bersuker, J. Garaj, M. Kebesova, J. Kohout, H. Langfelderova, M. Melnik, M. Serator and F. Valach, *Coord. Chem. Rev.*, 1976, **19**, 253.
24. F. S. Stephens, *J. Chem. Soc.*, 1969, 2233.

Acknowledgements.

The author wishes to thank Dr. T. W. Hambley, University of Sydney, Australia, for helpful discussions in this area.

Chapter 7

Molecular Modelling of Pt(II) Complexes

7.1. Introduction

Four-coordinate Pt(II) complexes exhibit square planar geometry. A notable characteristic of the chemistry of these species is the substitution reactions of these molecules. Because of the low coordination number these occur almost entirely by associative pathways (Figure 7.1).

Figure 7.1. Associative pathway for substitution reaction of Pt(II) complex.

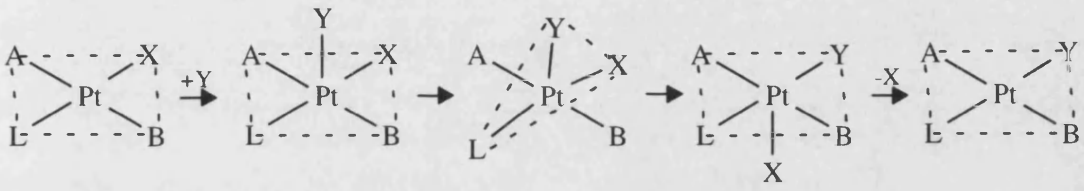

These ligand exchange reactions show distinct preferences for the site trans to one ligand rather than another. This effect of the ligand L on the rate of substitution in the position trans to itself is known as the trans effect.

Another feature usually discussed with respect to Pt(II) square planar complexes is the trans influence. This concept was first introduced by Pidcock et al.[1] and is reviewed by Appleton et al.[2]. It is defined as the extent to which a ligand can influence the strength of the bond that is trans to itself. This is a ground state property and can be evaluated, for example, from M-L bond lengths.

The trans effect is a kinetic phenomenon depending on activation energies, thus stabilities of both the ground state and the activated complex are important, whereas the trans influence is a thermodynamic, ground state property. The explanation of these concepts are not clear cut but it seems that both σ and π effects play a role.

7.1.1. σ Effects.

The length of the bond trans to a ligand L increases as the electronegativity of L decreases. For example, consider a trans L-M-X unit. A less electronegative L increases the electron density on M, and therefore the X to M σ donation is reduced and the X-M bond is weakened.

The polarisability of the ligand L can also have an influence. If L is a polarisable ligand then the metal will induce a dipole as shown in Figure 7.2.

Figure 7.2.

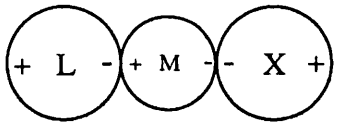

The dipole on M will then oppose the natural dipole of X, and thus weakens the X-M bond.

Both of the above factors are concerned with a ground state bond weakening and refer to the trans influence. However, they still have some relevance to the trans effect. Consider a pair of trans ligands interacting with the same metal orbital in the square planar geometry. On substitution, the reaction is postulated to go through a trigonal bipyramidal transition state, where neither of the ligands X or Y have a direct interaction with the metal orbital. (Figure 7.3.).

Figure 7.3.

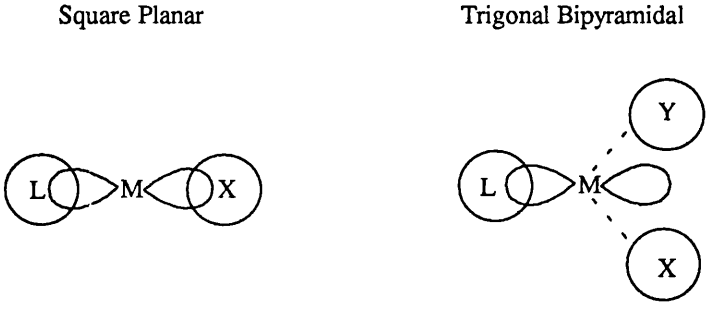

Thus the electronegativity and polarisation effects are going to be smaller in the transition state. Therefore, a ligand which weakens the trans bond in the ground state does not weaken it as much in the transition state and is, in effect, destabilising the ground state relative to the transition state, i.e. labilising the ligand.

7.1.2. π Effects.

Ligands exerting a strong trans effect, e.g. CO, PR_3, are those which are thought to have π acceptor character and thus remove π electron density from the metal. These cause the most significant reduction in electron density at the coordination site directly opposite, i.e. trans, and it is there that the attack of a nucleophile is most likely to take place.

If L and X are both π acceptors, then they will compete for the available d electron density on the metal (Figure 7.5).

Figure 7.5.

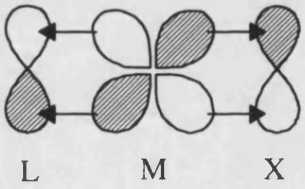

The greater the π acceptor ability of L, the more X is deprived of electron density and the weaker the M-X π bond. This is a ground state effect and can explain bond length variations when both L and X have π orbitals. π effects can also explain lability since a strong π acceptor will remove electron density from the metal, making it more willing to accept a fifth ligand.

7.1.3. Summary.

The trans effect and trans influence are often observed in square planar Pt(II) complexes, though it is not exclusive to these molecules.

This study concentrates on modelling the thermodynamic ground state phenomenon, the trans influence. Molecular Mechanics, as yet, is unable to model transition states so the trans effect is not simulated here, although it may form the basis of future studies.

7.2. Modelling of Pt(II) Complexes using Molecular Mechanics.

Extensive Molecular Mechanics studies of Pt(II) complexes have been carried out in the area of cis-platin binding to DNA[3-7] and other biologically related studies[8-12]. However, in these cases the Pt is usually complexed to four N donors, thus the trans influence does not need to be taken into account. Other studies have included macrocyclic complexes of platinum[13], where the donor atoms are equivalent, thus, again, the trans influence can be ignored.

So far, trans influences have only been simulated by using separate sets of force field parameters for the bonds that are trans to each other[14]. For example, if the system being studied was MX_3Y, in a square planar stereochemistry, then different force field parameters would define the M-X bond trans to Y, and the other M-X bonds. However, this strategy can only work with prior knowledge of the structure to be determined. In this way Molecular Mechanics loses its predictive power.

The only other attempt to model the trans influence has been by Rappé et al.[15]. They used the Universal Force Field to model π back bonding in transition metal complexes by considering the bond order between a metal and a ligand. They suggested that for phosphine ligands, a bond order of 2 should be used for M-P bonds which exhibit insignificant trans influence, but this bond order should be reduced for M-P bonds where there is notable trans influence. However, they have been unable to develop a general method which automatically generates the trans influence.

In this work, the trans influence of some $PtA_xB_yC_z$ systems (where $0 \leq x \leq 4$, $0 \leq y \leq 4$, $0 \leq z \leq 4$, A = Cl, B = S, C = P) were studied. The experimental compounds where

this type of donor system is demonstrated, exhibit Pt-Cl distances in the range of 2.30-2.37 Å, Pt-S distances range from 2.25-2.32 Å and Pt-P distances in the range of 2.22-2.32 Å.

As a preliminary study, only the hypothetical bare ligand systems were modelled to give an indication of the performance of the strategy implemented.

7.3. Theory

The general form of the CLFSE/MM method is,

$$E_{tot} = E_{str} + CLFSE \qquad (7.1)$$

The terms in equation 7.1 refer to the bond stretch and CLFSE interactions respectively, and have been described in chapters 1 and 2. As only bare ligand systems are being studied the other force field terms, the E_{bend}, E_{tors} and E_{vdw} are not required in these calculations.

The role of the CLFSE in the modelling of these systems was to ensure that a square planar geometry was obtained (as mentioned in Chapter 5, the inclusion of the CLFSE favours square planar geometry for 4-coordiante systems over tetrahedral stereochemistry).

To obtain the effect of the trans influence, an A---B Morse function was imposed (where A and B are ligands which are trans to each other). The M-A interaction of a MA_4 square planar complex would usually be described by the CLFSE+Morse function. If a MA_3B species was then studied the M-A distance (when A is trans to B) may differ from the M-A bond length (when A is trans to A) due to the trans influence. To account for this a Morse potential which describes the interactions of ligands trans to each other was introduced. Thus for ligands A in MA_4 an A--A bond stretch potential was introduced and in MA_3B an A--B function was included. In this way the

interaction of M-A in MA_4 can be described differently to that of M-A trans to ligand B in MA_3B.

For example, consider the 'bare' ligand systems in Figure 7.6.

Figure 7.6. The model systems determined using MM.

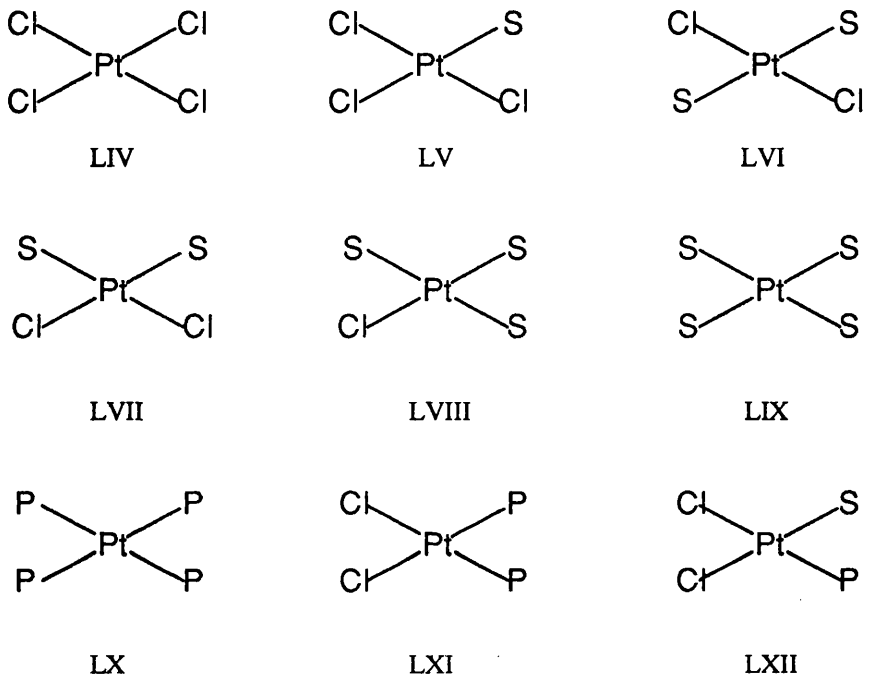

The equivalent experimentally observed structures to which these 'bare' ligand systems are compared are listed in Table 7.1 (overleaf).

Table 7.1.

Number	Calculated system	Experimental complex	Reference
LIV	$Pt(Cl)_4$	$[PtCl_4]^{2-}$	17
LV	$Pt(Cl)_3(S)$	$[PtCl_3(dms)]^-$	18
LVI	trans-$Pt(Cl)_2(S)_2$	trans-$[PtCl_2(dms)_2]$	19
LVII	cis-$Pt(Cl)_2(S)_2$	cis-$[PtCl_2(dms)_2]$	20
LVIII	$Pt(S)_3(Cl)$	$[PtCl(dms)_3]^+$	19
LIX	$Pt(S)_4$	$[Pt(dms)_4]^{2-}$	21
LX	$Pt(P)_4$	[bis(1,2bis(Diphenylphosphino)ethane P,P`)Pt] †	22
LXI	cis-$Pt(Cl)_2(P)_2$	cis-$[PtCl_2(PMe_2Ph)_2]$	23
LXII	$Pt(Cl)_2(S)(P)$	cis-$[PtCl_2(dms)(PMe_2Ph)]$	19

dms =dimethyl sulfide
PMe_2Ph = dimethylphenylphosphine
† A search of the Cambridge Structural Database[16] did not disclose a $Pt(PMe_2Ph)_4$ structure. However, by looking at a variety of PtP_4 square planar structures, e.g. bis (1,2 bis (Diphenylphophino)ethane P,P`) platinum (II) shown in Figure 7.7, it was concluded that the average Pt-P distance was 2.32 Å.

Figure 7.7

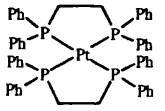

The strategy used in the development of the potential parameters was to see what extent the M-L bond length varied for a range of compounds. Then to determine a CLFSE + Morse potential which gave a minimum at one end of the range. An L--L Morse potential was then defined which would, in combination with the M-L Morse and CLFSE function, be able to reproduce a ML_4 structure. These parameters could then be tuned until a transferable force field encompassing a series of complexes was achieved. An example is described below.

The Pt-Cl bond length varies in the range of 2.30 - 2.37 Å, and the Pt-S distance is in the range of 2.26 - 2.32 Å. A Morse potential + CLFSE is chosen such that the minima of a Pt-Cl and Pt-S bond length is 2.37 and 2.32 Å respectively (see Figure 7.8 overleaf).

Figure 7.8.

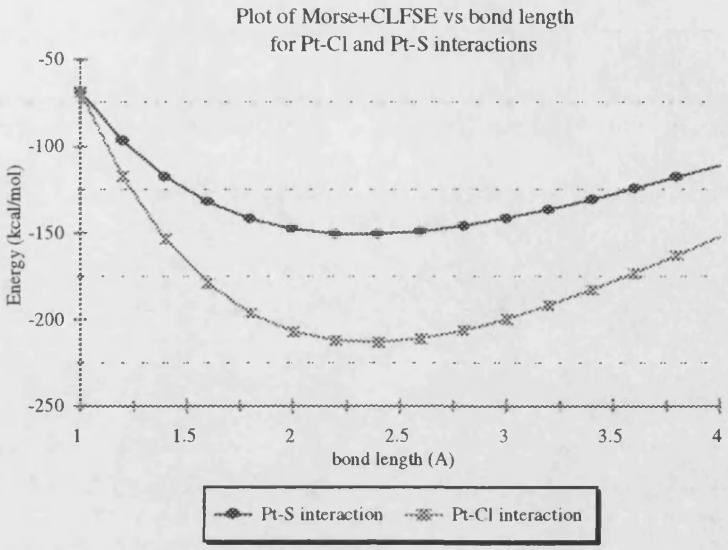

Now a Pt-Cl distance in $[PtCl_4]^{2-}$ is 2.30 Å thus, a Cl--Cl Morse function is introduced which has a steeper gradient than that shown in the graph which has an ideal equilibrium distance, r_e, of 4.58 Å. Thus, the Pt-Cl distance predicted from the Cl--Cl interaction alone would be 2.29 Å. However, from the graph it can be seen that the 'strain free' Pt-Cl bond length is estimated to be 2.37 Å. Thus, a combination of the Pt-Cl Morse + CLFSE and the Cl--Cl Morse potential yields a distance of around 2.30 Å.

The Pt-S distance in PtS_4 is 2.32 Å. A S--S Morse potential with an r_e of 4.64 Å would predict a Pt-S distance of 2.32 Å. This distance is also predicted from the CLFSE+Morse curve for Pt-S distance. However, when we look at $PtCl_3S$ then the Pt-Cl trans to S is 2.32 Å and Pt-S trans to Cl is 2.25 Å. A function describing the Cl--S interaction is introduced such that the r_e distance is 4.50 Å. If the potential for the Cl--S interaction is steeper than the Pt-S interaction then the Pt-S distance determined will be less than that predicted by the Pt-S interaction alone. Thus the trans influence of the S trans to the Cl can be reproduced.

Thus, by including a trans ligand-ligand bond stretch potential into the force field the trans influence of these model Pt(II) complexes may be studied.

7.4. Results and Discussion

The 'bare' ligand systems illustrated in Figure 7.6 were determined and compared with experimental data. A comparison of these is given in Table 7.2. A full listing of the force field parameters used is given in the Supplementary Data, Table S7.1.

Table 7.2

	observed			calculated		
	Pt-Cl / Å	Pt-S / Å	Pt-P / Å	Pt-Cl / Å	Pt-S / Å	Pt-P / Å
$Pt(Cl)_4$	2.30			2.30		
$Pt(Cl)_3S$	2.30$^{\nabla}$			2.30		
	2.32*			2.32		
		2.25			2.26	
trans $Pt(Cl)_2S_2$	2.30			2.30		
		2.31			2.31	
cis $Pt(Cl)_2S_2$	2.32			2.32		
		2.27			2.26	
$Pt(S)_3Cl$	2.31			2.33		
		2.31*			2.32	
		2.28$^{\nabla}$			2.27	
$Pt(S)_4$		2.32			2.32	
$Pt(P)_4$			2.32			2.32
cis $Pt(Cl)_2P_2$	2.36			2.35		
			2.25			2.23
$Pt(Cl)_2(S)(P)$	2.30*			2.33		
	2.37$^{\Diamond}$			2.35		
		2.27			2.27	
			2.22			2.23

∇ trans to Cl
$*$ trans to S
$\Diamond$ trans to P

As shown in Table 7.2 the calculated and observed bond lengths show excellent agreement, the worst case being in the calculation of the Pt-Cl distance in the $Pt(Cl)_2(S)(P)$ system where there is a deviation of 0.03 Å.

7.5. Conclusion

The trans influence for a series of $[PtA_xB_yC_z]$ systems (where $0 \leq x \leq 4$, $0 \leq y \leq 4$, $0 \leq z \leq 4$, A = Cl, B = S, C = P) has been successfully modelled by the inclusion of a trans ligand-ligand Morse potential to the CLFSE/MM methodology.

It should be noted that the force field developed here is only in the preliminary stages, the species calculated being hypothetical 'bare' ligand systems. Modelling the 'real' complexes would be the next logical step in providing a more applicable force field and will hopefully be the basis for future work in this area. However, the simulation of the trans influences in these case studies is still a significant advance in Molecular Mechanics modelling.

The force field used in this study has only been developed for a small range of systems. Thus, it needs to be extended to a wide variety of ligands so the transferability of the force field can be further tested. Once transferable parameters for a wide range of atoms have been developed then the predictive capability of this method can be tested.

It is hoped, that in the future, this methodology will be developed so that transition states may also be determined. If this succeeds then the trans effect could also be effectively studied using Molecular Mechanics.

7.6. Supplementary data.

Table S7.1. Potential parameters

	Morse function parameters			CLFSE parameters	
	D_0	r_e	α	a_0	a_1
Pt-S	80	2.70	0.45	35000	-5000
Pt-Cl	150	2.62	0.45	35000	-6000
Pt-P	120	2.46	0.45	35000	-4000
Cl--Cl	400	4.58	0.45		
S--S	100	4.64	0.45		
P--P	250	4.68	0.45		
Cl--S	100	4.50	0.45		
Cl--P	300	4.58	0.45		

7.8. References.

1. A. Pidcock, R. E. Richards and L. M. Venanzi, *J. Chem. Soc. (A)*, 1966, 1707.
2. T. G. Appleton, H. E. Clark and L. E. Mansen, *Coord. Chem. Rev.*,1973, **10**, 335.
3. J. Kozelka, G. A. Petsko, G. J. Quingley and S. J. Lippard, *Inorg. Chem.*, 1986, **25**, 1075.
4. J. Kozelka, G. A. Petsko and S. J. Lippard, *J. Am. Chem. Soc.*, 1985, **107**, 4079.
5. T. W. Hambley, *Inorg. Chim. Acta*, 1987, **137**, 15.
6. T. W. Hambley, *J. Chem. Soc., Chem. Comm.*, 1988, 221.
7. S. J. Yao, J. P. Plastaras and L. G. Marzilli, *Inorg. Chem.*, 1994, **33**, 6061.
8. M. D. Reily, T. W. Hambley and L. G. Marzilli, *J. Am. Chem. Soc.*, 1988, **110**, 2999.
9. T. W. Hambley, *Inorg. Chem.*, 1988, **27**, 1073.
10. J. Kozelka, R. Savinelli, G. Berthier, J. P. Flament and R. Lavery, *J. Comp. Chem.*, 1993, **32**, 478.
11. M. J. Bloemink, H. Engelking, S. Karentzopoulos, B. Krebs and J. Reedijk, *Inorg. Chem.*, 1996, **35**, 619.
12. G. Schroder, J. Kazelka, M. Sabat, M. H. Fouchet, R. Beverlepfuner and B. Lippert, *Inorg. Chem.*, 1996, **35**, 1647.
13. M. A. Watzky, D. Waknine, M. J. Hegg, J. F. Endicott and L. A. Ochrymowyzc, *Inorg.Chem.*, 1993, **32**, 4882.
14. P. Comba, H. Jakob, B. K. Keppler and B. Nuber, *Inorg. Chem.*, 1994, **33**, 3396.
15. A. K. Rappé, K. S. Colwell and C. J. Casewit, *Inorg. Chem.*, 1993, **32**, 3438.
16. Cambridge Structural Database, Version 4. Cambridge Crystallographic Data Centre, University Chemical Laboratory, Cambridge, 1994.
17. L. Bengtsson and Å Oskarsson, *Acta Chem Scand*, 1992, **46**, 707
18. V. Y, Kukushkin, K. Lövqvist, B. Norén, Å Oskarsson and L. I. Elding, *Inorg. Chim. Acta*, 1994, **219**, 155.
19. K. Lövqvist, *'A Crystallographic Study of Pt(II) Complexes'*, PhD Thesis, Lund, 1996.
20. G. W. Horn, K. Kumar, A. W. Maverick, F. R. Fronczek and S. F. Watkins, Acta Cryst, 1990, C46, 135
21. Z. Bugarcic, B. Norén, Å Oskarsson, C Stålhandske and L. I. Elding, *Acta Chem. Scand.*, 1991, **45**, 361.
22. G. Ferguson, A. J. Lough, A. J. McAlees and R. McCrindle, *Acta Cryst, C (Cr. Str. Com.)*, 1993, **49**, 573.
23. W. M. Attia, G. Balducci and M. Calligaris, *Acta Cryst. C (Cr. Str. Com.)*, 1987, **C43**, 1053.

Part 2

A study of Hexaaquo Metal Ion Acidity using Density Functional Theory

Introduction

The use of computational chemistry lies in its predictive nature and its ability to explain problems and concepts that the experimental scientist encounters. Here, an ab initio method, Density Functional Theory, (DFT), is discussed, and how it is used in enhancing understanding in an area of transition metal chemistry.

Density Functional programs are standard computational chemistry packages. In this study, the Amsterdam Density Functional package was used to investigate the acidity of metal hexaaquo ions. The justification of this work lies in the fact that a correlation of pK_a for the first hydrolysis step of metal ions and transferrin metal-binding has been suggested[1], and thus, the factors which govern the acidity, will also influence metal binding to transferrins.

There is significant interest in the biological role of transferrins, and the first chapter of this work introduces these proteins and the above mentioned correlation. An introduction to the chemistry of hexaaquo metal ions is given, and the modelling of these transition metal species is also discussed.

The second chapter explains the basic concepts of Density Functional Theory. However, the complex mathematics which lie at the heart of this computational technique have been omitted.

The final chapter discusses the results and conclusions drawn from this investigation, and future work which could be carried out.

Chapter 8

Background

8.1. Transferrins

Transferrins are a family of metal-binding proteins[2]. The fundamental role of transferrins is to control the levels of free iron in body fluid by binding, sequestering and transporting Fe^{3+} ions. These help to maintain the availability of iron while preventing the deposition of insoluble ferric hydroxide aggregates. The protein protects against the toxic effects of free iron that might otherwise catalyse the formation of the free radicals that damage cells. They are able to bind iron tightly so that is unavailable for bacterial growth.

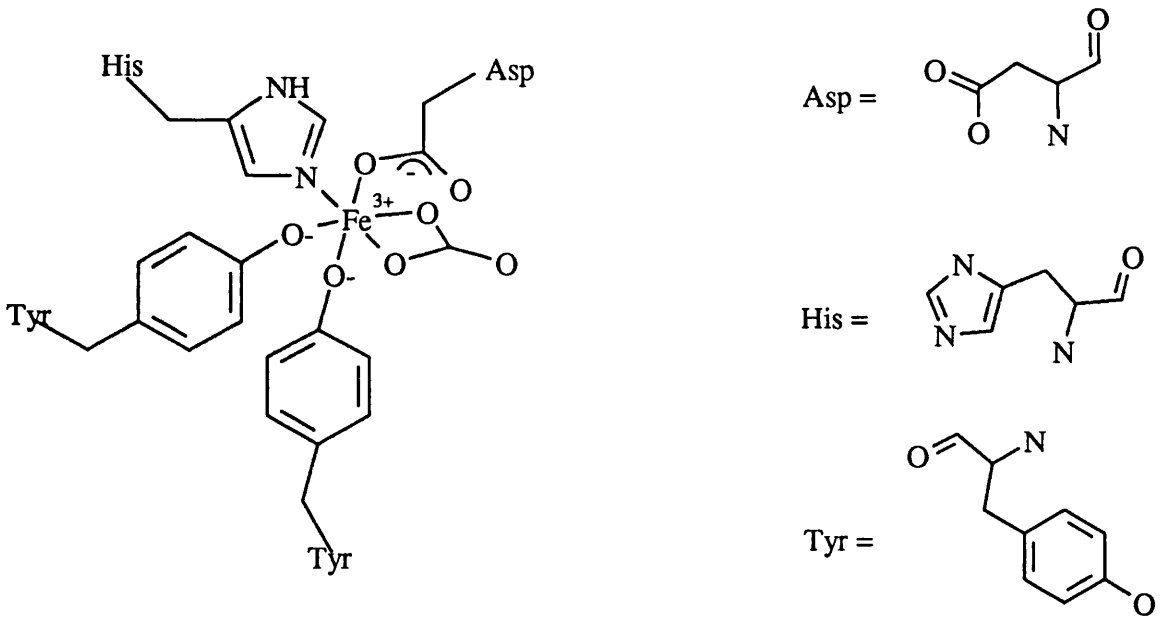

Figure 8.1. Schematic diagram of the characteristic transferrin metal and anion binding site.

The transferrins are primarily regarded as iron binding proteins because their affinity for Fe^{3+} is substantially greater than for any other metal ion. However, they can

accommodate a wide variety of other metal ions including most first row transition metals, several second row and third row transition metals, lanthanides, and actinides. Most of these are unlikely to be physiologically significant. However, as most of the first row transition elements are essential in biological systems, there is considerable interest in the possibility that transferrins may be involved in their binding and translocation.

Recent work by Sadler and co-workers[1] shows that there is an empirical correlation between pK_a values for the first hydrolysis step of metal ions, equation (8.1),

$$[M(H_2O)_x]^{n+} \rightarrow [M(H_2O)_{x-1}(OH)]^{(n-1)+} + H^+ \qquad (8.1)$$

and the first binding constant for metals to transferrin, TF, equation 8.2.

$$M^{n+} + HCO_3^- + TF \rightarrow [M(HCO_3)TF] \qquad (8.2)$$

This thus suggests that factors which govern pK_a's, will also determine metal binding to transferrin. Therefore, the work undertaken here was a theoretical study of the factors which govern pK_a's of some hexaaquo metal ion species.

8.2. Metal Ions in Solution

Aquo cations, especially those of 4+, 3+ and 2+ ions, tend to act as acids in solution[3]. At the simplest level, this behaviour can be ascribed to the influence of the positive charge on the metal ion facilitating the loss of a water proton to give a hydroxo-aqua species.

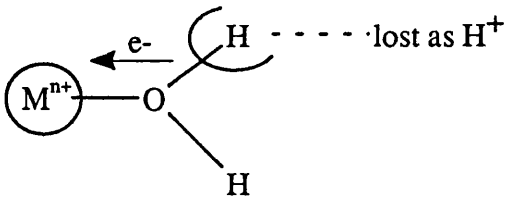

Figure 8.2. Diagram to show loss of proton

Such behaviour can lead into the area of polymerisation as many hydroxo-aquo cations can show tendencies to form bridged species, as seen in fig (8.3)

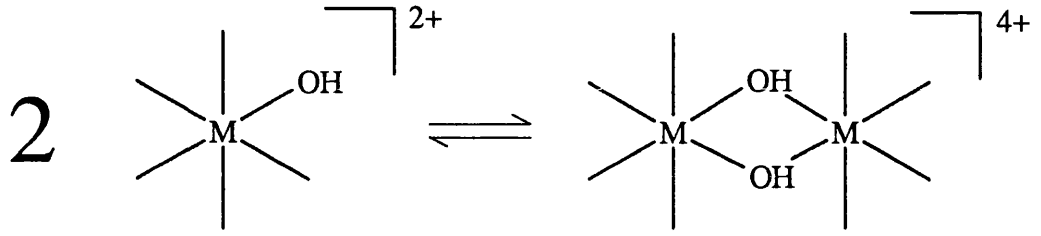

Figure 8.3. Hydroxo bridges formed between two cations

There are many complexes containing other ligands as well as aquo and hydroxo ligands, singly or in combination. The presence of such ligands can have a profound effect on acidity in several ways. For example, they may stabilise an unusually high or low oxidation state or assist a 'soft' metal ion to form a strong bond to water or hydroxide[4].

In general terms, the effects of coordinated ligands on the acidity of coordinated water molecules can to some extent be related to the electron releasing and withdrawing properties of the former. These effects can either be transmitted through or across the metal cation while the ease of transmission will depend on such properties of the cation such as its electron configuration and the availability of suitable orbitals.

The acidic properties of coordinated water in aquo cations vary enormously with the cation. There is an approximate correlation with electrostatics (charges and ionic radii), but such properties as oxidising power and 'softness' complicate the pattern[5].

The pK_a of a hexaaquo cation is a measure of its acidity. The more negative a pK_a the more acidic the complex. For example if you consider equation 8.1 then the equilibrium constant K_a is given by equation 8.3.

$$K_a = [M(H_2O)_5(OH)][H^+]/[M(H_2O)_6] \qquad (8.3)$$

The pK_a is then given in equation 8.4.

$$pK_a = -\log K_a \qquad (8.4)$$

To try to elucidate the factors which determine the pK_a of a variety of aquo cations, a computational method which has successfully been used in the modelling of properties of transition metal systems is required. An ab initio method, Density Functional theory, is one such method, and it is this theory which is used in this investigation.

8.3. Modelling of Aquo Ions.

A variety of theoretical studies have previously been carried out on hydrated metal ions. A brief summary will be given here.

Density Functional calculations[6] have been carried out on $[M(H_2O)_6]^{2+}$ ions, (where M is a metal ion from the first transition period), and the geometries and dissociation energies of water have been calculated.

Other ab initio methods have also been used successfully in the study of binding energies and ligand field effects for the hydrated divalent ions of the first row[7] and the second row[8] transition metals. The variation of binding energies in the hexaaquo complexes shows the double humped features expected, closely following the trends expected from ligand field theory and experimental hydration enthalpies.

Ab initio methods have also been used in the study of water exchange reactions[9] for the divalent ions of the first transition period. The smallest system which can be used to describe a water exchange process should contain seven water molecules, assuming a concerted associative process. If the mechanism goes via a 'dissociative' process then the activated complex will be an essentially pentahydrated complex with the two exchanging water molecules at a relatively large distance from the metal ion. In such a case the barrier to water exchange can be determined by the energy needed to remove one water from the hexahydrated complex. From the Arrhenius rate equation, it follows that a plot of dissociation energy versus the logarithm of the observed rate constant , k, should be linear. Ab initio calculations have shown that the theoretical bond dissociation values plotted against log k does indeed give a linear plot, and this has been interpreted in terms of a dissociative mechanism taking place.

8.4. Modelling of pK_a

In this study, Density Functional Theory has been used to investigate the factors affecting the acidity of hexaaquo metal ions.

The first assumption made is that the pK_a values are correlated with the dissociation energy of H^+.

Consider equation 8.5,

$$[M(H_2O)_6]^{n+} \rightarrow [M(H_2O)_5(OH)]^{(n-1)+} + H^+ \qquad (8.5)$$

The dissociation energy of H^+ will then be

$$E\{[M(H_2O)_5(OH)]\} + E\{H^+\} - E\{[M(H_2O)_6]\} \qquad (8.6)$$

In DFT, the basic assumption is that the energy, E, is a function of the electron density, ρ.

$$E = f(\rho) \quad (8.7)$$

as H^+ has no electrons then $E\{H^+\}$ will be equal to zero.

Thus the dissociation energy, ΔE, becomes

$$\Delta E = E\{[M(H_2O)_5(OH)]\} - E\{[M(H_2O)_6]\} \quad (8.8)$$

and this is assumed to be correlated to pK_a

$$pK_a \alpha \Delta E.$$

Solvation effects also need to be considered, thus ΔE becomes,

$$\Delta E = (E\{[M(H_2O)_5(OH)]\}+(\text{solvation energy}))-(E\{[M(H_2O)_6]\}+(\text{solvation energy})) \quad (8.9)$$

8.5. Solvation effects.

The effect that a polarisable environment (i.e. solvent effects) may produce on the electronic properties of atoms and molecules in solution has been found to significantly change their reactivity patterns, when compared to gas phase properties[10].

To take into account these solvation effects in computational simulations different models have been proposed. One method is the supermolecule approach where a finite number of solvent molecules are treated explicitly. This however can prove to be computationally demanding. Other methods utilise the dielectric continuum model to represent solvent electrostatic behaviour.

Pagleri et al[11] have used a model based on Onsager's reaction field theory[12]. Here the solvent effects are taken into account through a self consistent reaction field approach, which evaluates the electrostatic contributions to the solvation energy. In this model, the solute is placed in a cavity surrounded by a continuum characterised by a given dielectric constant, ε. The charge distribution due to the electron density, ρ, of the solute induces a polarisation of the solvent, so a reaction field is produced which in turn, interacts with the electronic density of the solute. This process is iterated until self consistency is achieved.

A similar approach, the polarisable continuum model, PCM, developed by Tomasi et al[13], again assumes the solvent to be a continuum dielectric, which reacts against the solute charge distribution generating a reaction field. However this method allows the boundary between the solute to take on an arbitrary shape. The implementation of Density Functional Theory within the polarisable continuum model for solvation has recently been reported by Fortunelli et al[14].

A simpler strategy is a 'virtual charge method' developed by Klopman[15]. In this model an imaginary particle, called a solvaton, is associated to each atom, A, of the solute. The charge of the solvaton, Q^S_A is equal in magnitude and opposite in sign to the Mulliken charge q_A. The positions of the solvaton are not fixed. In the calculation of the interaction between Q^S_A and another atom with charge q_B, the solvaton is placed at the position of atom A. The interaction of Q^S_A and Q_A is computed assuming a distance equal to the van der Waals radius of A. Interactions between solvatons are discarded. This formulation has been incorporated into a semiemperical procedure by Germer et al[16], and later re-elaborated by Mertus and Kysel[17], by Constanciel[18], and Contreras et al[19].

An even simpler approach still, and is the model used in the investigations described in this work, is the Born model[20]. Here the energy of solvation, E_{solv}, is given in equation (8.10).

$$E_{solv} = -1/2(z^2e^2N_A/4\pi\varepsilon_0 r)\,(1-\{1/\varepsilon_r\}) \qquad (8.10)$$

In the Born model z is the charge of the complex, e is the elementary charge, N_A is Avogadro's constant, ε_0 is the relative permitivity of a vacuum, r is the radius of the solvated complex and ε_r is the relative permitivity of the medium, in this case water.

After inserting the values of the appropriate constants, the E_{solv} in water approximates to

$$E_{solv} = -z^2/r(6.94x10^4) \text{ kJ/mol} \qquad (8.11)$$

(where r is measured in pm)

This model has been used successfully in work by Deeth[21] and also work by Langford[22], and thus was the model chosen in the investigation of pK_a values.

8.6. References

1. P. J. Sadler, private communication.
2. E. N. Baker, *Adv. Inorg. Chem.*, 1994, **41**, 389.
3. J. Burgess, *'Metal Ions in Solution'*, Ellis Horwood, Chichester, 1978.
4. J. Burgess, *'Ions in Solution'*, Royal Soc. of Chem., ETSG, London, 1984.
5. J. Burgess, in *'Comprehensive Coordination Chemistry'*, G. Wilkinson, R. D. Gillard and J. A. McCleverty, Eds.; Pergamon, Oxford, 1987, Vol. 2, Chapter 15.
6. K. Waizumi, H. Ohtaki, H. Masuda, N. Fukushima and Y. Watanabe, *Chem. Letts.*, 1992, 1489.
7. R. Åkesson, L. G. M. Petterson, M. Sandström, P. E. M. Siegbahn and U. Wahlgran, *J. Phys. Chem.*, 1992, **96**, 10773.
8. R. Åkesson, L. G. M. Petterson, M. Sandström and U. Wahlgran, *J. Am. Chem. Soc.*, 1994, **116**, 8691.
9. R. Åkesson, L. G. M. Petterson, M. Sandström, P. E. M. Siegbahn and U. Wahlgran, *J. Phys. Chem.*, 1993, **97**, 3765.
10. R. G. Pearson, *J. Am. Chem. Soc.*, 1986, **108**, 6109; M. M Karelson and M. C. Zerner, *J. Phys. Chem.*, 1992, **96**, 6949.
11. L. Paglieri, G. Corongui and D. A. Estrin, *Int. J. Quant. Chem.*, 1995, **56**, 615.
12. L.Onsager, *J. Am. Chem. Soc.*, 1936, **58**, 1486.
13. S. Miertus, E. Scrocco and J Tomasi, *Chem. Phys.*, 1981, **55**, 117.
14. A. Fortunelli and J. Tomasi, *Chem. Phys. Letts.*, 1994, **231**, 34.
15. G. Klopman, *Chem. Phys. Letts.*, 1967, **1**, 200.
16. H. A. Germer, *Theor. Chim. Acta*, 1974, **35**, 273.
17. O. Kysel and S. Miertus, *Chem. Phys. Letts.*, 1979, **65**, 395.
18. R. Constanciel, *Theor. Chim. Acta*, 1980, **54**, 123.
19. R. Contreras and A. Aizman, *Int. J. Quant. Chem.*, 1985, **27**, 293.
20. P. W. Atkins, *'Physical Chemistry'*, 3rd edt., Oxford University Press, 1986.
21. R. J. Deeth and L. I. Elding, *Inorg. Chem.*, 1996, **35**, 5019.
22. S. A. Langford, M. Phil. Thesis, University of Bath, 1996.

Chapter 9

Theory.

9.1. Introduction

Density Functional Theory (DFT) is an ab initio computational method which can be used to determine geometries, bond energies, transition states, etc[1]. It has been used in the modelling of many properties of transition metal systems and is used here in the study of pK_a values of hexaaqua systems.

9.2. Ab Initio Methods.

In principle, a molecular system can be described from first principles in terms of the Schrödinger equation (equation 9.1).

$$H\Psi = E\Psi \qquad (9.1)$$

H is the Hamiltonian operator which describes the energetic interactions between the particles in the system. In a molecule the particles involved are electrons and atomic nuclei. Ψ is the wave function which describes the positions and trajectories of the particles in the system. E is the total molecular energy. In order for an accurate energy, E, to be calculated, then the Hamiltonian, H, must include all possible inter and intra particle interactions, i.e. nuclear-nuclear interactions, nuclear-electron interactions and electron-electron interactions; and the wave function must be completely flexible.

An exact solution of the Schrödinger equation is not possible, except for the case of single electron systems like the hydrogen atom. For polyelectron systems an accurate description of the wave function would require an infinite number of components which cannot be achieved in practical implementation on a computer. Approximations are also necessary in evaluation of the Hamiltonian.

9.2.1. Wavefunctions

Molecular orbital theory uses a linear combination of atomic orbitals (LCAO)[2] to approximate the full wavefunction, equation (9.2).

$$\Psi = \Sigma c_i \Phi_i \qquad (9.2)$$

Where c_i is a coefficient and Φ_i is an atomic orbital.

These atomic orbitals are made up of angular functions and radial functions. The angular function describes the shape of the orbital and the radial function describes the distance dependence from the nucleus. The total set of angular and radial functions chosen for a given atom defines the basis set. One type of functional form to describe the basis set is known as Slater Type Orbitals (STO)[3], e.g.

$$\Phi 1s = (\zeta 3/\pi)1/2 \exp(-\zeta r) \qquad (9.3)$$

where ζ is a size constant

r is the distance from the nucleus

The simplest type of basis set is the minimal basis set where each atom is represented by a single orbital of each type as in descriptive organic chemistry. Thus, an oxygen atom would need 1x1s, 1x2s and 3x2p atomic orbitals. However, molecular orbitals are different to atomic orbitals, so extra functions can be added to allow for distortions occurring due to bond formation.

There are two types of distortion:-

i) radial

ii) angular

i) The radial distortion allows electrons to move closer to or further away from the nucleus. For example, one way to achieve this would be to double the minimal basis

set i.e. each 1s orbital being represented by two basis functions. This would then be known as a double zeta (DZ) basis set.

ii) In a molecule the electrons do not have to be centred on an atom. Thus, the basis set of an atom can include polarisation functions which allow the electron density to respond to the external field. These polarisation functions are atomic orbitals with angular momentum quantum number higher than the maximum necessary to describe the ground state of the neutral atom. For example, a p type function on hydrogen or a d type function on carbon allows displacements away from the nuclear position (as illustrated in Figure 9.1)

Figure 9.1. An illustration of polarisation functions.

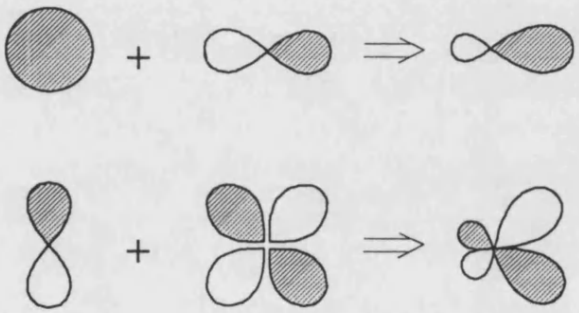

The resulting orbitals show deformation to one side of the atom and thus allow the electrons to move off centre.

The larger the basis set the more accurate the description of the wave function. However a large basis set will increase the computational time of a calculation. So an acceptable balance between accuracy and speed must be employed.

Another approximation often used in description of the basis set is that the core electrons are frozen, and that only the valence electrons are needed for an accurate description of molecular properties. This then reduces the number of functions used to define the basis set and thus increases the speed of the calculation.

9.2.2. Hamiltonian Operator.

In the complete Schrödinger equation, H is the many particle Hamiltonian for a molecule. As already mentioned, the particles thus involved are the electrons and atomic nuclei, thus the interactions are the nuclear-nuclear, nuclear-electron and electron-electron interactions.

The first approximation to be made is that the nuclei are fixed in space and the motions of the electrons are evaluated with respect to fixed nuclei. This is known as the Born-Oppenheimer approximation[4] and results in the nuclear-nuclear term reducing to a simple electrostatic interaction. It is also often assumed that relativistic effects are negligible. A further simplification is made in that the system is treated as a one electron problem. This leads to the so called one electron Schrödinger equation, (equation 9.4).

$$h\phi = \varepsilon\phi \qquad (9.4)$$

This equation is solved by self consistent field (SCF) theory. Here the energy and trajectory of each electron in turn is considered moving in the potential field generated by the nuclei and the other electrons. This requires an initial guess at a starting potential, followed by an iterative scheme where the potential is progressively retuned until it no longer varies. This process is said to be self consistent in as much as the potential at the start of the last cycle is essentially the same as that which emerges at the end.

The whole process is governed by the Variational Principle which states that given a particular wave function ϕ, the energy computed, ε, will always be greater than or equal to the lowest energy which can be obtained with the chosen method[4]. Hence, providing the energy decreases, a 'better' approximation to the 'best' wavefunction and energy is being obtained. Thus the calculation is driven by the minimisation of the energy.

The one electron hamiltonian, h, compromises essentially two terms, the kinetic and potential energy, K.E. and V respectively.

$$h=K.E. + V \qquad (9.5)$$

The potential energy V is then given by

$$V = V_{ne} + V_{ee} + V_{xc} \qquad (9.6)$$

where V_{ne} is the nucleus-electron interaction energy, V_{ee} is the electron -electron interaction energy and V_{xc} is the exchange-correlation energy. Exchange is the change in energy of the system when electrons in different orbitals are interchanged, while correlation is due to the fact that there is a tendency for electrons to avoid each other, i.e. their motions are correlated. These two terms together constitute the exchange-correlation energy. It is the treatment of the third term, V_{xc}, which essentially differentiates one ab initio method from another.

9.3. Density Functional Theory (DFT)

The Density Functional theorem states that the exact ground state energy can be determined from a unique functional of the electron density, ρ[5]. This means that if the true density is known then the exact energy including all correlation effects can be calculated. This idea goes back to early work by Thomas[6], Fermi[7], Dirac[8] and Wigner[9].

The true density can only be calculated by solving the many electron Schrödinger equation. This proves too complex, but in 1965 Kohn and Sham[10] developed a set of one electron equations, which for a so-called uniform electron gas, have an explicit functional form for the exchange and correlation energy.

9.3.1. Local Density Approximation.

From the theory of the homogeneous electron gas as a way to treat the exchange-correlation problem, the Local Density Approximation (LDA) was developed. The approximation is that the electron density of the system remains constant over all space, i.e. the electron density gradient is zero. For most real systems, this does not hold true, but it serves as a first approximation.

The exchange correlation energy for the homogeneous electron gas can be written as

$$Exc^{LDA} = Ex^{LDA} + Ec^{LDA} \qquad (9.7)$$

The exchange energy Ex^{LDA} can be calculated easily as it depends only on $\rho^{4/3}$. Ec^{LDA} is more complicated being a function of the spin densities of two correlated electrons. This can not be calculated exactly as the motion of an electron i, for example, will depend on the position of electron j, which in turn depends on the trajectory of electron i. However, Vosko et al[11] have carried out a series of calculations for a range of ρ and fitted their results to a function such that given any ρ, an appropriate Ec^{LDA} can be extracted.

Exchange and correlation energies for a number of atoms have been calculated[5] using LDA, and it has been shown that the error in exchange energy is approximately 10%, whereas the correlation energy can be overestimated by as much as 100%. The Ex^{LDA} is approximately 10 times bigger than Ec^{LDA}, thus, it is important to correct the exchange energy. However, an overall improvement of the both exchange and correlation energy is appropriate.

9.3.2. Stoll Corrections.

Stoll et al[12] suggest that the major part of the error due to correlation energy comes from correlation between electrons of the same spin. To amend this, the Ec^{LDA} is corrected such that correlation between electrons with the same spin is eliminated

altogether. Thus, contribution to the exchange-correlation energy from electrons of the same spin is given solely by the exchange part. This is known as the Stoll correction.

9.3.3. Gradient Corrections.

LDA is only a first approximation to the picture of electron density in real molecules. The acknowledgement that electron density is not constant across all space for molecules is important, and this deficiency can be corrected for by the inclusion of gradient corrected functionals. These have been developed for the exchange energy, by Becke[13], and for the correlation energy, by Perdew[14].

Use of these corrections has improved the description of some molecular properties[5], e.g. binding energies. However, Bray et al[15] have shown that for Werner type complexes, structural properties are more accurately determined using the LDA, while the geometries of organometallics are better described using gradient corrected methods. Thus, care should be taken when deciding which method to use.

9.3.4. Summary.

DFT makes use of the so called one electron Schrödinger equation (equation 9.4). The Hamiltonian is made up of a sum of kinetic and potential energy and is determined from a functional of the electron density. The basis set, for the molecule to be studied, is defined and thus the one electron Schrödinger equation may be determined using self consistent field (SCF) theory, the whole process being governed by the Variational Principle.

9.4. Amsterdam Density Functional.

The Amsterdam Density Functional (ADF) code is a FORTRAN program used to calculate structures and molecular properties. There are different levels of theory within ADF at present. The lowest level is the LDA, and the highest is the Non-Local-

SCF level in which gradient corrections are included within the SCF. A treatment where the SCF procedure is executed with only the LDA, and the gradient corrections are used to compute *a posteriori* a correction to the energy value, is also possible, and is known as post-scf, and the LDA can also be used with Stoll's corrections included. Therefore, each level, with a combination of basis sets, can be changed to improve the accuracy of the calculation.

In order to optimise molecular geometries, an initial structure for the molecule in question is postulated. The nearer this initial guess is to the final structure the shorter the calculation. The molecular energy as well as the corresponding energy gradients are then evaluated. Assuming this has not led to convergence an update matrix (Z) is then used to calculate the change in atomic coordinates for the next step. The molecular energy and energy gradients are subsequently recalculated using the new Z-matrix. This procedure is repeated until the values of the energy gradients fall below a specified value, i.e. convergence is reached. In order for this to happen, it is necessary to find the minima on the potential energy surface, thus each step should result in a reduction in the molecular energy. If the energy is found to increase the Z-matrix is reset to that from which the last successful step was taken and a smaller step size is taken, i.e. the change in atomic coordinates is reduced. The calculation of the Z-matrix and the step size are controlled by a set of limiting conditions in order to achieve minimisation as efficiently as possible.

In defining an initial structure, a symmetry may be imposed on the molecule, if appropriate, so as to shorten the length of the calculation. Instructions such as charge of the molecule are also necessary, and molecule can be described as paramagnetic or diamagnetic by stating how many electrons there are, and whether they are spin restricted or spin unrestricted. A restricted calculation implies that the orbitals are identical for up- and down-spin electrons. An unrestricted calculation specifies that the up-spin and down-spin electrons may be spatially different and the molecular orbitals may have different occupation numbers.

9.5. References.

1. R. G. Parr and W. Yang, '*Density Functional Theory of Atoms and Molecules*' Oxford University Press, 1989.
2. M. Orchin and H. H. Jaffé, '*Symmetry, Orbitals and Spectra*', John Wiley and Sons Inc., 1988.
3. R. McWeeny, '*Methods of Molecular Quantum Mechanics*', Academic Press Ltd., 1989.
4. A. Hinchliffe, '*Computational Quantum Chemistry*', John Wiley and Sons, 1988.
5. T. Ziegler, *Chem. Rev.*, 1991, **91**, 651.
6. L. H. Thomas, *Proc. Camb. Phil. Soc.*, 1927, **23**, 542.
7. E. Fermi, *Z. Phys*, 1928, **48**, 73.
8. P. A. M Dirac, *Camb. Phil. Soc.*, 1930, **26**, 376.
9. E. P. Wigner, *Phys. Rev. A*, 1965, **140**, 1133.
10. W. Kohn and L. J. Sham, *Phys. Rev. A*, 1965, **140**, 1133.
11. S. J. Vosko, L. Wilk and M. Nussair, *Can. J. Phys.*, 1980, **58**, 1200.
12. H. Stoll, E. Golka and H. Preuss, *Theor. Chim. Acta.*, 1978, **49**, 143.
13. A. D. Becke, *Int. J. Quantum Chem.*, 1983, **23**, 1915.
14. J. P. Perdew, *Phys. Rev.*, 1986, **B33**, 8822.
15. M. R. Bray, R. J. Deeth, V. J. Paget, P. D. Sheen, *Int. J. Quantum Chem.*, in press.

Chapter 10

Details of Investigation

10.1. Computational Details

Geometry optimisations are performed using the Amsterdam Density Functional program by Baerends et al[1]. This method employs Slater-type orbitals (STO) basis sets.

In this study, the uniform electron gas Local Density Approximation (LDA)[2] was used in conjunction with gradient corrected methods. The hexaaquo metal ions had a D_{2h} symmetry imposed, whilst the deprotonated form, $[M(H_2O)_5OH]^{(n-1)+}$, was constrained with C_{2v} symmetry. In the $[M(H_2O)_5OH]^{(n-1)+}$ complexes, the H-O-H angles were all fixed at the same value throughout the optimisation , as without this imposition the H's were bending up towards the OH ligand, i.e. intramolecular H bonding interactions were obtained. It is assumed that in solution, due to intermolecular hydrogen bonding with the solvent, that this intramolecular bonding would not take place. The solvent is not implicitly defined in the calculations as this would be too computationally demanding. However the effects of the solvation were considered by using the Born model as described elsewhere.

The lower core shells on the atoms (up to 2p for all the metals, and 1s for oxygen) were treated by the frozen core approximation. The basis set used was of triple-ζ quality for the valence orbitals with polarisation functions on the ligand atoms (2p for hydrogen and 3d for oxygen) and additional valence p orbitals on the metal atoms (ADF basis set IV)[3].

Relativistic corrections are not included as it has been shown[4] that the geometries and energies of complexes containing atoms as large as the 1st row transition metals are not affected significantly by the inclusion of these effects.

Calculations have used the spin unrestricted formalism so that the high spin configuration of the transition metals could be maintained.

10.2. Results and Discussion

The results of the geometry optimisations for the $[M(H_2O)_6]^{n+}$ and $[M(H_2O)_5OH]^{(n-1)+}$ complexes are displayed in Figure 10.1 and Tables 10.1 to 10.7.

Figure 10.1. Structures of $[M(H_2O)_6]^{n+}$ and $[M(H_2O)_5OH]^{(n-1)+}$

$[M(H_2O)_6]^{n+}$ $[M(H_2O)_5OH]^{(n-1)+}$

Table 10.1. Mn(II)

	LDA	LDA+stoll	LDA+gradcor	experimental
$[Mn(H_2O)_6]^{2+}$				
av Mn-O (Å)	2.13	2.15	2.20	2.18 [5]
$[Mn(H_2O)_5OH]^{+}$				
Mn-OH	1.81	1.82	1.82	
Mn-O_{ax} (Å)	2.22	2.24	2.34	
Mn-O_{eq} (Å)	2.22	2.24	2.34	
	2.22	2.24	2.34	
	2.18	2.02	2.30	
	2.18	2.20	2.30	
av Mn-O (Å)	2.14	2.16	2.24	

Table 10.2. Ni(II)

	LDA	LDA+stoll	LDA+gradcor	experimental
$[Ni(H_2O)_6]^{2+}$				
av Ni-O (Å)	2.00	2.02	2.07	2.07 [6]
$[Ni(H_2O)_5OH]^{+}$				
Ni-OH (Å)	1.83	1.85	1.84	
$Ni-O_{ax}$ (Å)	2.04	2.05	2.15	
$Ni-O_{eq}$ (Å)	2.04	2.05	2.15	
	2.04	2.05	2.15	
	2.00	2.01	2.08	
	2.00	2.01	2.08	
av Ni-O (Å)	1.99	2.00	2.08	

Table 10.3. Fe(II)

	LDA	LDA+stoll	LDA+gradcor	experimental
$[Fe(H_2O)_6]^{2+}$				
av Fe-O (Å)	2.06	2.08	2.13	2.10 [6]
$[Fe(H_2O)_5OH]^{+}$				
Fe-OH (Å)	1.76	1.77	1.78	
$Fe-O_{ax}$ (Å)	2.18	2.19	2.29	
$Fe-O_{eq}$ (Å)	2.11	2.15	2.27	
	2.11	2.15	2.27	
	2.15	2.19	2.24	
	2.15	2.19	2.24	
av Fe-O (Å)	2.08	2.11	2.18	

Table 10.4. Zn(II)

	LDA	LDA+stoll	LDA+gradcor	experimental
$[Zn(H_2O)_6]^{2+}$				
av Zn-O (Å)	2.07	2.08	2.13	2.09 [6]
$[Zn(H_2O)_5OH]^{+}$				
Zn-OH (Å)	1.79	1.80	1.80	
$Zn-O_{ax}$ (Å)	2.14	2.16	2.26	
$Zn-O_{eq}$ (Å)	2.14	2.18	2.23	
	2.14	2.18	2.23	
	2.11	2.11	2.20	
	2.11	2.11	2.20	
av Zn-O (Å)	2.07	2.09	2.15	

Table 10.5. Al(III)

	LDA	LDA+stoll	LDA+gradcor	experimental
$[Al(H_2O)_6]^{3+}$				
av Al-O (Å)	1.90	1.91	1.91	-----
$[Al(H_2O)_5OH]^{2+}$				
Al-OH (Å)	1.67	1.67	1.67	
Al-O_{ax} (Å)	1.96	1.92	2.03	
Al-O_{eq} (Å)	1.95	1.98	2.01	
	1.95	1.98	2.01	
	1.91	1.93	1.96	
	1.91	1.93	1.96	
av Al-O (Å)	1.89	1.92	1.94	

Table 10.6. Cr(III)

	LDA	LDA+stoll	LDA+gradcor	experimental
$[Cr(H_2O)_6]^{3+}$				
av Cr-O (Å)	1.96	1.97	2.01	1.96 [7]
$[Cr(H_2O)_5OH]^{2+}$				
Cr-OH (Å)	1.75	1.76	1.76	
Cr-O_{ax} (Å)	2.04	2.07	2.11	
Cr-O_{eq} (Å)	2.00	2.02	2.02	
	2.00	2.02	2.02	
	1.97	1.98	2.06	
	1.97	1.98	2.06	
av Cr-O (Å)	1.96	1.97	2.01	

Table 10.7. Fe(III)

	LDA	LDA+stoll	LDA+gradcor	experimental
$[Fe(H_2O)_6]^{3+}$				
av Fe-O (Å)	2.02	2.03	2.07	2.00 [7]
$[Fe(H_2O)_5OH]^{2+}$				
Fe-OH (Å)	1.74	1.75	1.78	
Fe-O_{ax} (Å)	2.08	2.03	2.17	
Fe-O_{eq} (Å)	2.08	2.10	2.16	
	2.08	2.10	2.16	
	2.04	2.05	2.10	
	2.04	2.05	2.10	
av Fe-O (Å)	2.02	2.03	2.08	

In all cases of the hexaaquo ions, except Al(III), experimental data for the M-O bond lengths were available for comparison with the computed M-O bond length. For the $[M(H_2O)_5OH]^{(n-1)+}$ ions, there were no experimental data available. So the calculated structures for these ions are predicted geometries.

When looking at the $[M(H_2O)_6]^{n+}$ ions , the LDA method underestimates the M-O bond length for Mn(II), Ni(II) and Fe(II) by approximately 0.06 Å, whereas for Zn(II), Cr(III) and Fe(III), excellent agreement between calculated and observed structures is observed, with the maximum deviation being only 0.02 Å.

When Stoll corrections are included there is good agreement in nearly all cases, the worst being Ni(II) where there is a deviation of 0.05 Å.

The inclusion of gradient corrections appears to give the 'opposite' results to those obtained using the LDA method, in that the Mn(II), Ni(II) and Fe(II) complexes are in excellent agreement with experimental structure, the maximum deviation being 0.03 Å. Whereas for Zn(II), Cr(III) and Fe(III) the calculated M-O bond lengths are over estimated, the greatest deviation being 0.07 Å for Fe(III).

As seen from Figure 10.1, the $[M(H_2O)_5OH]^{(n-1)+}$ complexes are predicted, using all methods, to have a slightly distorted octahedral structures, with the metal being slightly raised from the plane of the equatorial oxygen ligands. This may be due to repulsion between the extra electron density of the OH^- and the electron density of the other OH_2 ligands. In all cases, the M-OH bond length is greatly reduced when compared to the protonated form, and the M-OH_2 distance trans to the M-OH has increased in length. Also, the equatorial M-OH_2 bond lengths have increased. This may be indicative of a trans- and cis- influence occurring, whereby the OH^- ligand has weakened the bonds of the other ligands in the equilibrium state of the complex. Alternatively, the structures could be explained by consideration of Pauling's Electroneutrality Principle. This states that the electronic distribution in a molecule will tend to arrange itself such that all atoms are as close to being electrically neutral as

possible. Thus, the M^{n+} will have a strong interaction with the negatively charged OH^-, but not so strong with the neutral OH_2.

From a comparison of calculated hexaaquo M-O bond lengths and available experimental data, it was unclear which was the best computational method. Thus, in the investigation of pK_a values, all the different methods were used and the results obtained will now be compared.

10.2.1. Correlation of ΔE with pK_a

The relationship between ΔE with pK_a has been discussed in section 9.4, and was investigated using LDA, postscf, LDA+Stoll and NL-LDA.

The results are shown in Tables 10.8 to 10.11, and Graphs 10.1 to 10.4. The possibility of a linear relationship has been investigated and lines have been fitted to the graphs illustrated and will be discussed later.

The abbreviations used in the tables are: E (Maq) which is equivalent to $E[M(H_2O)_6]^{n+}$ in equation 8.9, solv aq is the solvation energy of $[M(H_2O)_6]^{n+}$, E(Moh) which is equivalent to $E[M(H_2O)_5OH]^{(n-1)+}$ in equation 8.9, and solv oh is the solvation energy of $[M(H_2O)_5OH]^{(n-1)+}$.

In all the results, ΔE (see equation 8.9) is correlated to the pK_a of $[M(H_2O)_6]^{n+}$ ions. These pK_a values were obtained from the IUPAC Stability Constants Database (1993)[8] and are listed in Table 10.8 (overleaf).

Table 10.8. pK_a values of metal ions

	pK_a
Mn(II)	10.5
Ni(II)	10.0
Fe(II)	9.5
Zn(II)	9.2
Al(III)	5.0
Cr(III)	3.8
Fe(III)	3.2

Table 10.9. Method 1 LDA

	E (Maq)	solv aq	E (Moh)	solv oh	E -(Maq) +E (Moh)	Δsolv	Δ E (M)
Mn(II)	-8224.68	-786.40	-8711.43	-196.05	-486.79	590.35	103.60
Ni(II)	-7681.42	-816.47	-8114.66	-204.72	-433.24	611.75	178.51
Fe(II)	-8073.04	-802.31	-8596.98	-199.43	-523.94	602.88	78.94
Zn(II)	-7466.14	-800.00	-7916.84	-200.00	-450.70	600.00	149.30
Al(III)	-6499.27	-1892.73	-7505.89	-843.77	-1006.62	1048.96	42.34
Cr(III)	-6744.55	-1858.93	-7767.67	-826.19	-1023.12	1032.74	9.62
Fe(III)	-6527.37	-1826.32	-7611.79	-811.69	-1084.42	1014.63	-69.79

All values in Table 10.9 are in kJ/mol.

Graph 10.1.

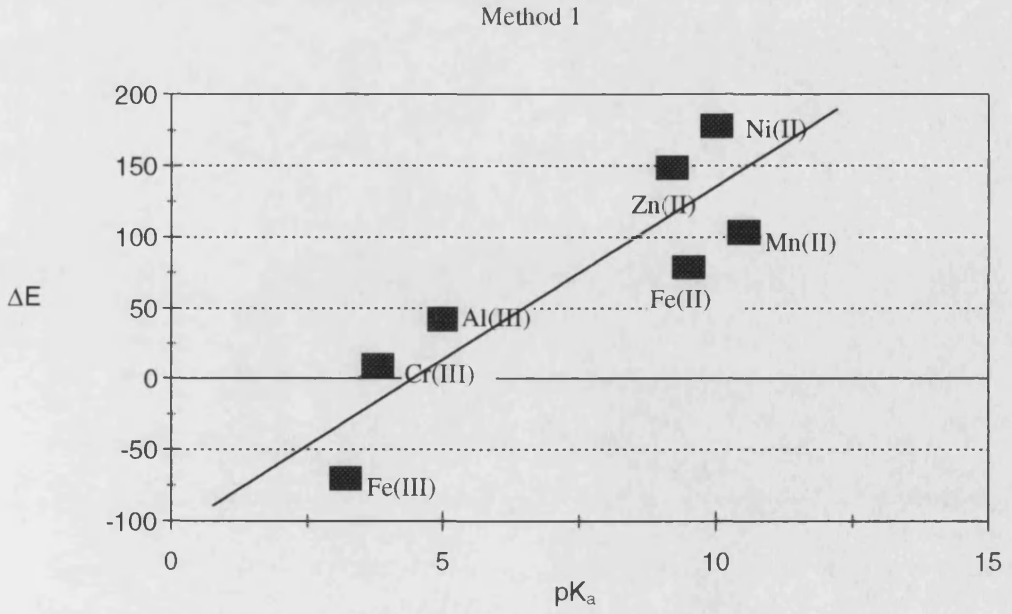

From first glance of graph 10.1, there seems to be a good linear relationship.

Table 10.10. Method 2 LDA+postscf

	E (Maq)	solv aq	E (Moh)	solv oh	E -(Maq) +E (Moh)	Δsolv	Δ E (M)
Mn(II)	-7613.51	-786.40	-8124.05	-196.05	-510.54	590.35	79.81
Ni(II)	-7029.93	-816.47	-7488.28	-204.72	-458.35	611.75	153.41
Fe(II)	-7439.76	-802.31	-7992.16	-199.43	-552.40	602.88	50.48
Zn(II)	-6808.47	-800.00	-7283.64	-200.00	-475.17	600.00	124.83
Al(III)	-5807.17	-1892.73	-6842.66	-843.77	-1035.49	1048.96	13.47
Cr(III)	-6064.84	-1858.93	-7116.89	-826.19	-1052.05	1032.75	-19.30
Fe(III)	-5863.81	-1826.32	-6978.25	-811.69	-1114.44	1014.65	-99.81

All values in Table 10.10 are in kJ/mol.

Graph 10.2.

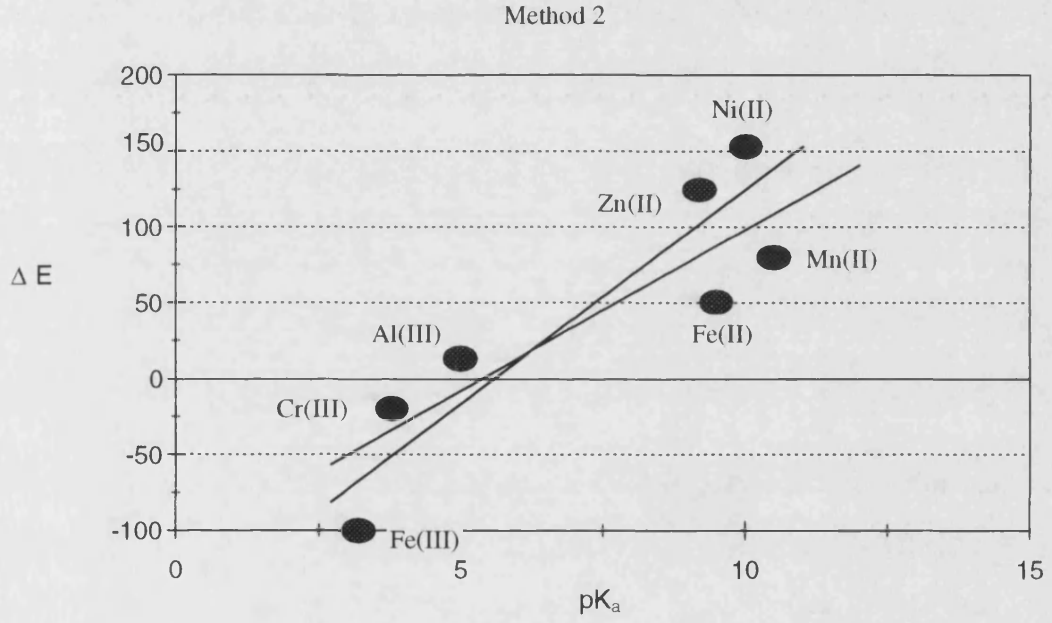

However, from the points plotted, a number of straight line graphs could be fitted.

Table 10.11. Method 3 LDA + Stoll

	E (Maq)	solv aq	E (Moh)	solv oh	E -(Maq) +E (Moh)	Δsolv	Δ E (M)
Mn(II)	-8026.49	-781.97	-8471.57	-194.94	-445.08	587.03	141.95
Ni(II)	-7505.37	-811.70	-7896.86	-204.12	-391.49	607.58	216.09
Fe(II)	-7877.86	-797.70	-8359.27	-197.72	-481.41	599.98	118.57
Zn(II)	-7285.25	-797.70	-7695.36	-198.85	-410.11	598.85	188.74
Al(III)	-6355.07	-1887.01	-7316.53	-836.14	-961.46	1050.87	89.41
Cr(III)	-6617.27	-1835.41	-7594.00	-823.74	-976.73	1029.67	52.94
Fe(III)	-6394.66	-1820.99	-7433.02	-809.33	-1038.36	1011.66	-26.70

All values in Table 10.11 are in kJ/mol.

Graph 10.3.

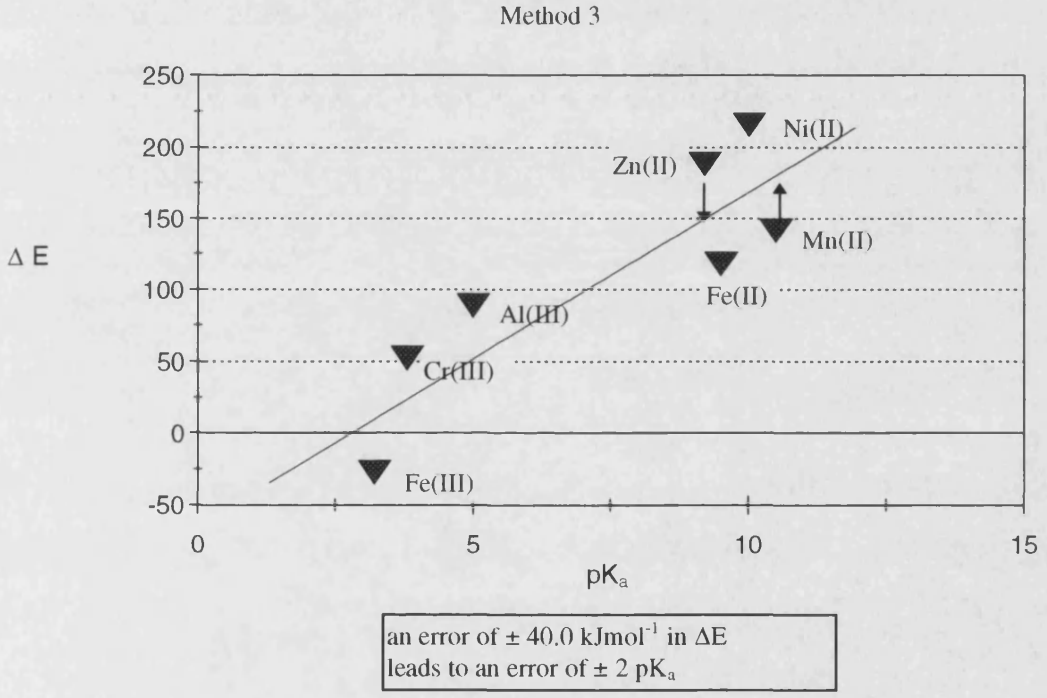

From analysis of this graph it can be seen that an error of ±40 kJ/mol in ΔE gives an error in pK_a of ±2 units.

Table 10.12. Method 4 LDA + gradient corrections.

	E (Maq)	solv aq	E (Moh)	solv oh	E -(Maq) +E (Moh)	Δsolv	Δ E (M)
Mn(II)	-7644.67	-771.11	-8154.99	-190.66	-510.32	580.45	79.81
Ni(II)	-7065.42	-800.00	-7525.48	-199.43	-460.06	600.57	153.41
Fe(II)	-7479.45	-786.40	-8027.73	-193.85	-548.28	592.55	44.27
Zn(II)	-6835.60	-786.40	-7313.45	-195.49	-477.85	590.91	113.06
Al(III)	-5827.51	-1887.01	-6866.35	-831.14	-1038.84	1055.87	17.03
Cr(III)	-6096.84	-1831.67	-7147.15	-814.08	-1050.31	1017.59	-32.72
Fe(III)	-5891.43	-1800.00	-7010.74	-797.70	-1119.31	1002.30	-117.01

All values in Table 10.12 are in kJ/mol.

Graph 10.4.

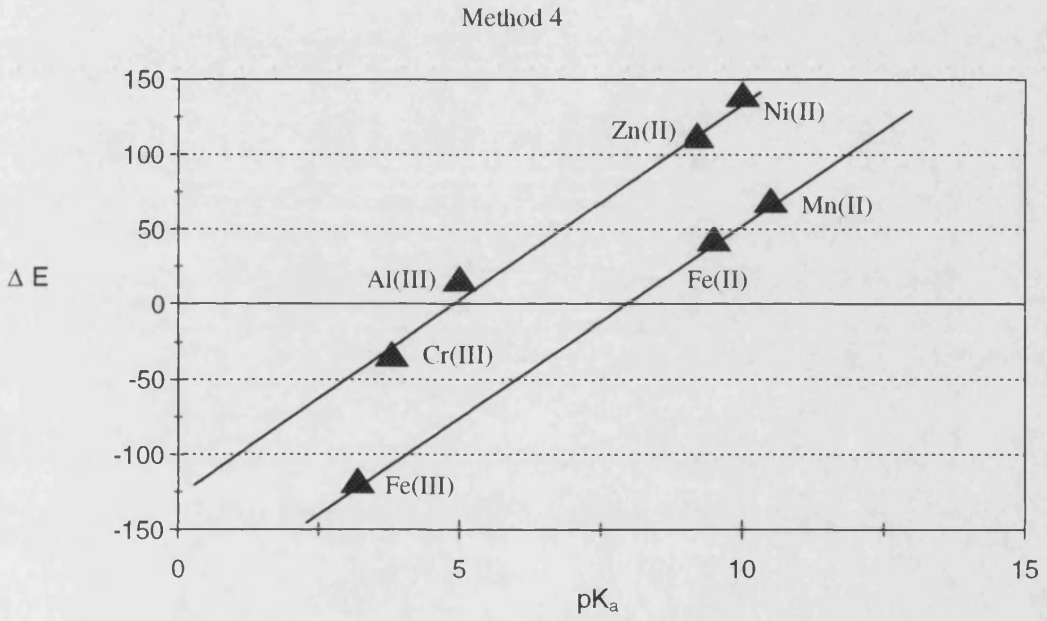

Lines can also be fitted through the points shown.

It can be seen that for all methods, even though the actual value of ΔE changes, the overall trends stay the same.

As defined earlier,

$$\Delta E \propto pK_a$$

thus from a plot of ΔE vs pK_a a linear correlation would be expected (Graph 10.1). However from the points plotted, a number of straight line graphs could be fitted (Graph 10.2), and this is obviously not satisfactory. Also, from analysis of Graph 10.3, it can be seen that an error of $\approx \pm 40$ kJ/mol in ΔE gives an error in pK_a of ± 2. This is very disappointing, as higher resolution was expected. From Graph 10.4 it can be seen that a line could be fitted through points Cr(III), Al(III), Zn(II) and Ni(II), and also through Fe(III), Fe(II) and Mn(II). This could suggest that for Fe(III), which has five unpaired electrons, Fe(II) which has four unpaired electrons and Mn(II) with five unpaired electrons that 'spin contamination' may be taking place.

10.2.2. Spin Contamination.

All the above calculations were spin unrestricted calculations. As mentioned in the previous chapter, spin unrestricted implies that the up-spin and down-spin electrons are spatially different.

Consider, Figure 10.2.

Figure 10.2.

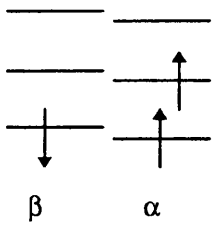

In Figure 10.2, S = 1/2.

If α and β are spatially different then excited states may be possible (Figure 10.3).

Figure 10.3.

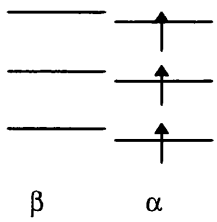

This excited state can mix in with the ground state, resulting in the overall spin being greater than 1/2, thus an impure spin state for the complex being considered. Spin contamination in this way will introduce errors into the calculation.

To overcome this problem, restricted single point calculations were carried out on all of the complexes. Single point calculations are calculations where the SCF solution is computed for the input geometry only. No geometry optimisations is performed. In the single point calculations carried out, the ground state structure determined from the previous calculations were used as the input structures and spin restriction was imposed. The results from these calculations are shown in Tables 10.13 to 10.16 and Graphs 10.5 to 10.8.

Table 10.13. Method 5 LDA + restricted

	E (Maq)	solv aq	E (Moh)	solv oh	E -(Maq) +E (Moh)	Δsolv	Δ E (M)
Mn(II)	-7950.68	-786.40	-8332.33	-196.05	-381.65	590.35	208.70
Ni(II)	-7581.02	-816.47	-7868.36	-204.72	-287.34	611.75	324.41
Fe(II)	-7989.14	-802.31	-8354.34	-199.43	-365.20	602.88	237.68
Zn(II)	-7466.14	-800.00	-7916.84	-200.00	-450.70	600.00	149.30
Al(III)	-6499.27	-1892.73	-7505.89	-843.77	-1006.62	1048.96	42.34
Cr(III)	-6744.54	-1858.98	-7621.13	-826.19	-876.59	1032.79	156.20
Fe(III)	-6367.71	-1826.32	-7400.56	-811.69	-1032.85	1014.63	-18.22

All values in Table 10.13 are in kJ/mol.

Graph 10.5.

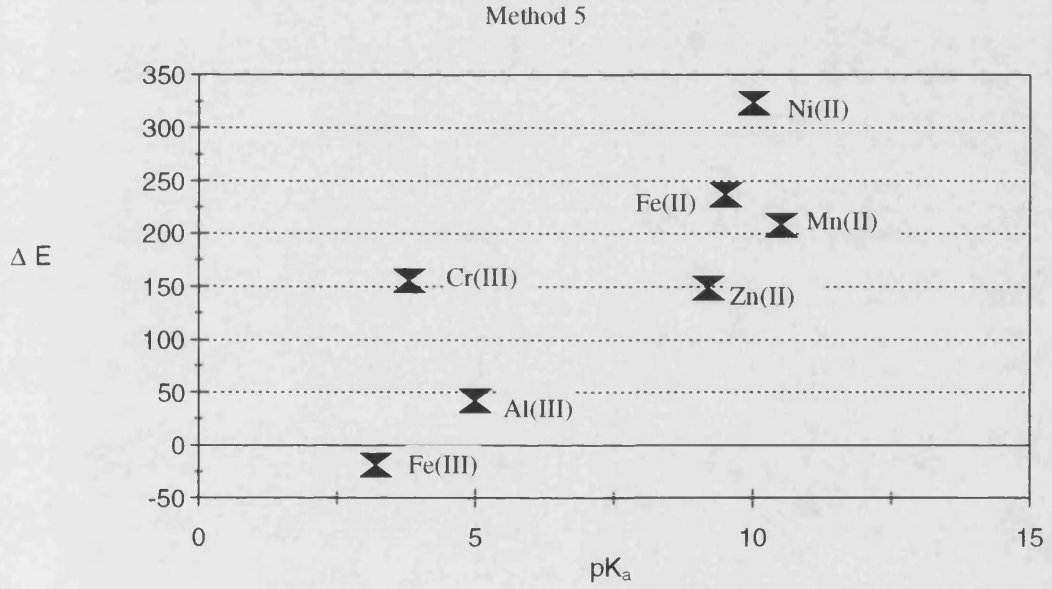

Table 10.14. Method 6 LDA + postcsf restricted

	E (Maq)	solv aq	E (Moh)	solv oh	E -(Maq) +E (Moh)	Δsolv	Δ E (M)
Mn(II)	-7323.60	-786.40	-7735.55	-196.05	-411.95	590.35	178.40
Ni(II)	-6897.42	-816.47	-7256.95	-204.72	-359.37	611.75	252.38
Fe(II)	-7346.92	-802.31	-7747.37	-199.43	-400.45	602.88	202.43
Zn(II)	-6808.47	-800.00	-7283.64	-200.00	-475.17	600.00	124.83
Al(III)	-5807.17	-1892.73	-6842.66	-843.77	-1035.49	1048.96	13.47
Cr(III)	-6064.79	-1858.93	-6949.81	-826.19	-885.02	1032.74	147.72
Fe(III)	-5694.11	-1826.32	-6760.01	-811.69	-1065.90	1014.63	-51.27

All values in Table 10.14 are in kJ/mol.

Graph 10.6.

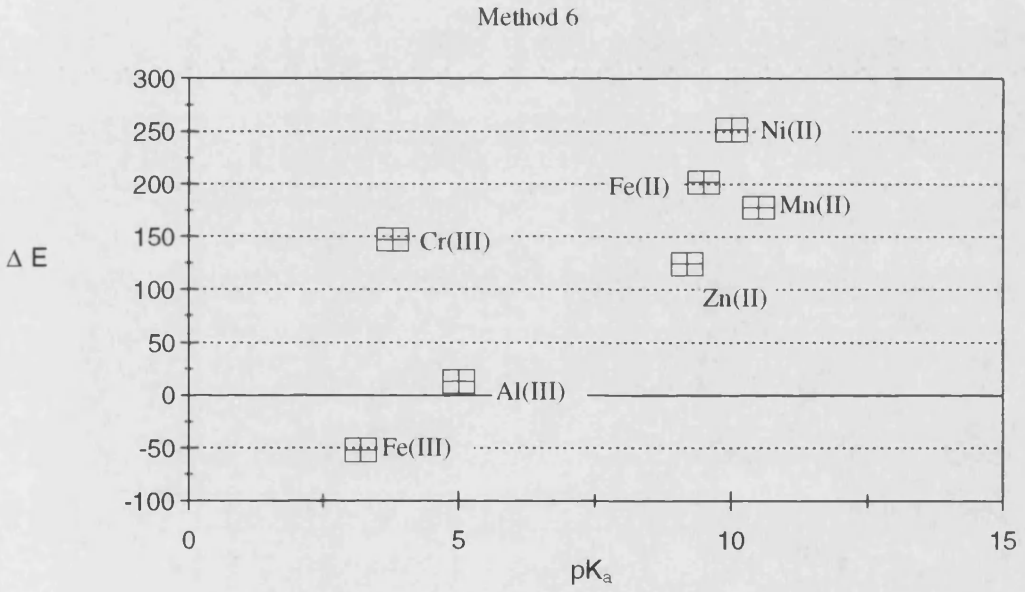

Table 10.15. Method 7 LDA + Stoll restricted

	E (Maq)	solv aq	E (Moh)	solv oh	E -(Maq) +E (Moh)	Δsolv	Δ E (M)
Mn(II)	-7694.12	-781.97	-8184.89	-194.94	-490.77	587.03	96.26
Ni(II)	-7365.19	-811.70	-7650.70	-204.12	-285.51	607.58	322.07
Fe(II)	-7741.74	-797.70	-8128.72	-197.72	-386.98	599.98	213.00
Zn(II)	-7285.25	-797.70	-7695.36	-198.85	-410.11	598.85	188.74
Al(III)	-6355.07	-1887.01	-7316.53	-836.14	-961.46	1050.87	89.41
Cr(III)	-6386.99	-1835.41	-7349.27	-823.74	-962.28	1029.67	67.39
Fe(III)	-6228.29	-1820.99	-6951.38	-809.33	-723.10	1011.66	288.56

All values in Table 10.15 are in kJ/mol.

Graph 10.7.

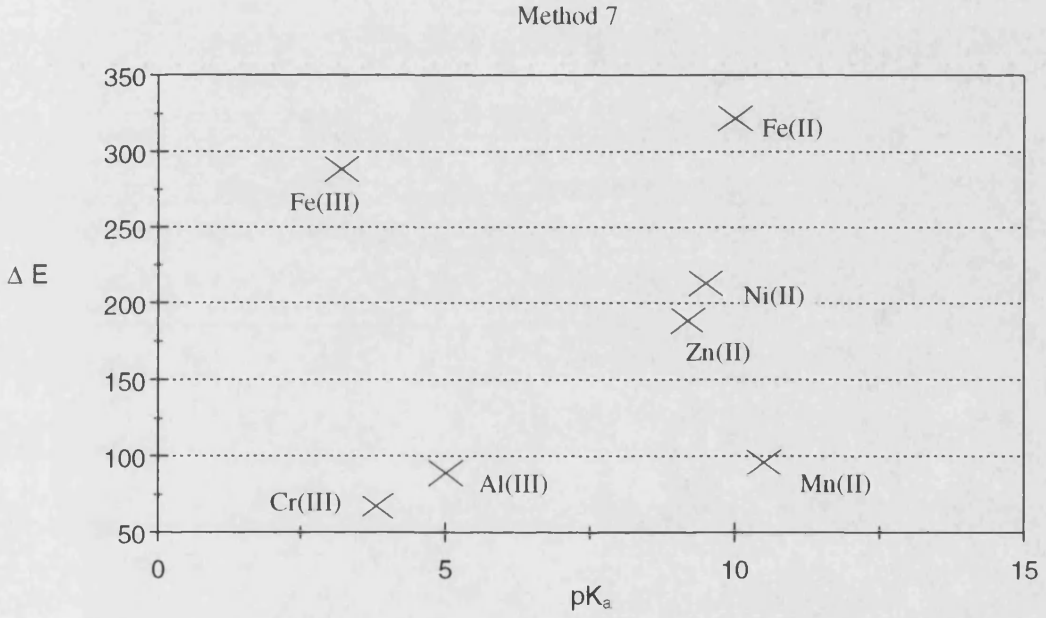

Table 10.16. Method 8 LDA + gradcor. restricted

	E (Maq)	solv aq	E (Moh)	solv oh	E -(Maq) +E (Moh)	Δsolv	Δ E (M)
Mn(II)	-7328.99	-711.11	-7760.18	-190.66	-431.19	580.45	149.26
Ni(II)	-6930.43	-800.00	-7265.49	-199.43	-335.06	600.57	265.51
Fe(II)	-7338.41	-786.40	-7705.39	-193.85	-366.98	592.55	225.57
Zn(II)	-6835.60	-786.40	-7313.45	-195.49	-477.85	590.91	113.06
Al(III)	-5827.51	-1887.01	-6866.35	-831.14	-1038.84	1055.87	17.03
Cr(III)	-5880.30	-1831.67	-6980.16	-814.08	-1099.86	1017.59	-82.27
Fe(III)	-5707.45	-1800.00	-6543.13	-797.70	-835.68	1002.30	166.62

All values in Table 10.16 are in kJ/mol.

Graph 10.8.

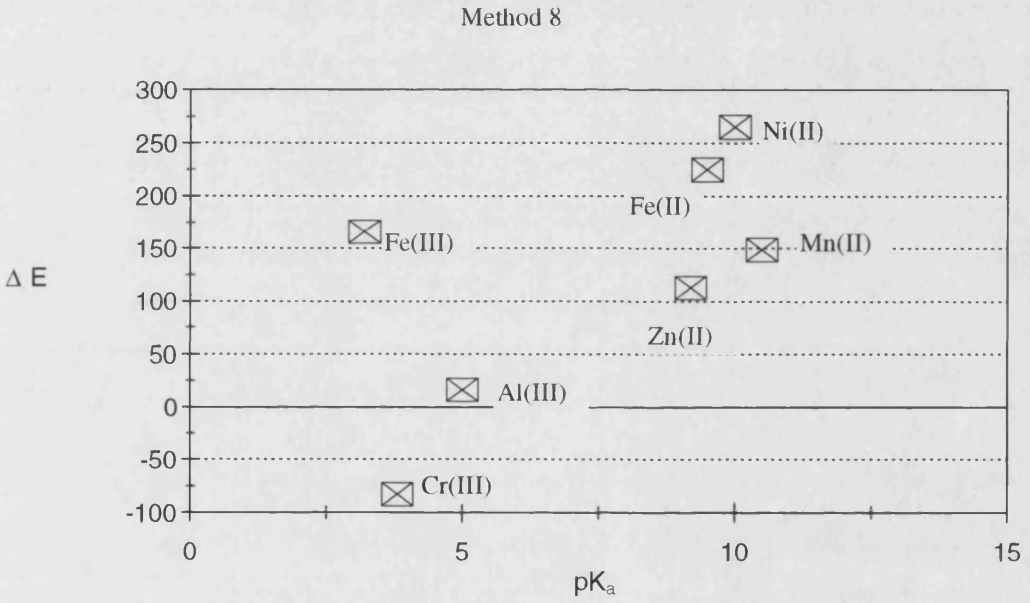

From analysis of Graphs 10.5 to 10.8, it can be seen that by correcting for 'spin contamination', the overall correlation of ΔE vs pK_a is not linear.

10.3. Conclusions and Future Work.

Using the methods described, it is clear that the M(III) ions have greater acidity than the M(II) ions. This would be expected as a larger positive charge will have a larger stabilising influence on the negatively charged OH^-. Thus, the $[M(H_2O)_6]^{3+}$ species

would be more acidic than the $[M(H_2O)_6]^{2+}$ species. The methods used were, however, unable to differentiate between the detailed variation of pK_a's in a series of 2+ or 3+ ions.

Future work must, therefore, be carried out to improve this resolution. A more accurate description of solvation may be one way of making improvements. Empirical calculations, for example, Molecular Dynamics calculations using the Car-Parrinello method, could be carried out on the cations with all the solvent being explicitly included. This may then give a more detailed analysis of the solution structure of these ions and thus be able to give a more accurate description of the pK_a.

This work also reports the calculated structures of the deprotonated aquo ions. The loss of the H^+ seems to have a profound effect on the equilibrium bond lengths of the other water ligands. Again, by including solvent explicitly in the calculations, it would be interesting to see what effects this would have on the structure.

A recent communication from Breza et al.[9] suggests that the water in $[Cu(H_2O)_6]^{2+}$ are in fact tilted. In the calculations carried out in this work, planar $M(OH_2)$ coordination was imposed. These symmetry constraints may have determined a calculated structure which was not at the true energetic minima.

Another consideration is that of the spin state of the complex. Spin transitions are feasible in six-coordinate complexes of d^4, d^5, d^6 and d^7. In this study this would include the d^5 Mn(II), Fe(III) and d^6 Fe(II). The restricted single point calculations carried out would have accounted for the low spin configurations of these complexes. However, it was observed from graph 10.5 to 10.8 that a linear correlation was still not observed. However, as spin transitions are not particularly feasible for d^8 or d^3 systems, then maybe a more rigorous investigation into which spin state of the metal would yield the most energetically favourable structure would be appropriate for the deprotonated complexes of Mn(II), Fe(III) and Fe(II) in this study.

10.4. References

1. E. J. Baerends, D. E. Ellis and P. Ros, *Chem. Phys.*, 1973, **2**, 41.
2. O. Gunnarsson and I. Lundquist, *Phys. Rev.*, 1976, **B13**, 4274.
3. J. G. Snijders, P. Vernooijs and E. J. Baerends, *At. Data Nucl. Data Tables*, 1981, **26**, 483.
4. J. Li, G. Schreckenbach and T. Ziegler, *J. Phys. Chem.*, 1994, **98**, 4838.
5. T. K. Sham, J. B. Hastings and M. L. Perlman, *J. Am. Chem. Soc.*, 1980, 102, 5904.
6. Y. Marcus, *Chem. Rev.*, 1988, **88**, 1475.
7. J. K. Beattie, S. P. Best, B. W. Skelton and A. H. White, *J. Chem. Soc., Dalton Trans.*, 1981, 2105.
8. IUPAC Stability Constants Database (1993), G. Pettit and L. D. Pettit, IUPAC and Academic Software.
9. M. Breza, S. Biskupic and J. Kozisek, private communication.

Part 3

General Conclusions

Chapter 11

Conclusions

This thesis has discussed two approaches of Computational Chemistry applied to transition metal systems.

11.1. Modelling of Transition Metal Centres using Density Functional Theory.

One such approach is Density Functional Theory. This is an ab initio technique which has often been used in the determination of geometries, bond energies, transition states and other molecular properties. Here it was used in the investigation of the acidic properties of some metal hexaaquo ions. This work was prompted by Sadler et al.[1], who suggested that there was a correlation between the pK_a of $[M(H_2O)_6]^{2+}$ ions and the binding of that metal, M, to the protein transferrin. Transferrins are of great biological interest. Their main role is in the binding, sequestering and transporting of Fe^{3+} ions, thus protecting against the toxic effects of the free iron whilst also maintaining its availability. However, transferrins can also bind many other metal ions and they, therefore, may also be involved in the binding and translocation of other metal ions.

The investigations of Sadler and co-workers have suggested that because of the observed correlation (mentioned above) then the factors which govern pK_a, would also influence metal binding to transferrins. This then led to the investigation of the acidity of metal hexaaquo ions (where the metal, M, was Fe(III), Cr(III), Al(III), Zn(II), Fe(II), Ni(II) and Mn(II)) using the ab initio method Density Functional Theory.

The geometries of the $[M(H_2O)_6]^{n+}$ ions were determined and generally agreed well with experimentally characterised structures. The structures of the deprotonated complexes $[M(H_2O)OH]^{(n-1)+}$ were also calculated, and showed some interesting characteristics. The M-OH distance in all cases was a relatively short bond and the OH_2 trans to this was elongated. It is suggested that the trans influence may be the cause of this.

In this study, it was assumed that the pK_a would be correlated with the dissociation energy of H^+, i.e. the energy difference between the deprotonated and protonated forms, ΔE. In the calculation of ΔE the solvation effects would play an important role. This was addressed using the Born model. This is a relatively simple approach, but it was used here as it has been successfully applied by Deeth and Elding[2] in the modelling of water exchange of $[Pd(H_2O)_4]^{2+}$ and $[Pt(H_2O)_4]^{2+}$. On calculation of ΔE, graphs were than plotted of ΔE vs pK_a to elucidate the correlation.

It was found that the 3+ ions were computed to be more acidic than the 2+ ions, as found experimentally. This is because the negative charge on the OH^- would be stabilised by the greater positive charge on the metal making it easier for the H_2O to lose a proton. The calculations were, however, unable to resolve the differences in acidity between the series of 2+ or 3+ ions, the error margin of 2 pK_a units being of the order of the spread of values for Mn^{2+} to Zn^{2+}. It is hoped, however, that by a more rigorous account of solvation, in future work, that a higher resolution will be obtained and, thus, the intimate factors governing the variations of pK_a, within a series of complexes with the same metal charge, could be determined.

11.2. Modelling of Transition Metal Centres using Molecular Mechanics.

Transition metals, which can play vitally important roles in a wide variety of biological processes, often display a wide variety of coordination numbers and geometries. For example, the active site of plastocyanin, a copper protein vital in photosynthesis, is a Cu(II) ion in a highly distorted tetrahedral environment. Modelling complexes is important for elucidating the metal ligand binding at the active site. However, ab initio methods are too expensive and computationally demanding for large systems. Thus, an empirical method, such as Molecular Mechanics, is required.

Molecular Mechanics has emerged as a popular method for modelling molecular geometry and energetics, and in this thesis it was applied to several coordination compounds.

For transition metal species, the partly filled d shells can have a profound effect on the bond lengths and coordination geometries around the metal centres. For example, a 6-coordinate Ni(II) high spin complex displays octahedral geometry, whereas a low spin Ni(II) complex , which can be viewed as a limiting case of tetragonal elongation, exhibits square planar stereochemistry. Cu(II) 6-coordinate species are Jahn Teller active and generally elongations are observed.

Geometry changes of this type can be generally rationalised in terms of ligand field stabilisation energies. Thus, for Molecular Mechanics to model these types of systems accurately, a term which can account for the ligand field stabilisation exhibited by these complexes was required. Thus, a Cellular Ligand Field Stabilisation Energy Term, based on Cellular Ligand Field theory was introduced. A transferable force field for a variety of systems has now been developed.

Consider the above example of high and low spin Ni(II) complexes. Conventionally, Molecular Mechanics treatments would have two separate force fields for paramagnetic and diamagnetic species, respectively. The CLFSE/MM methodology, however, is the first to be able to model both high and low spin systems with the same force field, as illustrated with the six- and four-coordinate Ni(II) amine systems. This is advantageous as it reduces the amount of parameterisation needed to develop the force field, but the full potential of this method lies in the following application. As the CLFSE depends on d orbital occupation, it is feasible that a possible future operation of the CLFSE/MM method would be the modelling of spin crossovers. Providing the initial and final spin states are well defined, one could imagine following the spin crossover by progressively mixing the relevant sets of d orbital occupations. The cross over region would then be associated with non-integral d orbital populations.

Calculations were also carried out on a hypothetical low spin NiN_6 'bare' ligand system. Consider the d orbital energy diagram of such a species (Figure 11.1).

Figure 11.1. Energy level diagram of d orbitals in hypothetical low spin NiN_6 system.

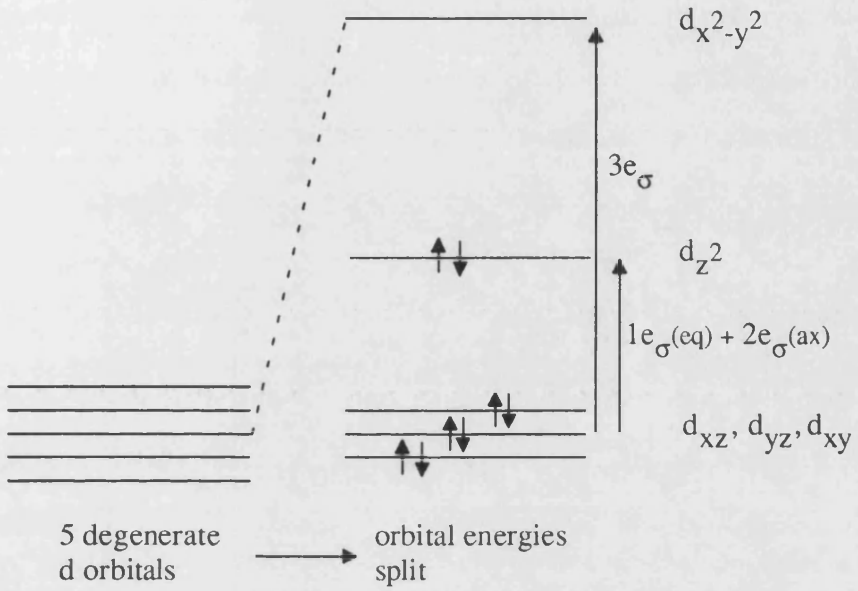

The CLFSE can thus be calculated to be

$$CLFSE = -22/5\ e_\sigma(eq) + 4/5\ e_\sigma(ax) \qquad (11.1)$$

Thus, a plot of CLFSE + Morse function (kcal/mol) vs bond length (Å) can be determined (Figure 11.2 overleaf).

Figure 11.2. Plot of CLFSE + Morse function (kcal/mol) vs bond length (Å) for a NiN_6 system.

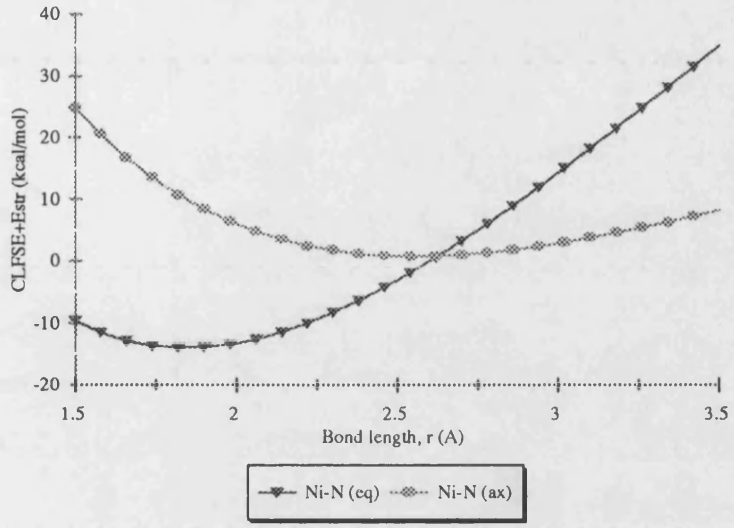

From the graph it can be seen that the Ni-N(eq) minimum lies at approximately 1.84 Å and the minimum for the Ni-N(ax) interaction lies at approximately 2.56 Å. When the van der Waals interactions are then included the CLFSE/MM method predicts an elongated geometry with Ni-N(ax) = 2.78 Å and Ni-N(eq) = 1.90 Å. Deeth and Hitchman[2] suggested that when a Ni(II) complex undergoes high → low spin conversion, the axial bond lengthens to such an extent that entropy effects make it energetically favourable for these ligands to be lost from the coordination sphere. Calculations carried out on a hypothetical 'bare' ligand system of low spin NiN_6 support this suggestion that low spin d^8 complexes can notionally be derived from a Jahn Teller distortion of an octahedral complex.

The Jahn Teller distortions of Cu(II) complexes have also presented many problems for molecular modellers. Many conventional force fields have tried to model these types of systems but have always needed to include external constraints, or to use two separate force field parameter sets for axial and equatorial ligands, thus, losing the predictive nature of the Molecular Mechanics calculations.

The CLFSE/MM strategy has been the first to be able to automatically generate the Jahn Teller distortions displayed by six-coordinate Cu(II) complexes, as shown by the excellent agreement between observed and calculated structures for a number of Cu(II) amine species. Therefore, this method is a significant advance in this computational area.

The force field developed for these Cu(II) amines can not only predict the elongated structures of the six-coordinate systems, but also the trigonal bipyramidal (TBP) and square based pyramidal structures (SBP) of the five-coordinate systems and the square planar stereochemistry of the four-coordinate species. It was also shown that the energy difference between the TBP and SBP is very small, within approximately ± 3 kcal/mol. This reflects the delicate energy balance between these two stereochemistries.

Also, consider the d orbital energy level diagram for the TBP system (Figure 11.3).

Figure 11.3. Energy level diagram of d orbitals for TBP system.

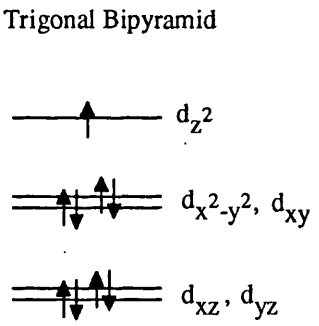

There is a 'hole' in the d_z^2 orbital. Thus, the d-electron density lying along the z axis is less than in the xy plane, i.e. the axial ligands are repelled to a lesser extent than the equatorial ligands, as reflected in the observed compressed structure. This is also calculated from the bare ligand system of CuN_5 where Cu-N(ax) = 1.88 Å and Cu-N(eq) = 2.28 Å. Thus, the stereochemical activity of the d electrons has been reproduced, and is a significant feature of the CLFSE/MM method.

It has been shown with the Cu(II) species, that the lattice effects play an important role in structure determination. Future work could include the modelling of these crystal packing effects.

Other future work could include investigations into static vs dynamic Jahn Teller effects. As Molecular Mechanics minimisations only find the local minima, it is suggested that the energies of compressed structures of Cu(II) species maybe determined as well as the elongated structures. The energy difference between them could then be related to whether or not static or dynamic Jahn Teller effects would occur.

Consider a Jahn Teller potential energy surface. Inclusion of second order terms warp the Mexican hat potential, and thus, a section could be represented as in Figure 11.4.

Figure 11.4. A representation of a section through a warped Mexican hat potential.

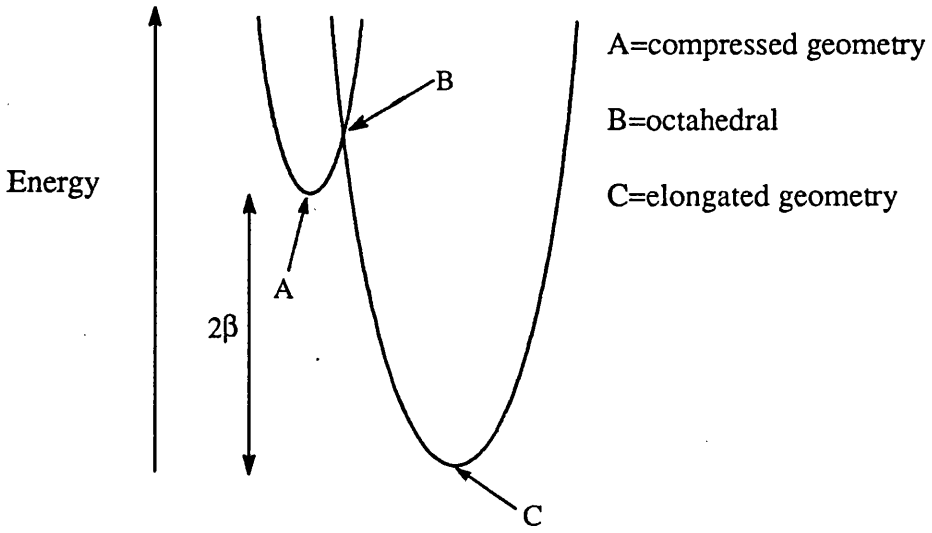

The Molecular Mechanics calculations could determine the energies of the compressed and elongated structures, and thus the difference, 2β, could then be determined. If $2\beta > kT$ then a static Jahn Teller effect would be predicted, but if $2\beta < kT$ then dynamic fluctuations would be expected. It is thought that lattice effects would also have to be

considered in this type of calculation, and this will hopefully form the basis of some future work.

The systems discussed so far have been amines and thus only σ interactions have been considered in the CLFSE. The next natural progression was to look at ligands which participate in π bonding. Thus, some complexes of Co(III) and Ni(II) where the ligands involved are chloride and amine donors, and Ni(II) and Cu(II) where the ligands involved are chloride and imine donors were studied. It was perceived that using the Cellular Ligand Field model within the Molecular Mechanics framework, then the M-L interaction could have been separated into its individual σ and π components.

The inclusion of e_π would affect not only the bond length, but also the bond angle and torsions as well. Within the CLFSE formalism, it was required that the shortening and strengthening of a given M-L bond should be energetically favourable i.e. be associated with an increasingly negative CLFSE. However, as the d orbitals of π symmetry are lower in energy than the global barycentre, increasing the e_π pushes the $d\pi$ orbitals up in energy which tends to reduce the magnitude of the CLFSE. Thus, it seems that the bond length dependence of e_π would prove to be an unnecessary complication, so it was neglected.

An angular dependence could still be incorporated by having a fixed a_0 value. However, as this could be mimicked within the e_σ parameterisation, it again seemed an unnecessary consideration.

π interactions also become important when considering that there is a torsional contribution to the CLFSE from e_π. For a d^8 system, for example, when considering the π interactions, if there is a rotation of the M-L bond along the y axis as shown in Figure 11.1 overleaf,

Figure 11.1. Illustration of π orbital orientation after rotation of M-L bond along the axis.

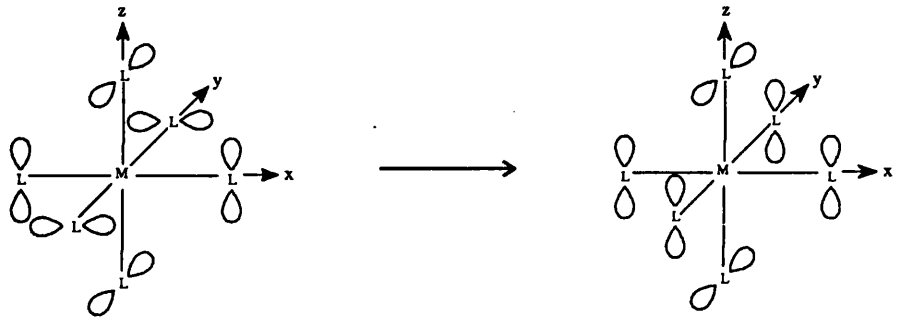

then although the qualitative d orbital energy level diagram changes, the CLFSE stays the same (see Figure 11.2).

Figure 11.2. The d orbital energy levels before and after rotation of the M-L bond.

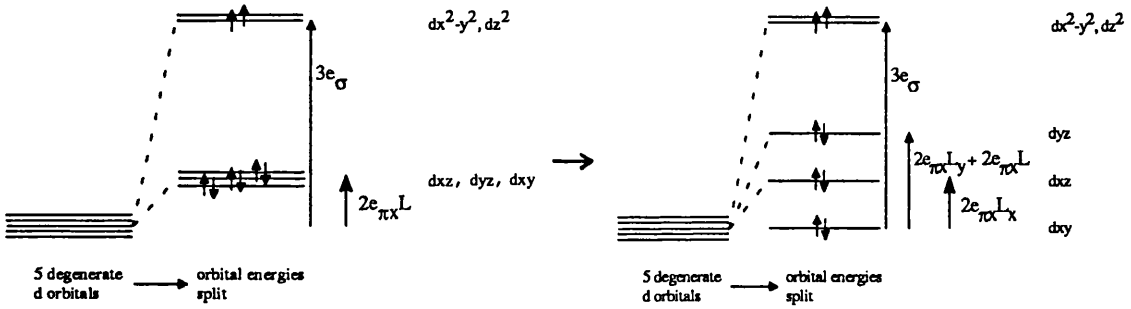

CLFSE = -18/5 e_σ + 12/5 e_π CLFSE = -18/5 e_σ + 12/5 e_π

In all the systems studied here, i.e. the low spin d^6 Co(III), d^8 Ni(II) and d^9 Cu(II), the t_{2g} orbitals are filled with electrons, thus, this torsional dependence is insignificant. However, if the d_π functions were not symmetrically filled, for example, a d^1, d^2, high spin d^6 and high spin d^7 system, then inclusion of a π interaction becomes more important. Thus, future work needs to be carried out to assess the magnitude of this effect in systems of this type.

Considering the above arguments, for the Co(III), Ni(II) and Cu(II) complexes studied, the M-Cl and M-imine bonds were parameterised by only considering the σ interaction, and excellent agreement between observed and calculated structures was still obtained.

The tetrahedral geometries exhibited by $[Ni(Cl)_4]^{2-}$ and $[Cu(Cl)_4]^{2-}$ presented another challenge, as it was shown that the CLFSE term would always favour a square planar structure over a tetrahedral geometry. It was found that by the inclusion of charges into the force field, that these, as well as the other stereochemistries mentioned above, could still be handled successfully. The inclusion of the electrostatic term into the force field can only prove advantageous, as future work may include extending the force field to look at biological systems, and in these systems the long range electrostatic interactions play an important role. If crystal packing influences were also to be included in future modelling then the inclusion of electrostatics in the calculations would become significant. Thus, a Coulombic term was introduced and a transferable force field was established for all the Ni(II) and Cu(II) complexes studied.

Another success which has not previously been achieved using conventional Molecular Mechanics, was the modelling of the trans influence of Pt(II) complexes by the introduction of a ligand-ligand Morse function, for ligands which are trans to each other. This work is only in the early stages but shows great promise. It is necessary to develop the force field to look at 'real' systems as opposed to the 'model' systems discussed and also to extend the force field to encompass a wider range of ligands before the full potential of this method can be realised.

The use of Molecular Mechanics lies in its predictive ability. Before this can be achieved, a force field must be tested so that a feel for the accuracy and ability of the method in calculating structures can be ascertained.

The accurate modelling of transition metal complexes has been tested for a number of systems using the CLFSE/MM method. The ultimate aim of any force field is to be able to

determine or predict the structure of any complex. Thus, there is quite a lot of work still to be done in extending the force field to include a wide range of ligands and metals.

Overall, the inclusion of the CLFSE term into the Molecular Mechanics force field has proved very successful in the determination of structures for transition metal complexes, providing a general Molecular Mechanics treatment which is independent of metal coordination number and/or stereochemistry. This method has made some significant advances in this area. These include:

i) the determination of the structures of high and low spin complexes using the same force field.

ii) the uniform treatment of four-, five- and six-coordinate Cu(II) complexes with a single force field.

iii) the automatic generation of Jahn Teller distorted Cu(II) complexes.

iv) the modelling of the trans influence of Pt(II) complexes (though this is still in the earlier stages of development).

This thesis has illustrated two methods of computational chemistry. It is hoped that the reader has gained an insight into how the application and development of these methods can be used in the elucidation of the chemistry of transition metal species.

11.3. References.

1. P. J. Sadler, private communication.
2. R. J. Deeth and M. A. Hitchman, *Inorg. Chem.*, 1986, **25**, 1225.

Part 4

Appendix

Force Field Parameters for calculations which do not include charges.

Complete listing of the Force Field parameters and functional forms used in this work. All energies are calculated in kcal/mol. This requires converting the CLFSE from wavenumbers.

Functional forms

Bond Stretch: $E_{str} = D_0[1\text{-}exp\text{-}^{\alpha(r-r_0)}]^2$

Angle Bend: $E_{bend} = (1/2)k_\theta(\theta-\theta_0)^2$

Torsion: $E_{tor} = K(1+S(cosn\omega)$

Van der Waals: $E_{vdw} = A/r^9 - B/r^6$

For Co(III):

CLFSE: $e_\sigma(N) = 33100 - 13000r\ (cm^{-1})$

CLFSE: $e_\sigma(Cl) = 12000 - 3200r\ (cm^{-1})$

For Cu(II) and Ni(II):

CLFSE: $e_\sigma(N) = 21629 - 8235r\ (cm^{-1})$

CLFSE: $e_\sigma(N5) = 21629 - 8235r\ (cm^{-1})$

CLFSE: $e_\sigma(N6) = 21629 - 8235r\ (cm^{-1})$

CLFSE: $e_\sigma(Cl) = 9000 - 2500r\ (cm^{-1})$

Bond stretch

	D_0 (kcal/mole)	r_0 (Å)	α
Co - N	75.0	2.663	0.45
Co - Cl	60.0	2.400	0.45
Ni - N	80.0	2.393	0.45
Ni - Cl	60.0	2.550	0.45
N - C	72.0	1.49	2.20
N - H	93.0	0.91	2.50
C - C	88.0	1.50	1.92
C - H	108.6	0.97	1.60
C5-H	108.6	0.970	1.60
N5'-H	93.0	1.030	1.00
C5-N5	80.0	1.350	1.60
C5-C5	80.0	1.350	1.60
C5-N5'	80.0	1.330	1.00
Cu-N5	80.0	2.333	0.45
C6-H	108.6	0.970	1.60
CJ-H	108.6	0.970	1.60
C6-C6	80.0	1.380	1.00
C6-C	72.0	1.490	1.92
C6-CJ	70.0	1.350	1.00
C6-CZ	70.0	1.350	1.00
C6-N6	80.0	1.350	1.60
CJ-N6	72.0	1.350	1.00
CZ-N6	80.0	1.350	1.60
Cu-N6	60.0	2.243	0.45
N5-N5'	72.0	1.34	2.00
Ni-N6	70.0	2.353	0.45
Ni-N5	80.0	2.373	0.45

Angle bend

	k_θ (kcal)	θ (°)
N - Ni - N	0.000	0.000
N - Ni - Cl	0.000	0.000
Cl - Ni - Cl	0.000	0.000
N -Co -N	0.000	0.000
N - Co - Cl	0.000	0.000
Cl - Co - Cl	0.000	0.000
N - Cu - N	0.000	0.000
Co - N - H	64.786	109.721
Co - N - C	28.786	118.008
Ni - N - H	64.786	109.721
Ni - N - C	28.786	118.008
H - N - H	47.497	108.977
N - C - H	64.786	109.492
C - N - C	28.786	109.492
C - C - C	64.786	109.492
N - C - C	64.786	110.492
H - N - C	64.786	109.492
H - C - C	51.815	109.378
H - C - H	47.497	108.977
H-N5'-C5	27.000	120.0
H-N5'-N5	27.000	120.0
N5-C5-H	90.000	114.0
C5-C5-H	90.000	110.0
C5-C5-N5'	90.000	110.0
C5-C5-N5	90.000	110.0
C5-N5-C5	90.000	110.0
C5-N5'-C5	90.000	110.0
N5-C5-H	50.000	120.0
N5'-C5-H	50.000	120.0
Cu-N5-C5	21.786	124.0
H-C6-C6	37.000	120.0
H-C6-CJ	37.000	120.0

H-C6-CZ	37.000	120.0
H-CZ-C6	37.000	120.0
N6-CJ-C6	90.000	120.0
N6-CZ-C6	90.000	114.0
N6-CJ-CJ	90.000	120.0
N6-CJ-C	64.000	115.0
C6-C6-C6	90.000	120.0
C6-CJ-CJ	90.000	120.0
C6-CJ-C	46.600	120.0
CJ-C6-C6	90.000	120.0
CZ-C6-C6	90.000	120.0
CJ-C-CJ	90.000	110.5
H-C-CJ	44.400	110.0
CJ-N6-CZ	75.100	114.0
CJ-N6-CJ	75.100	120.0
N6-C6-H	50.000	120.0
N6-CZ-H	50.000	120.0
N-C-CJ	64.786	110.5
Cu-N6-CJ	14.786	120.0
Cu-N6-CZ	14.786	130.0
N6-Cu-N6	0.0	0.0
N6-Cu-N	0.0	0.0
C5-N5-N5'	90.000	110.000
N5-N5'-C	75.000	114.000
N5-N5'-C5	90.000	114.000
CJ-N6-CJ	75.100	120.000
C-N5'-C5	75.100	114.000
N5-C-CJ	60.000	120.000
C6-CJ-C5	46.600	120.000
C5-C5-C5	75.000	104.000
N6-CJ-C	64.786	110.492
Ni-N6-CJ	14.785	124.008
Ni-N5-C5	7.786	128.008
Ni-N5-N5'	7.786	124.008
N6-Ni-N6	0.000	0.000
N6-Ni-N5	0.000	0.000
C-C-CJ	14.000	120.000
N5-C-N5	64.786	109.492
N5-Ni-N5	0.000	0.000

Torsion

	K (kcal)	n	S
Co - N - C - H	0.000	0.0	0.0
Co - N - C - C	0.000	0.0	0.0
Ni - N - C - C	0.000	0.0	0.0
Ni - N - C - H	0.000	0.0	0.0
Cu - N - C - C	0.000	0.0	0.0
Cu - N - C - H	0.000	0.0	0.0
H - C - C - C	0.474	3.0	1.0
H - C - C - H	1.423	3.0	1.0
H - C - N - H	0.474	3.0	1.0
H - C - C - N	1.423	3.0	1.0
C - C - C - N	0.474	3.0	1.0
C - N - C - C	0.474	3.0	1.0
C - N - C - H	0.474	3.0	1.0
H-C5-N5'-H	4.0	2.0	-1.0
C5-N5-C5-H	4.0	2.0	-1.0
C5-N5-C5-N5'	4.0	2.0	-1.0
H-N5'-C5-N5	4.0	2.0	-1.0
H-C5-N5'-C5	4.0	2.0	-1.0
H-C5-C5-N5	12.0	2.0	-1.0
H-C5-C5-H	4.0	2.0	-1.0
H-C5-C5-N5'	4.0	2.0	-1.0
C5-N5'-C5-C5	4.0	2.0	-1.0
C5-N5'-C5-N5	4.0	2.0	-1.0
C5-N5-C5-C5	4.0	2.0	-1.0
N5'-C5-C5-N5	12.0	2.0	-1.0
H-N5'-C5-C5	4.0	2.0	-1.0
C5-N5-Cu-N5	0.0	0.0	0.0
H-C5-N5-Cu	0.0	0.0	0.0
Cu-N5-C5-H	0.0	0.0	0.0
Cu-N5-C5-C5	0.0	0.0	0.0
H-C6-C6-C6	12.000	2.0	-1.0
H-C6-CJ-C	12.000	2.0	-1.0
C6-C6-CJ-C	12.000	2.0	-1.0
H-C6-C6-CJ	12.000	2.0	-1.0
H-C6-CJ-CJ	12.000	2.0	-1.0
H-C6-C6-CZ	12.000	2.0	-1.0
H-CZ-C6-C6	12.000	2.0	-1.0
H-C6-CZ-H	12.000	2.0	-1.0
H-C6-C6-H	12.000	2.0	-1.0
H-C6-CZ-N6	12.000	2.0	-1.0
H-C6-CJ-N6	12.000	2.0	-1.0
C6-CJ-C-CJ	0.474	3.0	1.0
N6-CJ-C-CJ	0.474	3.0	1.0
C6-CJ-C-H	0.474	3.0	1.0
N6-CJ-C-H	0.474	3.0	1.0
C6-CJ-C-N	0.474	3.0	1.0
N6-CJ-C-N	0.474	3.0	1.0
C6-CJ-CJ-N6	1.000	2.0	-1.0
C6-C6-CJ-N6	12.000	2.0	-1.0
C6-C6-CZ-N6	12.000	2.0	-1.0
C6-C6-CJ-CJ	12.000	2.0	-1.0
C6-CJ-CJ-C6	1.000	2.0	-1.0
CZ-C6-C6-C6	12.000	2.0	-1.0
CJ-C-N-H	0.474	3.0	1.0
CZ-N6-CJ-CJ	4.000	2.0	-1.0
CZ-N6-CJ-C6	4.000	2.0	-1.0
CJ-N6-CZ-C6	4.000	2.0	-1.0
CJ-N6-CZ-C	4.000	2.0	-1.0
CJ-N6-CJ-C6	4.000	2.0	-1.0
CJ-N6-CZ-H	4.00	2.0	-1.0
N6-CJ-CJ-N6	1.000	2.0	-1.0
CZ-N6-Cu-N6	0.000	0.0	0.0
CJ-N6-Cu-N6	0.000	0.0	0.0
Cu-N6-CJ-CJ	0.000	0.0	0.0
Cu-N6-CZ-C6	0.000	0.0	0.0
Cu-N6-CJ-C6	0.000	0.0	0.0
Cu-N6-CJ-C	0.000	0.0	0.0
Cu-N-C-CJ	0.000	0.0	0.0
N-Cu-N6-CJ	0.000	0.0	0.0
N-Cu-N6-CJ	0.000	0.0	0.0
N6-Cu-N-H	0.000	0.0	0.0
N6-Cu-N-C	0.000	0.0	0.0
H-CZ-N6-Cu	0.0	0.0	0.0
H-CZ-N6-Cu	0.0	0.0	0.0
H-CZ-N6-Cu	0.0	0.0	0.0
H-C-C-H	0.474	3.0	1.0
H-C5-N5-N5'	4.000	2.0	-1.0
H-C-N5'-C5	0.474	3.0	1.0

H-C-N5'-N5	0.474	3.0	1.0
C5-C5-C5-H	12.0	2.0	-1.0
C5-C5-C5-N5'	12.0	2.0	-1.0
CJ-C-N5'-C5	0.474	3.0	1.0
CJ-C-N5'-N5	0.474	3.0	1.0
C5-C5-C5-N5	4.000	2.0	-1.0
C5-C5-N5' N5	4.000	2.0	-1.0
H-C5-C5-N5'	12.000	2.0	-1.0
H-C5-C5-N5	4.000	2.0	-1.0
N5'-C-CJ-N6	0.474	3.0	1.0
N5'-C-CJ-C6	0.474	3.0	1.0
C5-N5-N5'-C5	4.000	2.0	-1.0
C5-N5-N5'-C	4.000	2.0	-1.0
H-C5-N5'-N5	4.000	2.0	-1.0
CJ-N6-CJ-C	4.000	2.0	-1.0
C-N5'C5-C5	4.000	2.0	-1.0
C6-N6-Ni-N6	0.000	0.0	0.0
C5-N5-Ni-N6	0.000	0.0	0.0
C5-N5-Ni-N5	0.000	0.0	0.0
N5-Ni-N5-N5'	0.000	0.0	0.0
N6-Ni-N5-N5'	0.000	0.0	0.0
H-C6-N6-Ni	0.000	0.0	0.0
H-C5-N5-Ni	0.000	0.0	0.0
C5-N5'-N5-Ni	0.000	0.0	0.0
C-N5'-N5-Ni	0.000	0.0	0.0
N5-Ni-N6-CJ	0.000	0.0	0.0
N6-Ni-N6-CJ	0.000	0.0	0.0
Ni-N6-CJ-C	0.000	0.0	0.0
Ni-N6-CJ-C6	0.000	0.0	0.0
Ni-N5-N5'-C5	0.000	0.0	0.0
Ni-N5-N5'-C	0.000	0.0	0.0
Ni-N5-C5-C5	0.000	0.0	0.0
N5-N5'-C-N5'	0.474	3.0	1.0
Cu-N5-N5'-C	0.000	0.0	0.0
C5-N5'-C-N5'	0.474	3.0	1.0
C5-C5-N5'-C	12.000	2.0	-1.0
H-C-C-CJ	0.474	3.0	1.0
N-C-C-CJ	0.474	3.0	1.0
C-C-CJ-N6	0.474	3.0	1.0
C-C-CJ-C6	0.474	3.0	1.0
N - C - C - N	0.474	3.0	1.0

Van der Waals

	A	B
Co	0.0	0.0
Ni	0.0	0.0
Cu	0.0	0.0
H	654.295	41.085
N	10155.9	326.517
N6	10155.9	326.517
C6	14539.0	397.436
CJ	14539.0	397.436
CZ	14539.0	397.436
N5	10155.900	326.517
N5'	10155.900	326.517
C5	14539.000	397.436
C	14539.0	897.436
Cl	49496.2	1154.4

Symbols used.

	Description
C	Aliphatic C
C6	C in 6 membered ring
H	Hydrogen atom
N	Aliphatic N
N6	N in 6 membered ring
CJ	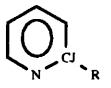
CZ	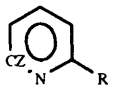
N5	N in 5 membered ring (attached to metal)
N5'	N in 5 membered ring
C5	C in 5 membered ring

Force Field Parameters for calculations which include charges.

Complete listing of the Force Field parameters and funcional forms used in this work. All energies are calculated in kcal/mol. This requires converting the CLFSE from wavenumbers.

Functional forms

Bond Stretch: $E_{str} = D_0[1-\exp^{-\alpha(r-r_0)}]^2$

Angle Bend: $E_{bend} = (1/2)k_\theta(\theta-\theta_0)^2$

Torsion: $E_{tor} = K(1+S(\cos n\omega)$

Van der Waals: $E_{vdw} = A/r^9 - B/r^6$

CLFSE: $e_\sigma = a_0 + a_1 r\ (cm^{-1})$

Charge $E_{el} = q_i q_j / r_{ij}$

CLFSE

	Ni(II), Cu(II)	
	a_0	a_1
N	21629	-8235
N6	21629	-8235
N5	21629	-8235
Cl	9000	-2500

Bond stretch

	D_0 (kcal/mole)	r_0 (Å)	α
Ni - N	120.0	2.460	0.45
Ni - Cl	120.0	2.520	0.45
N - C	72.0	1.49	2.20
N - H	93.0	0.91	2.50
C - C	88.0	1.50	1.92
C - H	108.6	0.97	1.60
C5-H	108.6	0.970	1.60
N5'-H	93.0	1.030	1.00
C5-N5	80.0	1.350	1.60
C5-C5	80.0	1.350	1.60
C5-N5'	80.0	1.330	1.00
Cu-N5	120.0	2.233	0.45
Cu-N	120.0	2.283	0.45
C6-H	108.6	0.970	1.60
CJ-H	108.6	0.970	1.60
C6-C6	80.0	1.380	1.00
C6-C	72.0	1.490	1.92
C6-CJ	70.0	1.350	1.00
C6-CZ	70.0	1.350	1.00
C6-N6	80.0	1.350	1.60
CJ-N6	72.0	1.350	1.00
CZ-N6	80.0	1.350	1.60
Cu-N6	120.0	2.233	0.45
N5-N5'	72.0	1.34	2.00
Ni-N6	120.0	2.420	0.45
Ni-N5	120.0	2.430	0.45

Angle bend

	k_θ (kcal)	θ (°)
N - Ni - N	0.000	0.000
N - Ni - Cl	0.000	0.000
Cl - Ni - Cl	0.000	0.000
N - Cu - N	0.000	0.000
Ni - N - H	64.786	109.721
Ni - N - C	28.786	118.008
H - N - H	47.497	108.977
N - C - H	64.786	109.492
C - N - C	28.786	109.492
C - C - C	28.786	112.492
N - C - C	64.786	110.492
H - N - C	64.786	109.492
H - C - C	51.815	109.378
H - C - H	47.497	108.977
H-N5'-C5	27.000	120.0
H-N5'-N5	27.000	120.0
N5-C5-H	90.000	114.0
C5-C5-H	90.000	110.0
C5-C5-N5'	90.000	110.0
C5-C5-N5	90.000	110.0
C5-N5-C5	90.000	110.0
C5-N5'-C5	90.000	110.0
N5-C5-H	50.000	120.0
N5'-C5-H	50.000	120.0
Cu-N5-C5	21.786	124.0
H-C6-C6	37.000	120.0
H-C6-CJ	37.000	120.0
H-C6-CZ	37.000	120.0
H-CZ-C6	37.000	120.0
N6-CJ-C6	90.000	120.0
N6-CZ-C6	90.000	114.0
N6-CJ-CJ	90.000	120.0
N6-CJ-C	64.000	115.0
C6-C6-C6	90.000	120.0
C6-CJ-CJ	90.000	120.0
C6-CJ-C	46.600	120.0
CJ-C6-C6	90.000	120.0
CZ-C6-C6	90.000	120.0
CJ-C-CJ	90.000	110.5

H-C-CJ	44.400	110.0
CJ-N6-CZ	75.100	114.0
CJ-N6-CJ	75.100	120.0
N6-C6-H	50.000	120.0
N6-CZ-H	50.000	120.0
N-C-CJ	64.786	110.5
Cu-N6-CJ	14.786	120.0
Cu-N6-CZ	14.786	130.0
N6-Cu-N6	0.0	0.0
N6-Cu-N	0.0	0.0
C5-N5-N5'	90.000	110.000
N5-N5'-C	75.000	114.000
N5-N5'-C5	90.000	114.000
CJ-N6-CJ	75.100	120.000
C-N5'-C5	75.100	114.000
N5-C-CJ	60.000	120.000
C6-CJ-C5	46.600	120.000
C5-C5-C5	75.000	104.000
N6-CJ-C	64.786	110.492
Ni-N6-CJ	14.785	124.008
Ni-N5-C5	7.786	128.008
Ni-N5-N5'	7.786	124.008
N6-Ni-N6	0.000	0.000
N6-Ni-N5	0.000	0.000
C-C-CJ	14.000	120.000
N5-C-N5	64.786	109.492
N5-Ni-N5	0.000	0.000

Torsion

	K (kcal)	n	S
Ni - N - C - C	0.000	0.0	0.0
Ni - N - C - H	0.000	0.0	0.0
Cu - N - C - C	0.000	0.0	0.0
Cu - N - C - H	0.000	0.0	0.0
H - C - C - C	0.474	3.0	1.0
H - C - C - H	1.423	3.0	1.0
H - C - N - H	0.474	3.0	1.0
H - C - C - N	1.423	3.0	1.0
C - C - C - N	0.474	3.0	1.0
C - N - C - C	0.474	3.0	1.0
C - N - C - H	0.474	3.0	1.0
H-C5-N5'-H	4.0	2.0	-1.0
C5-N5-C5-H	4.0	2.0	-1.0
C5-N5-C5-N5'	4.0	2.0	-1.0
H-N5'-C5-N5	4.0	2.0	-1.0
H-C5-N5'-C5	4.0	2.0	-1.0
H-C5-C5-N5	12.0	2.0	-1.0
H-C5-C5-H	4.0	2.0	-1.0
H-C5-C5-N5'	4.0	2.0	-1.0
C5-N5'-C5-C5	4.0	2.0	-1.0
C5-N5'-C5-N5	4.0	2.0	-1.0
C5-N5-C5-C5	4.0	2.0	-1.0
N5'-C5-C5-N5	12.0	2.0	-1.0
H-N5'-C5-C5	4.0	2.0	-1.0
C5-N5-Cu-N5	0.0	0.0	0.0
H-C5-N5-Cu	0.0	0.0	0.0
Cu-N5-C5-H	0.0	0.0	0.0
Cu-N5-C5-C5	0.0	0.0	0.0
H-C6-C6-C6	12.000	2.0	-1.0
H-C6-CJ-C	12.000	2.0	-1.0
C6-C6-CJ-C	12.000	2.0	-1.0
H-C6-C6-CJ	12.000	2.0	-1.0
H-C6-CJ-CJ	12.000	2.0	-1.0
H-C6-C6-CZ	12.000	2.0	-1.0
H-CZ-C6-C6	12.000	2.0	-1.0
H-C6-CZ-H	12.000	2.0	-1.0
H-C6-C6-H	12.000	2.0	-1.0
H-C6-CZ-N6	12.000	2.0	-1.0
H-C6-CJ-N6	12.000	2.0	-1.0
C6-CJ-C-CJ	0.474	3.0	1.0
N6-CJ-C-CJ	0.474	3.0	1.0
C6-CJ-C-H	0.474	3.0	1.0
N6-CJ-C-H	0.474	3.0	1.0
C6-CJ-C-N	0.474	3.0	1.0
N6-CJ-C-N	0.474	3.0	1.0
C6-CJ-CJ-N6	1.000	2.0	-1.0
C6-C6-CJ-N6	12.000	2.0	-1.0
C6-C6-CZ-N6	12.000	2.0	-1.0
C6-C6-CJ-CJ	12.000	2.0	-1.0
C6-CJ-CJ-C6	1.000	2.0	-1.0
CZ-C6-C6-C6	12.000	2.0	-1.0
CJ-C-N-H	0.474	3.0	1.0
CZ-N6-CJ-CJ	4.000	2.0	-1.0
CZ-N6-CJ-C6	4.000	2.0	-1.0
CJ-N6-CZ-C6	4.000	2.0	-1.0

CJ-N6-CZ-C	4.000	2.0	-1.0
CJ-N6-CJ-C6	4.000	2.0	-1.0
CJ-N6-CZ-H	4.00	2.0	-1.0
N6-CJ-CJ-N6	1.000	2.0	-1.0
CZ-N6-Cu-N6	0.000	0.0	0.0
CJ-N6-Cu-N6	0.000	0.0	0.0
Cu-N6-CJ-CJ	0.000	0.0	0.0
Cu-N6-CZ-C6	0.000	0.0	0.0
Cu-N6-CJ-C6	0.000	0.0	0.0
Cu-N6-CJ-C	0.000	0.0	0.0
Cu-N-C-CJ	0.000	0.0	0.0
N-Cu-N6-CJ	0.000	0.0	0.0
N-Cu-N6-CJ	0.000	0.0	0.0
N6-Cu-N-H	0.000	0.0	0.0
N6-Cu-N-C	0.000	0.0	0.0
H-CZ-N6-Cu	0.0	0.0	0.0
H-CZ-N6-Cu	0.0	0.0	0.0
H-CZ-N6-Cu	0.0	0.0	0.0
H-C-C-H	0.474	3.0	1.0
H-C5-N5-N5'	4.000	2.0	-1.0
H-C-N5'-C5	0.474	3.0	1.0
H-C-N5'-N5	0.474	3.0	1.0
C5-C5-C5-H	12.0	2.0	-1.0
C5-C5-C5-N5'	12.0	2.0	-1.0
CJ-C-N5'-C5	0.474	3.0	1.0
CJ-C-N5'-N5	0.474	3.0	1.0
C5-C5-C5-N5	4.000	2.0	-1.0
C5-C5-N5' N5	4.000	2.0	-1.0
H-C5-C5-N5'	12.000	2.0	-1.0
H-C5-C5-N5	4.000	2.0	-1.0
N5'-C-CJ-N6	0.474	3.0	1.0
N5'-C-CJ-C6	0.474	3.0	1.0
C5-N5-N5'-C5	4.000	2.0	-1.0
C5-N5-N5'-C	4.000	2.0	-1.0
H-C5-N5'-N5	4.000	2.0	-1.0
CJ-N6-CJ-C	4.000	2.0	-1.0
C-N5'C5-C5	4.000	2.0	-1.0
C6-N6-Ni-N6	0.000	0.0	0.0
C5-N5-Ni-N6	0.000	0.0	0.0
C5-N5-Ni-N5	0.000	0.0	0.0
N5-Ni-N5-N5'	0.000	0.0	0.0
N6-Ni-N5-N5'	0.000	0.0	0.0
H-C6-N6-Ni	0.000	0.0	0.0
H-C5-N5-Ni	0.000	0.0	0.0
C5-N5'-N5-Ni	0.000	0.0	0.0
C-N5'-N5-Ni	0.000	0.0	0.0
N5-Ni-N6-CJ	0.000	0.0	0.0
N6-Ni-N6-CJ	0.000	0.0	0.0
Ni-N6-CJ-C	0.000	0.0	0.0
Ni-N6-CJ-C6	0.000	0.0	0.0
Ni-N5-N5'-C5	0.000	0.0	0.0
Ni-N5-N5'-C	0.000	0.0	0.0
Ni-N5-C5-C5	0.000	0.0	0.0
N5-N5'-C-N5'	0.474	3.0	1.0
Cu-N5-N5'-C	0.000	0.0	0.0
C5-N5'-C-N5'	0.474	3.0	1.0
C5-C5-N5'-C	12.000	2.0	-1.0
H-C-C-CJ	0.474	3.0	1.0
N-C-C-CJ	0.474	3.0	1.0
C-C-CJ-N6	0.474	3.0	1.0
C-C-CJ-C6	0.474	3.0	1.0
N - C - C - N	0.474	3.0	1.0

Van der Waals

	A	B
Ni	0.0	0.0
Cu	0.0	0.0
H	654.295	41.085
N	10155.9	326.517
N6	10155.9	326.517
C6	14539.0	397.436
CJ	14539.0	397.436
CZ	14539.0	397.436
N5	10155.900	326.517
N5'	10155.900	326.517
C5	14539.000	397.436
C	14539.0	897.436
Cl	49496.2	1154.4

Charge

	q
Ni	0.9
Cu	0.5
N	-0.41
N6	-0.41
N5	-0.41
Cl	-0.7

Symbols used.

	Description
C	Aliphatic C
C6	C in 6 membered ring
H	Hydrogen atom
N	Aliphatic N
N6	N in 6 membered ring
CJ	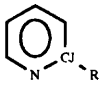
CZ	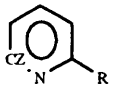
N5	N in 5 membered ring (attached to metal)
N5'	N in 5 membered ring
C5	C in 5 membered ring